UNIVERSITÉ DU LUXEMBOURG

PhD-FSTM-2021-020
The Faculty of Science, Technology and Medicine

DISSERTATION

Defense held on 29/03/2021 in Luxembourg
to obtain the degree of

DOCTEUR DE L'UNIVERSITÉ DU LUXEMBOURG

EN *SCIENCES DE L'INGÉNIEUR*

by

Mohammed OUALLAL
Born on 25 April 1985 in Berkane, (Morocco)

ENTRAINMENT OF DROPLETS FROM WATER POOLS

Dissertation defense committee

Prof. Dr. Stephan LEYER, dissertation supervisor
Université du Luxembourg, Luxembourg

Dr. Sanjeev GUPTA
Becker Technologies, Eschborn,Germany

Prof. Dr. Frank SCHOLZEN
Université du Luxembourg, Luxembourg

Prof. Dr. Abdelouahab DEHBI
Paul Scherrer Institute, Switzerland

Prof. Dr. Marco KOCH
Ruhr University Bochum, Germany

Abstract

The aim of this work is to study the phenomena of droplet entrainment from water pool. This phenomenon could be either a consequence of boiling or depressurization. In a bubble column, droplets are released from the surface of the pool by bubble burst (in bubbly flow regime) or by detachment from liquids sheets (in churn turbulent flow regime) depending on the hydrodynamics inside the pool. Eventually, these droplets will be entrained by the streaming gas (superficial gas velocity) or fall back due to gravity.

Many experimental studies have been conducted, and several numerical simulations were performed for a better understanding of the phenomena of entrainment. Numerical simulation are a good tool to simulate an experiment due to limitations of data. To that end, CFD showed to be a good candidate to perform such a simulation, yet these it demand high computational performance and are time consuming. However, Lumped Parameter codes (LP) are widely used due to their simplicity and fast running.

The number of correlations that quantify the entrainment previously developed based on empirical, semi-empirical and theoretical approaches are limited to a specific regime in the water pool, thermal hydraulic conditions or even to a specific geometry

For this purpose, after an extensive study, an empirical correlation is proposed to cover the flow regimes from bubbly to churn turbulent, and could be applied to a wide range of geometries.

The current correlation shows an increase until a maximum entrainment of about 2.10^{-4}, corresponding to gas velocity of 0.05 m/s for bubbly flow regime, a slight decrease to 2.10^{-5}, for the transition regime for superficial gas velocities up to 0.1 m/s, and a sharp increase as the superficial gas velocity goes up to 5 m/s

The experimental database used to develop the present empirical correlation covers a broader range of boundary conditions, namely pressure [1 bar – 15 bar], water pool thermal condition [subcooled – boiling], vessel diameter[0.19m- 3.2 m], pool diameter [0.1 m – 1.4 m], superficial gas velocity up to 5.0 m/s and for soluble and insoluble aerosols. Therefore, the proposed empirical correlation aims to constitute an important tool to transfer the experimental results to reactor application.

Acronyms

ACE	Advanced Containment Experiments
ALPHA	Assessment of Loads and Performance of Containment in a Hypothetical Accident
BUSCA	Bubble Scrubbing Algorithm
BUSCA-PSI	Updated version of BUSCA by PSI
BWR	Boiling water reactor
CFD	Computational Fluid Dynamics
CV	Control Volume
COCOSYS	Containment Code System
CNC	Condensation Nuclei Counter
ECART	Enel Code for Analysis of Radionuclide Transport
ENEL	**E**nte **N**azionale per l'**E**nergia E**l**ettrica
EPRI	Electric Power Research Institute
FP	Fission Products
FS	Filter Station
GF	Gesamtfilter (in German), Integral Filter (in English)
GS	Gas Scrubber
IPRESCA	Integration of Pool Scrubbing Research to Enhance Source-term Calculations
JAERI	Japan Atomic Energy Research Institute
LOCA	Loss of Cooling Accident
LP	Lumped Parameter code
OECD	Organization for Economic Co-operation and Development
POSEIDON	Pool Scrubbing Effect on Iodine Decontamination
PSI	Paul Scherrer Institute
PWR	Pressurized Water Reactor

RPV	Reactor Pressure Vessel
RECOM	A code for the simulation of radionuclide resuspension at bubbling water
REST	REsuspension Source Term(Bunz et al., 1992)
SMPS	Scanning Mobility Particle Sizer
SGTR	Steam Generator Tube Rupture
SPARC-90	Suppression Pool Aerosol Removal Code
SPARC-B/98	Updated version of SPARC
SPARTA	Suppression Pool Aerosol Retention Test Apparatus
SUPRA	Suppression Pool Retention Analysis
THAI	Thermal-hydraulic Hydrogen Aerosol Iodine
RUB	Ruhr-Universität Bochum
UKAEA	United Kingdom Atomic Energy Authority

Nomenclature

A	Vessel cross section$[m^2]$
A_j	Junction cross section$[m^2]$
A_d	Turbulent diffusion coefficient$[m^2.s^{-1}]$
a	Capillary length$[m]$
a'	Correlation constant equation
C	Droplet concentration in the atmosphere$[m^{-3}]$
$C(x)$	Droplet concentration in the atmosphere as a function of x$[m^{-3}]$
C_0	Initial droplet concentration on the atmosphere$[m^{-3}]$
C_1	Droplet concentration on the atmosphere to be determined from experimental data$[m^{-3}]$
C_K	Constant of Kruzhilin correlation.
C_{cond}	The concentration of the tracer in the condensate$[m^{-3}]$
C_{BP}	The concentration of the tracer in the pool$[m^{-3}]$

b'	Correlation constant
DF	Decontamination factor
$DEPEFF$	Depletion efficiency
d_{vm}	Bubble Sauter diameter $[m]$
d_b	Bubble diameter$[m]$
$d_{b,crit}$	Critical bubble diameter$[m]$
$\overline{d_b}$	Mean bubble diameter$[m]$
D_H	Vessel diameter$[m]$
d_{dr}	Droplet diameter$[m]$
D	Pipe diameter in equation (14) Chapter 2$[m]$
D_{BP}	Diameter of Bubbling Pool (BP) $[m]$
E_{fg}	Liquid entrainment $[-]$
f_i	Mass fraction of particle
$f(d)$	Bubble size distribution
$F(d_{dr,crit})$	Fraction of ejected droplets less than $d_{dr,crit}$
f	Correlation constant equation (9) Chapter 2
g	Acceleration due to gravity$[m.s^{-2}]$
G_{kj}^{a}, G_{kj}^{e}	Mass flow rate for all component *k* of inlets and outlets. $[kg.s^{-1}]$
G_{ij}^{e}, G_{ij}^{a}	Mass flow rate of non-condensable gases, inlet and outlet respectively. $[kg.s^{-1}]$
G_{Wj}^{e}, G_{Wj}^{a}	Mass flow rate of liquid water, inlet and outlet respectively$[kg.s^{-1}]$
G_{Dj}^{e}, G_{Dj}^{a}	Mass flow rate of steam, inlet and outlet respectively. $[kg.s^{-1}]$
G_{VD}^{vol}	Mass evaporation rate describing the phase change. $[kg.s^{-1}]$
G_W, G_D	Mass flow rates of water and steam respectively
G_j	Mass flow rate through the junction $j[kg/s]$
h_d	Height of drop trajectory$[m]$
h_i	Initial height above the water surface (no bubbling pool)$[m]$
h	Height above the water surface in the case of bubbling $[m]$
h_l	Liquid level without bubbles$[m]$
h_{fg}	Two phase flow level (swell level) $[m]$
h_{film}	Bubble film thickness $[m]$
H_D	Steam enthalpy$[J]$

H_W	Water enthalpy$[J]$
i_W, i_D	Specific enthalpy of water and steam respectively$[J.kg^{-1}]$
j_g	Superficial gas velocity $[m.s^{-1}]$
j_t	Transition gas velocity $[m.s^{-1}]$
j	Correlation constant equation
k_i, with$i = 1 \dots 5$,	Correlation constant of Cosandey's correlation
K_j	Junction resistance$[Pa.m^{-3}.s]$
l_j	Junction length$[m]$
N_{dr}	Number of jet droplets produced by a single bubble
m	Mass of liquid drop $[kg]$
$\dot{m}_g, \dot{m}_l$	Mass flow rate of gas and liquid respectively$[kg.s^{-1}]$
$\dot{m}_{st,cond}, \dot{m}_{st,w}$, $\dot{m}_{ncg}$	Mass flow of condensate, mass flow condensed steam on vessel walls, mass flow of non-condensable gases$[kg.s^{-1}]$
M_1	Bubble mass sitting on the water surface $[kg]$
M_W, M_D	Masses of water and steam respectively $[kg]$
p_{js}, p_{jt}	Pressure at the source and target point$[bar]$
$P(j_g)$	Probability of the existence of suspended droplet at a given j_g
P_i	Pressure inside the bubble $[bar]$
P_o	Pressure of the surrounding $[bar]$
Q^a, Q^e	Heat exchange with the surrounding, heat acquired and given respectively.$[J]$
R_0	Radius of the bubble $[m]$
S_f	Acceleration inside the bubble due to centripetal force$[m.s^{-2}]$
T_{gas}	Gas temperature$[K]$
t	Time$[s]$
u'	Drop velocity $[m.s^{-1}]$
u_i'	Initial drop velocity $[m.s^{-1}]$
v_b	Bubble rise velocity$[m.s^{-1}]$
v_t	Droplet terminal velocity$[m.s^{-1}]$
V_0	Average droplet velocity$[m.s^{-1}]$
V_{dr}	Total volume of liquid droplet per volume bubble $V_b[m^3]$
$\dot{V}_{dr}$	Droplets volume flow rate$[m^3.s^{-1}]$

V_b	Bubble volume $[m^3]$
V	Volume time dependent $[m^3.s^{-1}]$
V_{tc}	The roll film velocity (Taylor – Culick velocity)$[m/s]$
w_j	Weight of junction column $(\rho g \Delta h)[N]$
x_{BP}	Mass fraction of the boiling pool
x_{ncg}	Mass ratio of non-condensable gases

Dimensionless groups

$Eo = Bo = D^* = \frac{D}{\sqrt{\frac{g\Delta\rho}{\sigma}}}$	Dimensionless vessel diameter also is the Bond number
$Fo = \frac{j_g^2}{g.D_H}$	Froude number
$h^* = h \Big/ \sqrt{\frac{g\Delta\rho}{\sigma}}$	Dimensionless height above the water surface
$j_g^* = j_g \Big/ \left(\frac{\sigma g \Delta\rho}{\rho_g^2}\right)^{1/4}$	Wallis number
$N_{\mu g} = \frac{\mu_g}{\sqrt{\sigma \rho_g \sqrt{\frac{\sigma}{g\Delta\rho}}}}$	Dimensionless viscosity
Ra	Rayleigh number
$We = \frac{j_g^2.D_H.\rho_l}{\sigma}$	Dimensionless viscosity

Greek symbols

α	gas volumetric fraction
α_j	Heal loss
β	reciprocal of average drop energy$[J^{-1}]$

Φ	Correction factor
μ_g	Gas viscosity$[N.s.m^{-2}]$
ρ_l	Liquid density$[kg.m^{-3}]$
$\Delta\rho = \rho_l - \rho_g$	Density difference$[kg.m^{-3}]$
σ	Surface tension$[N.m^{-1}]$
γ_i	Current correlation constants
$\Phi_{\mathrm{dr}}, \Phi_b$	Droplets an bubble size distribution functions respectively

Table of Contents

Acknowledgment

I would like to express my deep and sincere gratitude to my research supervisor, Dr. Stephan Leyer, Professor and Head of the Department of Engineering, University of Luxembourg, for giving me the opportunity to do research and providing guidance throughout this research. Thanks to him, I could accomplish many things during this period. Through his recommendations and criticism, I could improve this thesis. I was remarkably fortunate to work under his supervision, since I met people who have extremely marked me. I would like to thank my advisor Dr. Sanjeev Gupta, Head of Reactor Safety & Engineering, Becker Technologies, Germany, for his dynamism and sincerity that have deeply inspired me. He has showed me the methodology to carry out the research and to present the research works as clearly as possible. I thank my second advisor, Dr. Frank Scholzen, associate professor, University of Luxembourg, for his commitment and recommendations to accomplish this thesis.

I would like to express my special appreciation and thanks to Dr. Karsten Fischer, retired from Becker Technologies, Germany, for his uncompelled dedication and fruitful enlightening discussions.

I would like to thank deeply Dr. Dehbi Abdel, Senior Scientist at PSI, Switzerland, for his hospitality at PSI, and for showing devotion, cheering and spontaneous assistance.

I thank Dr. Nowack Holger, Engineer at GRS, Cologne, for his hospitality at GRS, assistance and long discussion to accomplish the numerical part of this work.

Many thanks to Dr. Abdel Dehbi, Senior scientist of the Paul Scherrer Institute, Switzerland, and Dr. Marco Koch, Engineer and Professor at Ruhr University Bochum, Germany for accepting the invitation to be part of the committee.

I am extremely grateful to my parents for their love, caring and sacrifices for educating and preparing me for my future. I am very much thankful to my brothers and sister for their love, assistance and positivity to accomplish this work. Words will not be enough to thank enough to my elder brother who covered all my expenses during this period of research in Luxembourg. Besides, he was a source of motivation and advices.

I would like to thank my friend Dr. Nabil Bella, Professor at Université Tahri Mohammed Béchar, Algeria, for his assistance and valuable advices.

I would like to say thanks to my friends and research colleagues, for their genuine support throughout this research work.

Finally, my thanks go to all the people who have supported me to complete the research work directly or indirectly.

List of Figures

List of Tables

I. Introduction

The entrainment of liquid phase by a gas phase is found in a numerous industrial process, where mass and heat transfer intervene. During the interaction liquid-gas, the formation of the droplets is a common phenomenon. Taking their size into account, and the exchange with the gas phase, they can be entrained by this latter to a specific height above the water surface. The superficial gas velocity characterizes the gas phase.

The superficial gas velocity is calculate from the volume flow rate of the gas coming from the pool surface of a certain cross section area. Therefore, for different superficial gas velocities comes different flow regimes in the water pool. At low superficial gas velocities, the regime is attributed to a bubbly flow regime, where bubble are defined in shapes and size (Shah et al., 1982). At high superficial gas velocities, where the irregular shapeless bubble are formed, the regime is attributed to churn turbulent flow. As a function of the flow regimes, the droplet generation mechanism differs from bubble burst to detachment from liquid ligaments due to momentum exchange gas-liquid (**Figure I-1**). The present study concerns the release of these droplets, or so-called droplet entrainment from water pool that cover the mentioned flow regimes.

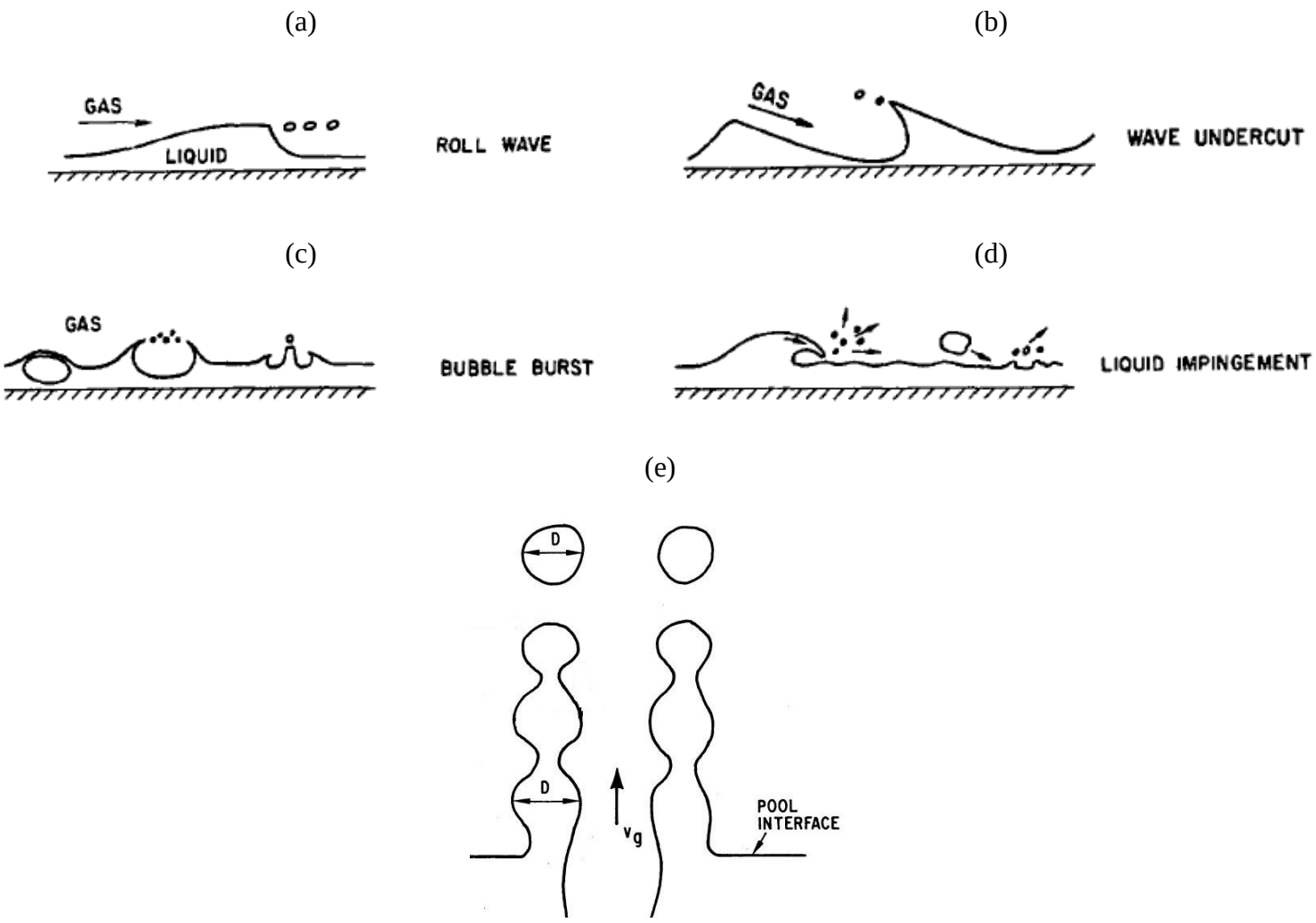

Figure I-1 *Droplets generation mechanisms* (Santiago and Marvillet, 1991)(Kataoka and Ishii, 1984)

The phenomenon of entrainment is found in industrial processes as in natural phenomena, from geophysics (release of salt from the surface of the sea), water treatment (desalination) to nuclear applications (release of aerosol from water pool).

In natural phenomena, the entrainment is responsible of mass transfer at the surface of the sea. Sea spray, which is the amount of droplets generated either from bubble burst or roll wave or by splashing containing salts and bacteria from the sea surface (Blanchard, 1989)(Donald E Spiel, 1998) are entrained by the wind and could be problematic for human health as it could affect the climate. The released aerosol might form large clouds that could affect the air quality as well as

reflecting the sun light. The weather in coastal region is mainly determined by quantifying the amount of airborne aerosols. (**Figure I-2**).

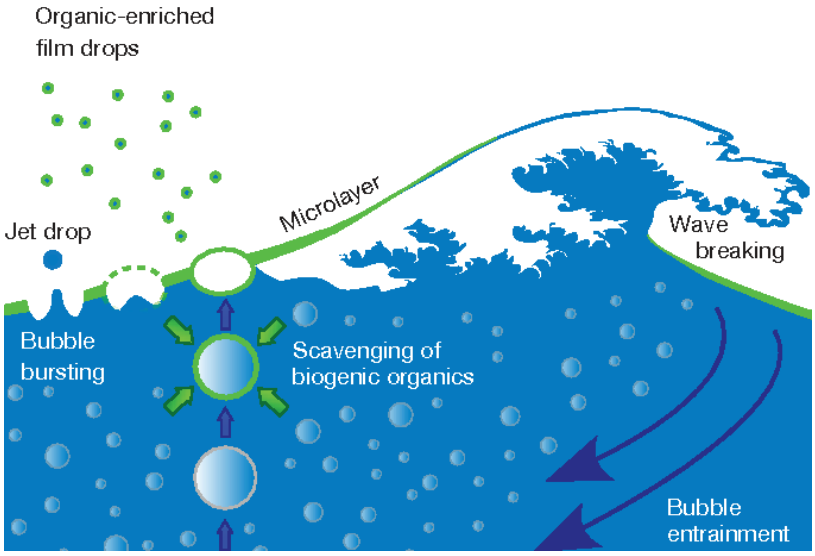

Figure I-2 *Re-entrainment of droplets from the surface of the Sea*(Wilson et al., 2015)

In the sector of water treatment, in order to separate solid from liquid phase, desalination plants use evaporator. The process is to entrain droplet by injecting steam. As the bubbles rise to reach the surface, they burst to generate small droplets that are partly entrained in the distillate (Cosandey, 1999).

In horizontal and vertical separators in gathering centres (**Figure I-3**), to separate phases (gas, oil and liquid), a mixture of gas-water-oil or gas-oil is feed into a static vessel. The inflow causes agitation of the interface by entraining gas into the mixture of oil-liquid in form of bubbles. This latter rise on the surface and burst producing droplets. Therefore, for phase separation, gas is exhausted by a vent at the top of the vessel, carrying liquid droplet with it. One of the principle of separation is coalescence. Coalescing is related to the agitation process. During coalescence, water droplets come together to form larger drops. In vane type mist eliminators, droplets are removed from the vapour stream through inertial impaction. The wet gas is forced to change direction causing mists droplets to strike the vanes and coalesce with other droplets eventually falling. However, some of the droplets escape without coalescing. Therefore, the amount of droplet needs

to be quantified in order to measure the purity of the gas (Viles, 1993)(Kharoua et al., 2013)(Wurster et al., 2015).

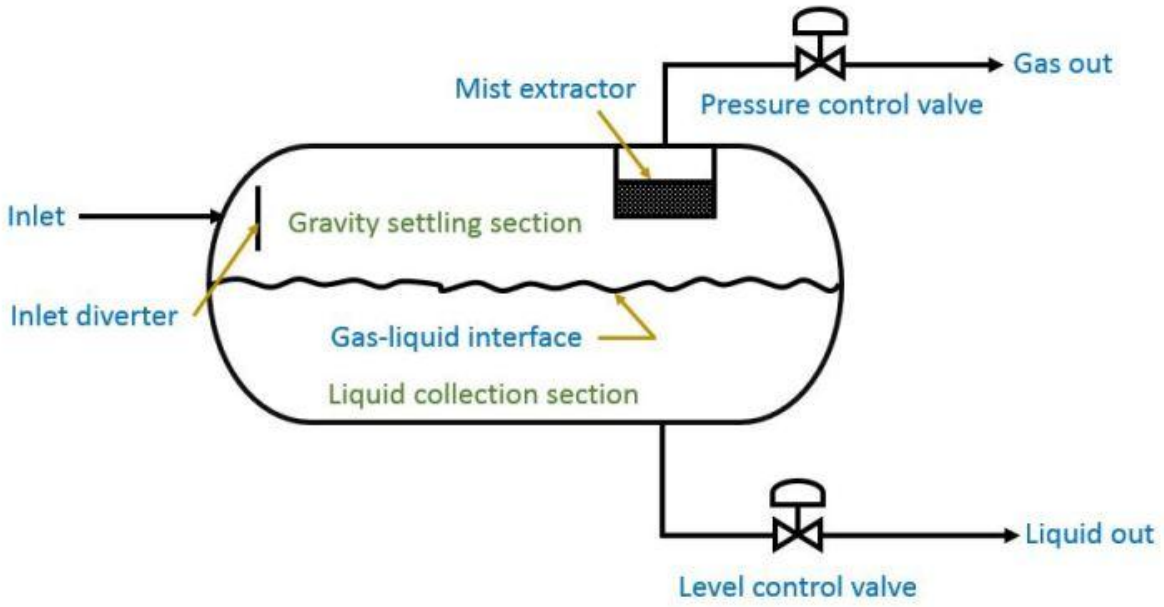

Figure I-3 *Two phase flow horizontal separator*

In nuclear engineering, the Steam Generator Tube Rupture (SGTR) events often occurs during PWR operation. The steam generator tube might experience degradations that cause leakage or rupture (Dehbi et al., 2016) (**Figure I-4**, left). Water from the primary circuit passes in the secondary circuit by large quantities transporting fission products along. The steam generator is rapidly filled with water, and droplets might be released due to boiling from the pool to the environment through vents. Therefore, the quantification of these droplet is necessary from the design point of view (Berzal et al., 1995)(Bagul et al., 2018b)(Qiu et al., 2015).

In BWR severe accident, after the core damage, a mixture of steam/non-condensable gases and FPs is transported via pipe into large water pool (**Figure I-4**, right). Some of the FP will become trapped in the water pool and some of them will be re-entrained by the streaming gas due to the continuous heat release or boiling. The consequence of the gas release into the containment building atmosphere, also caused by release of H_2 and CO from MCCI, could jeopardize the

containment integrity. Therefore, the building is depressurized using vents placed at a certain height above the water pool. The depressurization may induce boiling, and the rate of depressurization defines the hydrodynamic of the pool. High depressurization rates cause large agitation in water pool by producing large bubble (Kudo et al., 1994), whereas low depressurization rates engender small bubbles at the water surface (Freitag and Schmidt, 2017). In either case, the release of droplet from water pool as a function of the flow regime is inevitable. These droplets re-entrain contaminants (such as aerosol) and might contribute to their release to the environment.

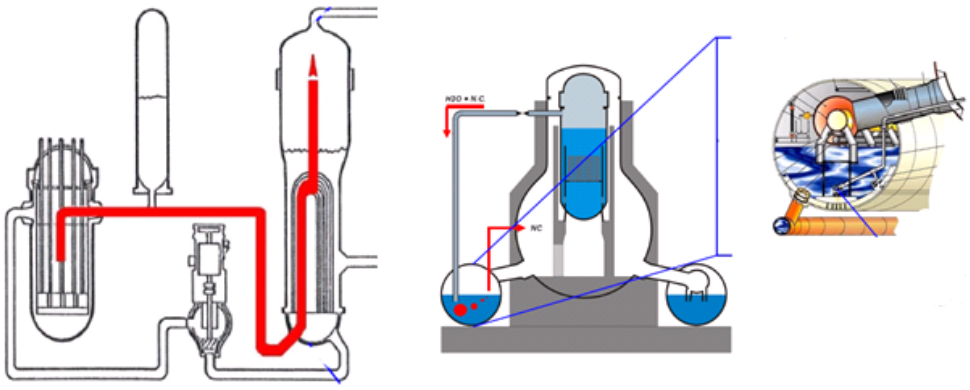

Figure I-4 *Accident scenario in PWR (left), accident scenario in BWR (right)*(Herranz, 2017)

The assessment of the entrainment phenomena is conducted by numerical simulation. CFD and LP codes are used for this purpose. CFD simulations require computational resources to simulate small droplets in the micron range and provide as well results on the characteristics of the droplets including their size and velocity distributions at different height above the water pool, in addition to their concentration. Nonetheless, this amount of information are time consuming to acquire. Whilst LP codes are characterized by short time execution and providing results in a couple of minutes due to their empirical aspect. LP code are popular in simulating severe accidents scenarios in power plants.

A. Work Objective

In the open literature, experiments conducted on entrainment in large pool and large vessel are limited to low superficial gas velocities (Dapper, 2009) (bubbly flow regime), and experiments conducted in small pools used high superficial gas velocities. In addition, entrainment models that could be found in literature have limited range of applicability in terms of the flow regime (high superficial gas velocity) and/or geometry. At the current knowledge, there is no model that englobes the full range of the boundary conditions (superficial gas velocity and geometry).

A prior understanding of the dynamics of the bubble is imperative, such as the effect of thermal hydraulics, physical properties of the liquid, bubble behaviour at the surface of the pool before and after the burst for simple cases such as the study of a single bubble to quantify the entrainment. Then, the information on the single bubble could be translated to bubble swarm by analysing the behaviour of the bubbles at the water surface under low (Günther et al., 2003)and high gas flow rates. The main objective of this PhD thesis is to quantify the entrainment as a function of the hydrodynamics of the pool (flow regimes) for different scenarios that implies different geometries by one correlation.

The outcome of this works might provide information for lumped parameter codes that could be used in nuclear applications.

B. Structure of thesis

This thesis is composed of five chapters:

Chapter II is devoted to a detailed re-entrainment literature survey, including experimental, empirical, and theoretical works.

Chapter III includes the analysis of re-entrainment phenomena using COCOSYS based on THAI experiments.

Chapter IV presents the empirical correlation development for bubbly flow, transition and churn turbulent flow regime.

Chapter V concludes the present work providing the main achievement, and possible future works and perspectives.

II. Literature review

In this chapter, an extensive literature review is presented. The first part is devoted to experimental work on entrainment. The second part presents the analytical work. The third part discusses the main finding of the review by providing factors that affect the entrainment phenomenon.

A. Experimental work

The phenomena of entrainment require the study of the geometry and the dynamics of the bubble in addition to the mechanisms affecting their ability to generate droplets. The study of bubble dynamics as a swarm arises from the study of single bubble. The outcome of single bubble analysis then could be correlated to swarm (Günther et al., 2003).

Poulain et al.(Poulain et al., 2018) investigated this phenomenon in detail for an air-water system. First, they examine the effect of temperature on the time required for a bubble before its burst or so-called "ageing", by producing discrete bubbles in a stainless steel tube from an air pump. They controlled the temperature (between 5° to 90° C) by putting coiled tubing connected to a recirculating water heating or cooling pump which is wrapped around the tube. As water temperature increases the bubble ageing time decreases due to the decrease of surface tension with increasing temperature.

Moreover, the effect of surfactants on the life time of the bubble was examined by Poulain et al. (Poulain et al., 2018). The diffusion of soluble surfactant blob of a specified size across the film of a certain thickness initiates the Marangoni effect, and a perturbation of that surfactant blob could rupture the cap if the size of the blob is twice as bigger as the cap thickness. The surfactant in a bubble cap of size d_b diffuses from one side of a film of thickness h_f to the other side over time $\tau_{diff}\ h_f^2/D$. The Schmidt number ($Sc = \nu/D$) has to be significantly small for bubble rupture to occur.

Zhang et al. (Zhang et al., 2012) considered a dimensionless approach to study the characteristics of droplets generated by bubble burst at a free surface for various liquids. They developed

correlations to predict the critical bubble size as a function of the physical properties of the liquid as equation II.*1*shows, and the number of produced jet droplets per bubble (equationII.*2*).

$$d_{b,crit} = 10^{0,1914}\sigma_l^{0,5517}\rho_l^{-0,4830}g^{-0,5170}\mu_l^{-0,0688} \quad \text{II.1}$$

$$N_{dr} = 7{,}9e^{\left(\frac{-d_b}{0{,}338d_{b,crit}}\right)} - 0{,}41 \quad \text{II.2}$$

From equation II.*2*, the number of the jet drops depends on Bond number square root $= \left(\frac{d_b}{d_{b,crit}}\right)^2$. For significantly large bubbles, practically no jet droplets are produced $d_b \rightarrow \infty;\ N_{dr} \rightarrow 0$, and the only drops that can be generated from such bubbles are from the thin film at the surface.

As equation *II.2* shows, the critical bubble size where no jet droplet is produced, depends on properties of the liquids. The critical bubble size is large for fluids with low density and low viscosity. When the bubble is resting on the liquid surface, it is submitted to two forces: surface and centripetal forces, assuming no interactions with its surroundings. The bubble will burst under the condition (Donald E. Spiel, 1998);

$$\frac{M_1 S_f^2}{R_0} > 2\sigma$$

Therefore, the critical bubble size, in equation II.*1* increases when surface tension increases. This equation resulted from a dimensionless and regression analysis, considering a combination of the Froude, Reynolds and Weber numbers and plot it against Morton number. The combination of Re, Fr and We were made in order to cancel the velocity term, so it eventually yields the critical bubble size.

The experiment of Zhang (Zhang et al., 2012) is relevant to quantify the droplet entrainment for pure and contaminated water. As demonstrated, high fluid viscosity, produce fewer droplets. Toba (Toba, 1959) and Spiel (Donald E Spiel, 1998) used sea water to investigate the number of

droplets, under T=10°C and T=28°C respectively. More droplets was produced under Spiel condition (Donald E Spiel, 1998) than Toba's (Toba, 1959). Concluding that droplets production increase with decreasing temperature accordingly. Since, the decrease in temperature engender an increase of surface tension, which increase the ageing of the bubble (Poulain et al., 2018). That leaves enough time for the film cap to drain, eventually the bubble produce more droplet, unless the bubble size exceed the critical size, then the bubble burst under the condition of instability.

The drops generated by bubble whether from film or from jet contribute to the entrainment taking into account the bubble size and flow regimes, hence interaction between bubbles.

Such droplet might be entrained by the streaming gas to different location above the water pool. Kataoka and Ishii (Kataoka and Mamoru, 1983), subdivided these location into three regions: 1) near the surface where the entrained droplets consist of all sizes, 2) the momentum controlled region which is considered as a transition region where droplets are either carried over or fall back, and 3) the deposition controlled region where droplets are small enough to be carried over and suspended, unless deposited onto wall. **Figure II-1** illustrate these three regions. Some authors conducted experiment to quantify the entrainment of droplet in the momentum controlled regions (Kim and No, 2003)(Lebel et al., 2020)(Garner et al., 1954), and others conducted experiment to measure the entrainment in the deposition controlled region (Freitag and Schmidt, 2017)(Cosandey, 1999)(Müller and von Rohr, 1997). The near surface region is a challenging zone to measure the entrainment due to high water surface agitation from multiple bubble burst. However, since the entrainment consists of all droplet at the near surface region, Kataoka and Ishii (Kataoka and Mamoru, 1983), stated that the droplets mass flux is 4 times larger than the gas mass flux. This value is validated by previous authors as well (Bagul et al., 2019)(Kim and No, 2003).

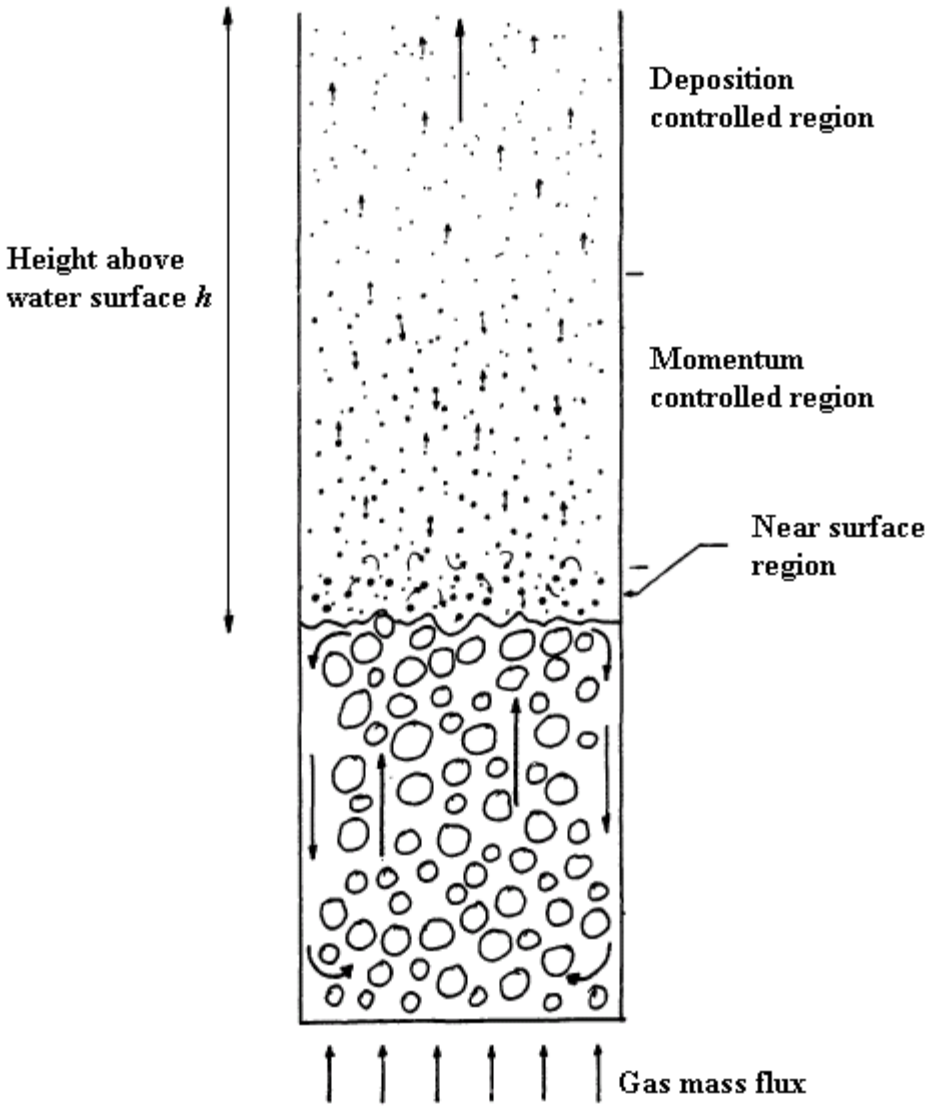

Figure II-1 *Entrainment of droplet at different regions above the water pool (adapted from* (Santiago, 1991)*)*

Experiments on water entrainment could be conducted in large and small vessel. As for large vessel, it could be attributed to containment buildings (Freitag and Schmidt, 2017; Fritz, 2006; Kudo et al., 1994), (where entrainment is measured in the deposition controlled region) while small vessel corresponds to scenarios such as SGTR, SBLOCA(Kim and No, 2003) (where entrainment is measured in the momentum controlled region).

Kim and No (Kim and No, 2003),(Kim, Hyun and No, Cheon, 2005) conducted experiments on pool entrainment to simulate the depressurization system of Advanced Power Reactor 1400 in the case of TLOFW. The facility consisted of a pool and a break at the top to measure the amount of water droplets. Kim and No's data (**Figure II-2**) were compared against previous work of Sterman (Rozen et al., 1970), Golub (Sterman, 1958) and Styrikovich (Styrikovich et al., 1964). As could be seen in **Figure II-2**, initially, Sterman used the same height as Kim and No (Kim and No, 2005), that explains the agreement at the beginning. Despite the use of higher superficial gas velocity in the experiment of Sterman (Sterman et al., 1957), the entrainment is lower than the entrainment measured by Kim and No. The possible reason is related to thermal-hydraulics conditions. Kim and No conducted their experiment under atmospheric conditions, while Sterman et al. conducted their experiments with a pressure of 185 bar. Further discussion about this effect is given at the end of this chapter. Same explanation is applied to Styrikovich (Styrikovich et al., 1964)who conducted a his experiment under a pressure of 36 bar. As for Garner (Garner et al., 1954) and Golub (Golub et al., 1980), even for the use of higher superficial gas velocities, they calculated lower value of entrainment. This is due to the use of higher distance above the water pool. Furthermore, the entrainment decrease with increasing the location of the measurement point above the water pool (height above the water pool).

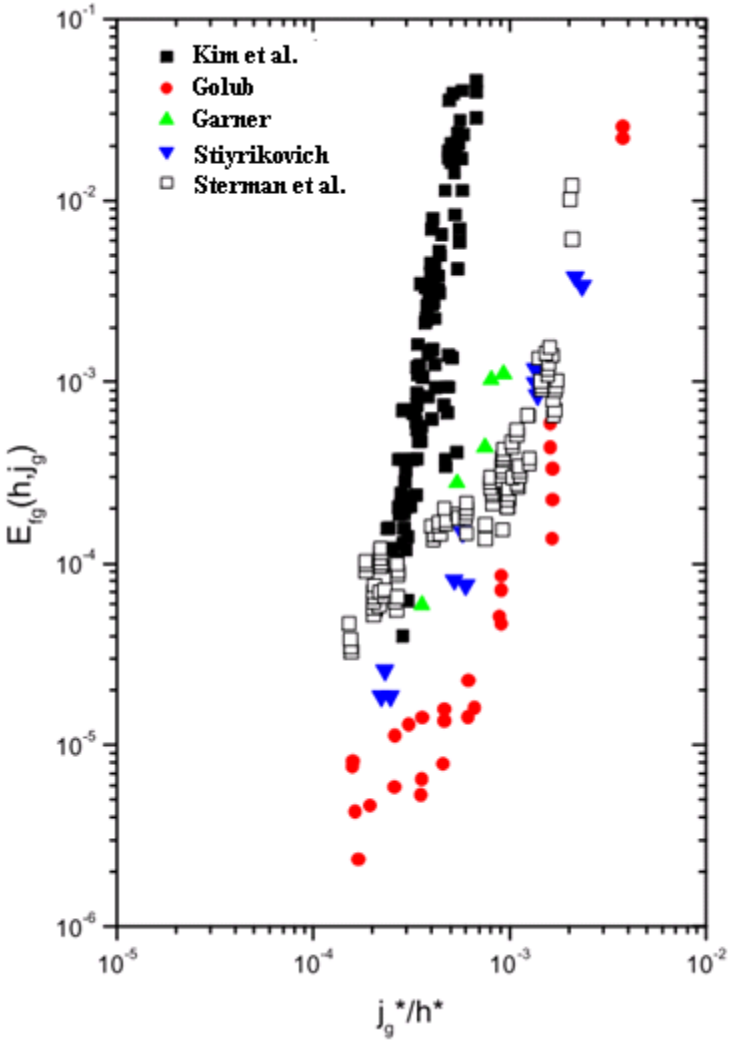

Figure II-2 *Comparison of the experiment of Kim* (Kim, Hyun and No, Cheon, 2005) *and experimental data*

Kim and No (Kim and No, 2005) adapted the Kataoka's model to their experimental data in order to ascertain a correlation, which depends on superficial velocity to 7th power, as could be seen in equation *II.3*. That is due to substantial momentum in the top break – as shown in **Figure II-3**– with the entrainment in that case being a strong function of the ratio of the break diameter to the distance between the water surface and the break, along with the gas superficial velocity.

$$E_{fg} = 7{,}706.10^{20} j_g^7 h^{-7} \qquad \text{II.3}$$

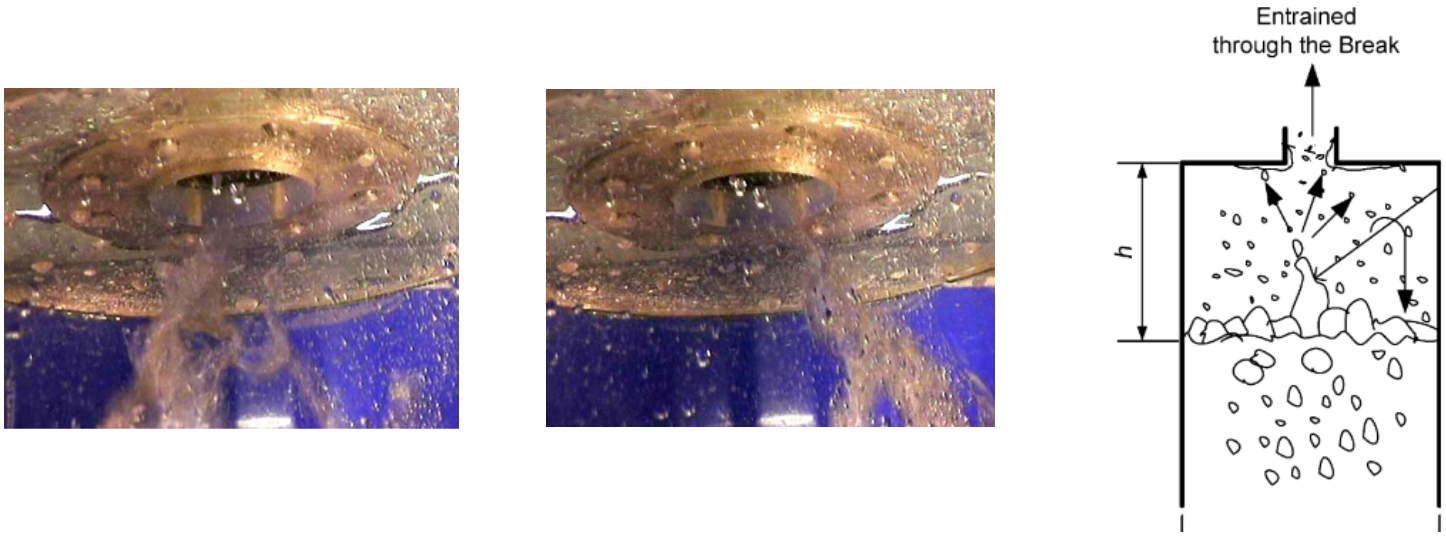

Figure II-3*Entrainment of water droplet through the break* (Kim, Hyun and No, Cheon, 2005)

Bagul (Bagul et al., 2018a) simulated experimentally the AHWR heat transport to drums, where steam is transported and condensed in the scaled down, Air Water Loop AWL facility. The entrainment was measured near the surface, close to the drum exit. This could be equivalent to the pool entrainment near the surface and in the momentum-controlled region. This is due to the swell level of the two-phase mixture, which limits the gas space above the water pool. Bagul's experimental results successfully validated the previous mechanistic models and correlations of entrainment for high swell level and high gas flow rates. This later has to be high enough to capture large amount of droplets. Since some droplets will be deposited at the exit walls or even fall back, it could be approximated to Kataoka's statement that entrainment at near surface consisted of all droplets, and that the mass flow rate of the entrained liquid is 4 times the gas flow rate (Kataoka and Mamoru, 1983) (**Figure II-4**).

The entrainment recorded by Bagul is from 0.3 to 4. The Kataoka's correlation plotted in **Figure II-4** at swell level 1.8m indicates the momentum controlled region from low gas flow rate to high gas flow rates, and the line where it shows a constant entrainment value (approximately 4) and a swell level between 1.8 m and 1.95 m, corresponds to the near surface region. The data of Bagul agree with Kataoka's correlation for momentum-controlled region at high gas flow rates and near

surface. This is evident, since the swell level increases with increasing gas flow rate to reach the drum exit, eventually allowing more droplet to pass through.

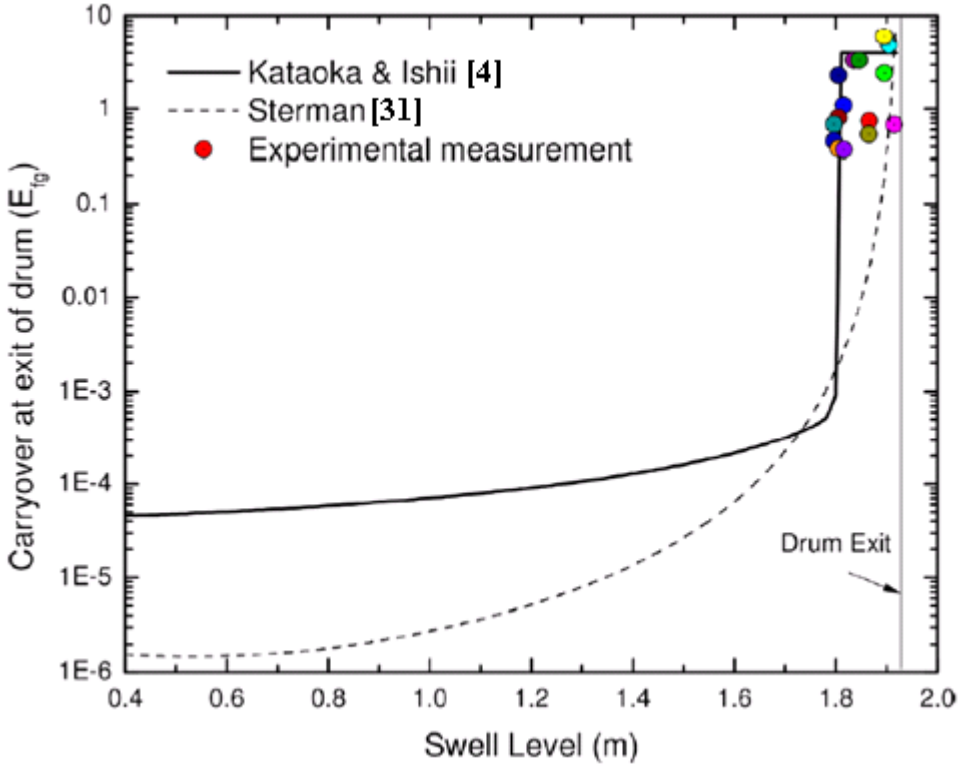

Figure II-4 *Comparison of entrainment measurement and correlations* (Bagul et al., 2018a)

The experiments of Kim (Kim and No, 2003) (discharge pipe *50 mm, 5 mm* -holes injection) and Bagul (Bagul et al., 2018a) (Drum exit *102.26 mm*) are similar as regards the entrainment mechanisms, however there are still some differences in the boundary conditions, as could be seen in the **Table II-1** below.

Table II-1 *Comparison of Bagul's and Kim's experiments*

	Bagul experiments	**Kim experiments**
Superficial gas velocity [m/s]	0.277	0.35
Two phase flow level [m]	1.798 – 1.915	1.0 – 1.9
Entrainment [-]	0.371 to 4.900	1E-2to 1E-1
System	Air – water	Air – water
Temperature [°C]	Atmospheric	Atmospheric
Pressure [bar]	Atmospheric	Atmospheric

In the experiment of Kim and No (Kim and No, 2003) high air flow rate was used, and the distance from the swell level to the break was from 0.4 m to 0.1 m. While in Bagul's it was no less than 0.015 m, which is very close to the exit, allowing more droplets to be entrained. Even so, Bagul's experiments showed higher values of liquid entrainment than those of Kim's. That could be explained as follows: the height above the pool for Kim is much higher than in the Bagul's experiment, even if Kim (Kim and No, 2005) used higher superficial gas velocity, the Bernoulli Effect is more significant in Bagul experiments.

The height above the water pool was calculated by Sterman (Sterman, 1957) via an equation he developed for the volume gas fraction above the two-phase flow mixture during bubbling (swell level)(equation *II.4*):

$$\alpha = 0.26\left(\frac{j_g^2}{g\sqrt{\frac{\sigma}{g\Delta\rho}}}\right)^{0.4}\left(\frac{\rho_g}{\Delta\rho}\right)^{0.12} \qquad \text{II.4}$$

$$h = h_i - \frac{h_l \alpha}{1 - \alpha} \qquad \text{II.5}$$

Table II-2 *The effect of the height of the vapour space in a bubbling pool and superficial gas velocity on entrainment*

	$j_g(m/s)$	$h_{fg}(m)$	$h(m)$	E_{fg}
Bagul et al. (Bagul et al., 2018a) $P = 1atm$	0.099 – 0.277	1.798 – 1.915	0.122 - 0	0.371 – 4.900
Kim and No (Kim and No, 2003) $P = 1atm$	0.09 – 0.33	1.0 – 1.9	1.0 - 0.1	1E-2 - 1E-1
Sterman (Sterman et al., 1957) $P = 151atm$ $P = 185atm$	0.166 0.075	0.2537 0.244	0.5663 0.4060	0.12 6E-2
Styrikovich (Styrikovich et al., 1955) $P = 36atm$ $P = 91atm$	0.524 – 0.535 0.260 – 0.266	0.3668 0.2819	0.4782 0.5631	0.1 4E-2

The value of h could also be validated experimentally from equation II.*4* and II.*5*.

Table II-2 shows a comparison between Kim (Kim and No, 2003), Bagul et al. (Bagul et al., 2018a), Sterman (Sterman et al., 1957) and Styrikovich (Styrikovich et al., 1955) data on water carry-over. First, the criterion to compare these results is that the condition $Bo \leq 260 \left(\frac{\rho_g}{\Delta\rho}\right)^{-0.2}$ has to be

fulfilled. From **Table II-2**, as the superficial gas velocity increases, the height above the two-phase flow level decreases, therefore the entrainment increases.

De Santiago (Santiago and Marvillet, 1991) in the frame of PhD work, also investigated experimentally the phenomenon of the pool entrainment, with an emphasis on the droplet size and velocity distribution. The performed study focused on the droplet entrainment at different height above the water pool for superficial gas velocities in the range [0.13 m/s – 0.4 m/s]. It was found that the gas velocity have a clear impact of the droplet size distribution in the deposition controlled region. In this region, the droplet are whether entrained or deposited due to turbulent diffusion as the height above the water pool increases.

Kudo (Kudo et al., 1994) experimentally investigated the entrainment phenomenon from flashing pool in the frame of the ALPHA program in a BWR Mark 1 containment facility in order to quantify the re-entrained aerosol from a contaminated pool.

The facility was a model containment vessel with 3.9 m of inner diameter and 5.7 m of height, and a volume of 50 m^3. Inside the vessel was placed a 2 m deep steel water pool. For the depressurization, a discharged pipe equipped with a valve was used and a condensation tank that connect the containment vessel by the pipe. The opening or the breach area of the containment during the flashing was simulated by scaling the containment volume and the containment breach size.

Two experiments were conducted and the differences between them is the water mass in the pool and the mass of dissolved sodium sulfate.

Three samplings were taken, and as a result, the size distribution of the airborne aerosols was surprisingly bimodal (two peaks) for some samplings (figure 6 of (Kudo et al., 1994)). Kudo stated that the reason is not clear and the generated droplet mechanisms might be one of the explanations, which is a consequence of the rate of the depressurization and the position of the vent. Another explanation could be related to the instrumentation used for entrainment measurement. Kudo used a cascade impactor to measure the particle size distribution, which traps particle from larger to smaller ones in collection plates. The problem encountered might be related to some particles deposition in the collection plates. In both experiments, the superficial gas velocity was below 0.04

m/s. Mass entrainment from the pool at the surface measured does not agree with Kataoka and Ishii's correlation. Kataoka and Ishii(Kataoka and Ishii, 1984) assumed that the pool bubbles in a uniform fashion. The scenarios under which the pool could bubble in a uniform fashion are the flashing pool under low depressurization rates (which is enough to generate bubbles across the entire pool surface,) as investigated by (Cosandey, 1999) and (Freitag and Schmidt, 2017) or a well distributed quencher in such way to make the entire pool bubbling (Schmidt et al., 2015).

Kudo's experiments show an increase of superficial gas velocity near the walls, and a decrease towards the centre of the pool. The flow regimes in the pool that was observed are churn turbulent flow is near the walls and bubbly flow is in the centre. That might explain the discrepancy between the measured entrainment and Kataoka and Ishii's (Kataoka and Mamoru, 1983)correlation. The experiments of Kudo is of extreme relevance, as it showed a coexistence of two flow regime at the same time, unfortunately a full set of data is not available in the open literature.

Aerosol re-entrainment by droplets was extended to a non-Newtonian fluid/gas system. The complexity of treating non-Newtonian fluid lies in the physical properties of the liquid, and more precisely, the viscosity. This latter is no longer assumed constant, but is a function of the shear stress. The behaviour of the fluid depends on the shear stress, and it has a threshold value where the non-Newtonian fluid behaves like a Newtonian fluid. Fritz (Fritz, 2006), simulated the radioactive wastes from the Hanford site in Washington that are stored in underground tanks. The experiment was conducted in a half-scaled tank filled with a waste simulant processing Bingham plastic rheological properties **Figure II-5** which is similar to the expected properties of the nuclear waste. The simulant consisted of a mixture of 80% kaolin clay and 20% bentonite clay mixed with water. Filtered air was used as injected gas via 9 spargers under different flow rates. The entrainment was measured in three different heights above the liquid surface(Kataoka and Ishii, 1984). The expected flow in the experiment of Fritz in bubbly flow, and the measured entrainment was compared with the Rozen correlation (Rozen et al., 1976a) and Kataoka and Ishii's correlation (Kataoka and Ishii, 1984). Fritz adapted the Kataoka and Ishii's correlation for the deposition region to the bubbly flow regime, by reducing the exponent of the superficial gas velocity from 3 to 1, as can be seen in equation II.*6*.

$$E_{fg}(h, j_g) = 7{,}13.\,10^{-4}(0{,}025)\,j_g^{*}N_{\mu g}^{0.5}\left(\frac{\rho_g}{\Delta\rho}\right)^{-1} e\left(-0{,}205\left(\frac{h}{D_H}\right)\right) \qquad \text{II.6}$$

As for the Rozen's formula, the entrainment agrees with experimental data for the momentum controlled and deposition regions (**Figure II-6**). Rozen's correlation is as accurate as the modified Kataoka and Ishii's correlation by Fritz (equation II.*6*). As reported by Fritz (Fritz, 2006), the lack of efficiency of the aerosol samplers resulted in a disagreement with the Kataoka and Ishii correlation for the momentum controlled region. At the experimental condition, the fluid at such low superficial gas velocities behave as a Newtonian fluid. The entrainment of droplets in non-Newtonian fluid system cannot be applied to high superficial gas velocity for the behaviour of the viscosity (the resistance to the gas motion).

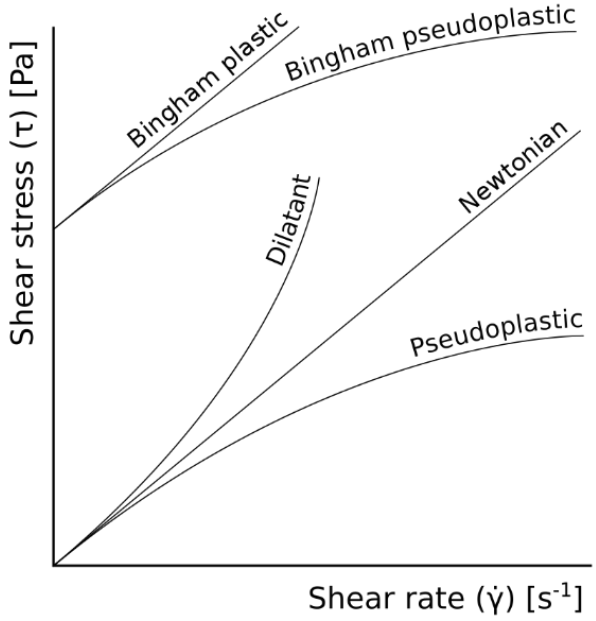

Figure II-5 *Classification of fluids with shear stress*

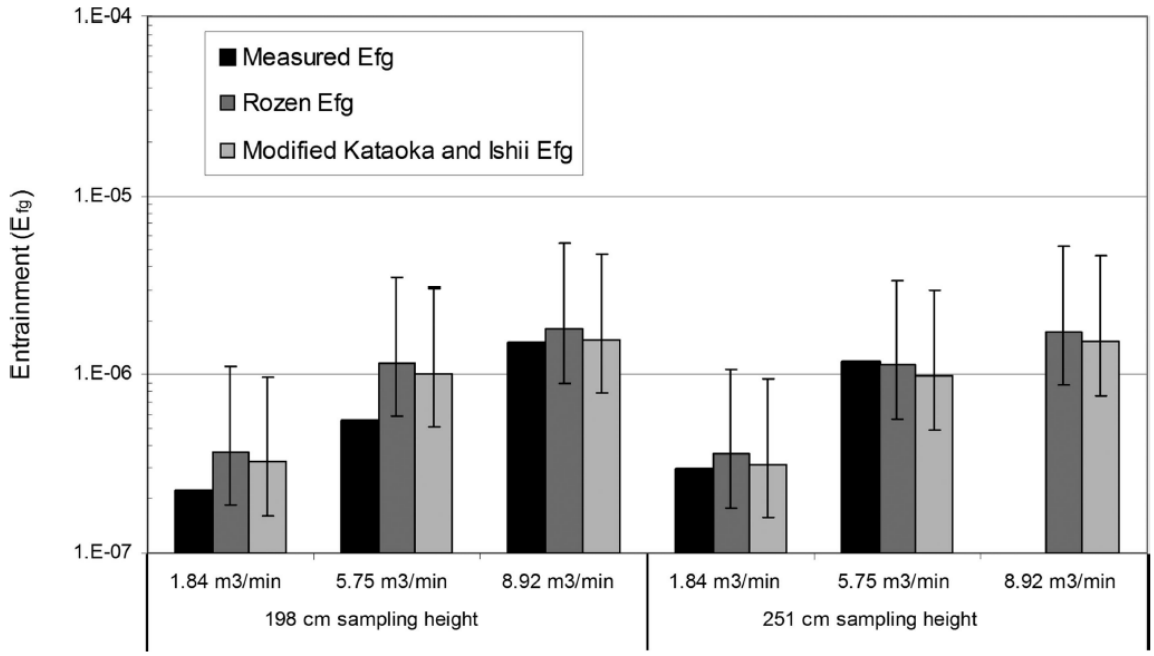

Figure II-6 *Comparison of measured entrainment and modified Kataoka and Ishii correlation* (Fritz, 2006) *and Rozen correlation* (Rozen et al., 1976a) *in the deposition controlled region under a bubbly flow regime.*

The modified Kataoka and Ishii correlation by Fritz (Fritz, 2006), the Rozen (Rozen et al., 1970) correlation and the measured entrainment show no dependence on sampling height above the water pool in the deposition-controlled region. This non dependence effect was also observed in previous THAI experiments(Schmidt et al., 2015) (TH25), as shown in **Figure II-7**. This figure reads the entrainment as a function of the gas flow rates at locations 6.5 m and 7.7 m respectively. The entrainment measured at h=6.5 m is similar to the entrainment measured at location h=7.7 m. The zone is considered uniformly distributed; therefore, the entrainment is the same at every point in the deposition-controlled region for a given superficial gas velocity.

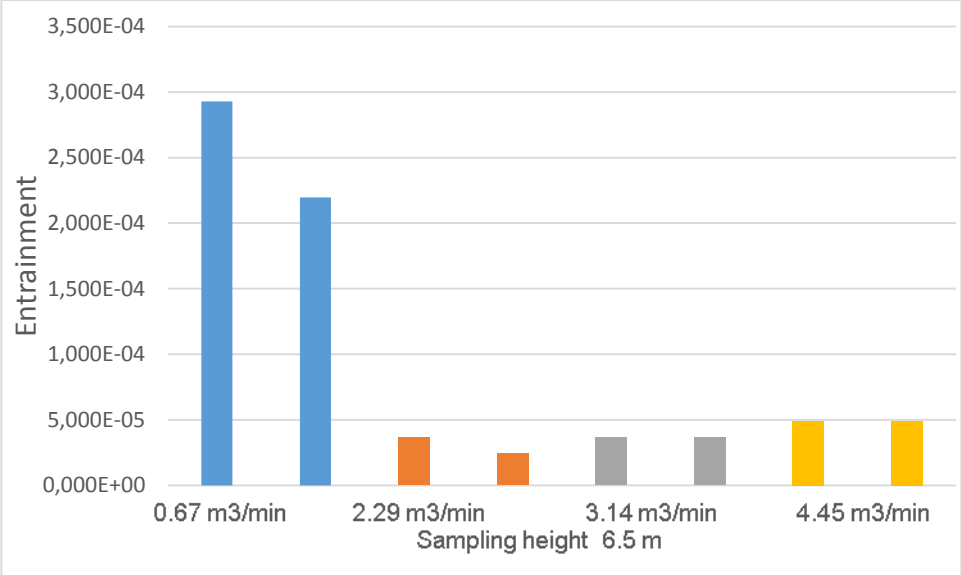

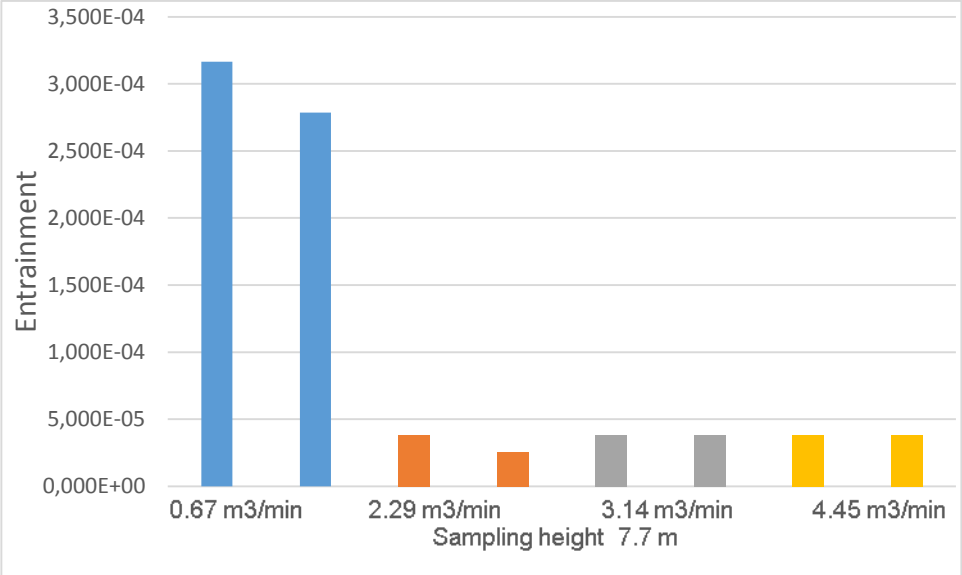

Figure II-7 *Entrainment measured in TH25 THAI experiment*

B. Analytical work

Beginning with the bubbly flow regime, the bubble shapes range from spherical over elliptic to spherical cap (Clift et al., 1978). The bubble trajectory from the injection to the water surface is not a straight motion: the gas flow rate, the buoyancy force, and the interaction between bubbles

yield a zig zag motion until they reach the water surface (Özdemir, 2005). When reaching the surface, the bubbles form a cap, or remain spherical in shape depending on their sizes (Toba, 1959), (Lhuissier and Villermaux, 2012). The capillary length *a* which is the maximum stable bubble size of the critical bubble size, indicates at which scale the gravitational and the surface forces are in balance (Poulain et al., 2018). It is an important magnitude when analysing the bubble burst at the water surface, however bubbles have multiple size and therefore multiple shape. The bubble static stability then is achieved by analysing the bubble Bond number equation *II.7*.

$$Bo_{bub} = \frac{d_b g\, \rho_g}{\sigma}\left(\frac{\Delta\rho}{\rho_g}\right) = \left(\frac{d_b}{a}\right)^2 \qquad \text{II.7}$$

Surface tension produces the centripetal force on the bubble lamellae sitting on the water surface. It is counteracted by the bubbles' internal overpressure. The bubble is submitted to two forces done by the bubble, and one force is due to the pressure of the surrounding.

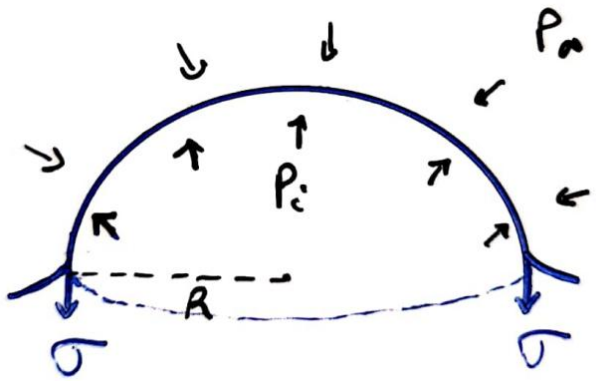

Figure II-8 Force acting on a bubble at water surface

The figure above (Figure II-8) shows the forces acting on a bubble sitting on the water surface. The force balance yields: force due to internal pressure ($P_i R\pi^2$) = force due to surface tension ($2\sigma R\pi$) + force due to pressure surrounding ($P_\infty R\pi^2$). This yields what is known as, the Young – Laplace equation $P_i - P_\infty = 2\sigma/R$. The pressure of the surrounding is the pressure of the system, while the pressure inside the bubble depends on its size. The bubble loses its integrity when the pressure inside the bubble and that of the surrounding are balanced.

The bursting process is also initiated by local thinning of the lamellae (which is more likely occur at the bubble foot) and hydrodynamic instability (Rayleigh–Taylor instability). Two families of drops are generated from the burst; film droplets produced from the bubble cap, and jet droplets, which are eventual consequence of film drops. The jet droplets are produced from the agitation of the water liquid inside the bubble after the burst, caused by the bubble pressure, and the drained film cap into the water bulk.

After the burst, the film (that produces film droplets) depart with a certain velocity. This velocity depends on the bubble size (Donald E Spiel, 1998) and how soon it burst (Poulain et al., 2018). The disintegration of the film into droplet could be achieved by analysing the Weber number ($We_{film} = \frac{\rho S_f^2 l_{film}}{\sigma}$) on how stable the film is and its ability to produce droplets.

The mechanisms of droplet generation (c, d and e of **Figure I-1**) are mostly encountered in pools. In a vessel filled with water, the bubbles are produced either by boiling due to continuous heat release or depressurization. The swell level of the pool surface depends on the gas injection patterns and pool dimensions.

The cumulative water droplets generated from the bursting bubbles at the water pool surface are ejected with different sizes and velocities in a parabolic movement like a projectile. Spiel (Donald E Spiel, 1998) investigated the angle of ejection of film droplets burst at the centre, and found that the angles do not depend on the bubble size. Against the gas velocity, the droplets might settle down, or be carried over by the streaming gas to eventually stay airborne at specific heights. In Stokes flow regime, the terminal velocity, which is the maximum velocity reached by the droplet as it falls back in the vertical direction, of the droplets larger than the superficial gas velocity results in settling down. With terminal velocity smaller than the superficial gas velocity, the droplets continue to rise to the top vessel to stay volatile unless they deposit onto vessel structure or walls. These droplets constitute the entrainment. Sterman and Antonov (Sterman et al., 1957) summarize the dependence of entrainment on superficial gas velocity and height above the water surface for small values of Bond number (small vessel) and heights above the water surface as shown in **Figure II-9** and **Table II-3**.

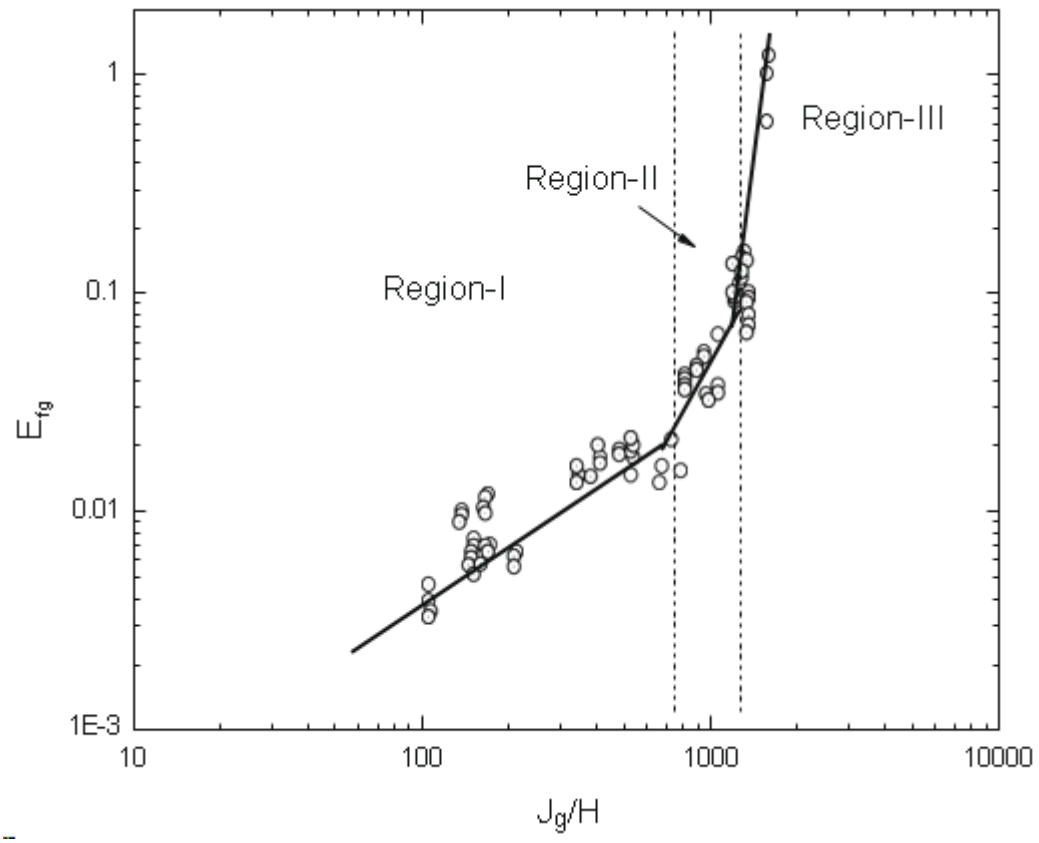

Figure II-9 *Entrainment as a function of superficial gas velocity and height above the water surface* (Sterman et al., 1957)

Table II-3*Superficial gas velocity exponent with respect to zone above the water pool* (Sterman et al., 1957)

Zone	I (near surface)	II (momentum controlled)	III (deposition)
n	0 → 1	3 → 4	7 → 20
Condition for water droplet volatility	$v_t > j_g$	$v_t \leq j_g$	$v_t < j_g$

The entrainment is defined as the ratio of the droplets mass flow rate to the gas mass flow rate regardless the zone showed in **Table II-4.**

$$E_{fg} = \frac{\dot{m}_l}{\dot{m}_g} \qquad \text{II.8}$$

There have been several attempts to predicted the entrainment by either theoretical, semi-empirical or even purely empirical approaches. Zenz and Weil (Zenz and Weil, 1958) developed a theoretical approach to quantify the entrainment of solid particle by a gas phase. Gordon and Zuber (Yeh and Zuber, 1960) adapt Zenz and Weil approach to calculate the entrainment for a liquid-gas system through drop dynamics above the liquid surface as a function of the initial drop velocity $u_i{}'$ and the physical properties of the liquid and gas. However, a number of considerations were assumed to quantify the entrainment numerically; first, the droplets sizes are log-normally distributed. The physical properties of the operating system air-water are constant and the initial droplet velocity is known. Davis (Davis, 1940) calculated this velocity assuming movement of a projectile, by balancing initial droplet kinetic energy and terminal potential energy, which yields $u_i' = \sqrt{2gh_m} = 140\,cm/s$. The droplets are separated by the gas stream and carried away if the terminal velocity $v_t > 0$, or return back to the liquid surface if$v_t < 0$. The droplet velocity can be calculated as a function of time from equation II.*9*(Zenz and Weil, 1958)(Yeh and Zuber, 1960).

$$u' = v_t\left(1 - e^{\frac{-18\mu_g t}{\rho_l d_{dr}^2}}\right) + u_i' e^{\frac{-18\mu_g t}{\rho_l d_{dr}^2}} \qquad \text{II.9}$$

At $t = 0$ the droplet has an initial velocity ($u' = u_i'$), then depending on its size, the droplet reach a terminal velocity ($u' = v_t$).

The height of rising droplets as a function of time can be calculated by equation II.*10*.

$$h = u_t' t - (u_t' - u_i')\frac{\rho_l d^2}{18\mu_g}\left(1 - e^{\frac{-18\mu_g t}{\rho_l d^2}}\right) \qquad \text{II.10}$$

Finally, the entrainment of the droplets carried away is calculated. The numerical scheme proposed by the Zenz and Weil (Zenz and Weil, 1958) requires knowledge of the number of droplets produced by bubble size and u_i' or j_g, which are already available from experimental works of

Zhang et al (Zhang et al., 2012), Koch et al. (Koch et al., 2000) and Ramirez (Santiago and Marvillet, 1991).

Gordon and Zuber (Yeh and Zuber, 1960) modified the work of Andrews (Andrews, 1960) on entrainment of fluidized solids to calculate the entrainment rate of droplets. Initially, Andrews assumed that the entrained droplets need a sufficient amount of kinetic energy to detach. Gordon and Zuber added the following: a steady state must be maintained. The total energy of droplets remains constant. The number of particles must remain unchanged. All these assumptions match those of the kinetic theory, therefore, Andrews assumed that the energy distribution of droplets at the interface follows the Maxwell Boltzmann distribution $f_i = \beta e^{-\beta \epsilon_i}$.

The entrainment rate of droplets (equation II.*12*) is obtained considering the inventory of droplets in the vessel (equation II.*11*) with kinetic energy $\epsilon_i = \frac{m u_i^2}{2}$.

The initial velocity is obtained from the energy balance between the kinetic energy that a droplet need to be entrained at a maximum height and its potential energy $u_i' = \sqrt{2gh_m}$.

$$\frac{dE_{fg}}{dt} = \frac{-A\rho_l u_i'}{6} f_i \qquad \text{II.11}$$

whence

$$E_{fg} = \frac{1}{2\beta mg}\sqrt{\frac{\pi}{\beta mg}}\left[1 - \Phi\sqrt{\beta mgh}\right] + \frac{\sqrt{h}e^{-\beta mgh}}{\beta mg} \qquad \text{II.12}$$

The entrainment rate developed by Andrews (Andrews, 1960) and modified by Zuber (Yeh and Zuber, 1960) does not depend on the superficial gas velocity, it only gives information about the droplets' velocity distribution. Regardless the pool size, the gas velocity changes the droplet size distribution, therefore, the entrainment rate as stated by Zuber (Yeh and Zuber, 1960).

However, the formulation of Andrews (Andrews, 1960) is evaluated considering that the droplets velocity distribution follows the Boltzmann-Maxwell distribution, therefore at steady-state conditions. It is not the case in a containment building. The thermal hydraulics condition change

continuously due to gas release to the containment atmosphere, and more in case of depressurization.

Kruzhilin (Kruzhilin, 1951) adopted a semi-empirical method to determine the entrainment, assuming that the contribution of the film droplets produced by the disintegration of the bubble cap is neglected. The droplets that contribute to the entrainment are those carried away by sufficient gas kinetic energy, and interaction between droplets is neglected. The amount of entrained droplets depends upon the kinetic energy of the gas and physical properties of the liquid. Based on a dimensional analysis, Kruzhilin (Kruzhilin, 1951) obtained the following:

$$E_{fg} = C_K \frac{\rho_g j_g^4}{\sigma g} \sqrt{\frac{\rho_g}{\rho_l}} \qquad \text{II.13}$$

C_K is determined experimentally.

The effect of height is not considered in the formulation of Kruzhilin (Kruzhilin, 1951), thus, his model is suitable to calculate the entrainment near the water surface. The correlation of Kruzhilin is limited, for the reason that the entrainment depend only of jet drops. Moreover, the superficial gas velocity in equation II.*13* is power 4, which means at such superficial gas velocity, the only droplet that can be generated are from the liquid ligaments. Thus, neglecting the film droplets in Kruzhilin's assumptions, is consistent with equation II.*13*. Moreover, the omission of the droplets interaction might also have a noticeable impact on entrainment, since the outcome of such interactions might be coalescence or breakup. The void fraction increase with increasing gas velocity, therefore formation of large bubbles. It exists an upper limit for a bubble size to produce jet and film droplets(Santiago and Marvillet, 1991)(Poulain et al., 2018)(Zhang et al., 2012). That makes the equation II.*13* limited in application, however, it gave an insight for later entrainment prediction.

Panasenko and Antonov (Panasenko and Antonov, 1959), later on, decided that the formulation of Kruzhilin (Kruzhilin, 1951) needed to be evaluated and adapt it to their considerations. This implies introducing the height of the vapour space above the water surface. Kruzhilin's (Kruzhilin,

1951) correlation is suitable for the second region, while the Panasenko and Antonov correlation is evaluated for the transition point (**Figure II-9**).

$$E_{fg} = 1.96 * 10^{7} \frac{\left(\rho_g g\right)^{0.48} \mu_l^{1.8} j_g^{1.96}}{g^{0.08} (\rho_l g)^{1.03} \sigma^{1.25} h^{1.18}} \qquad \text{II.14}$$

Equation II.*14* was correlated with experimental data of Sterman(Sterman et al., 1957), (Sterman et al., 1958) and Styrikovich et al. (Styrikovich et al., 1955)[1].

Sterman (Sterman, 1958) studied the effect of pressure on pool entrainment based on dimensional analysis in churn turbulent flow regime for pressure up to 185 bar. The equation II.*15* is based on previous experiments (Sterman et al., 1957)(Styrikovich et al., 1955)(Sterman et al., 1958)(Sterman, 1952) and (Kolokoltzev, 1952).

$$E_{fg} = 6{,}1.10^{9} \frac{\left(\frac{j_g^2}{gh}\right)^{1.38} \left(\frac{a}{h}\right)^{0.92}}{\left(\frac{g a^3}{\nu_l^2}\right)^{1.1} \left(\frac{\Delta\rho}{\rho_g}\right)^{1.124}} \qquad \text{II.15}$$

$$a = \left(\frac{\sigma}{g\Delta\rho}\right)^{0.5}$$

The parameter h in equations II.*14* and II.*15* is the height above the water surface. This height decreases with increasing gas flow rate. Sterman (Sterman, 1958) in his correlation adopted a formulation for gas volume fraction which depends upon superficial gas velocity (Sterman, 1957).

$$\alpha = 0.26 \left(\frac{j_g^2}{g\sqrt{\frac{\sigma}{g\Delta\rho}}} \right)^{0.4} \left(\frac{\rho_g}{\Delta\rho}\right)^{0.12} \qquad \text{II.16}$$

[1] These data are found in the Appendix of Yeh and Zuber work (Yeh and Zuber, 1960).

Under the condition:

$$Bo \leq 260\left(\frac{\rho_g}{\Delta\rho}\right)^{-0.2}$$

For an air-water system at Sterman's conditions (Sterman et al., 1957) (P=185 atm and vessel diameter d=0.255 m): $Bo = 287.25 < \left[260\left(\frac{\rho_g}{\Delta\rho}\right)^{-0.2} = 357.30\right]$

Golub (Rozen et al., 1970) considered a normal law to describe the droplet size distribution, and analyse the entrainment from the forces acting on a single droplet; weight, buoyancy and drag. Then, he validated the model against experimental data to find the following relationship (equation II.*17*):

$$E_{fg} = [A.K^{0,5} + B.K^{2,1}]\sqrt{\frac{\Delta\rho}{\rho_g}}e^{-0,23h/D_H} \qquad \text{II.17}$$

With

$$A = 9{,}011.10^{-5}\Delta\rho^{0,625}\rho_g^{-0.25}\sigma^{-0,375}g^{-0,25}$$

$$B = 0{,}753\Delta\rho^{1,025}\rho_g^{-0.5}\sigma^{-1,575}g^{-1,25}$$

$$K = d_{dr}j_g$$

From this equation, one might deduce that the entrainment is decreasing with increasing height above the water pool. Which make the Golub's formulation limited for very small droplets. The normal distribution considered in Golub (Golub, 1970) correlation might not be the adequate choice to describe the droplet size distribution, due to the fact that the independent variable in the normal distribution takes negative value by definition. Therefore, the droplet size could not take negative value, unless the phase of change is taken into account in the entrainment analysis where droplets evaporate. A possible choice might be a lognormal distribution instead of a Gaussian to describe the droplet size distribution.

Reed's Correlation (equation II.*18*) (Westgarth, 1964) is obtained from the paper of Paradissiadis and Widmer (Paradissiadis and Widmer, 1984). Unfortunately, the work of Reed could not be found in the open literature, nor a detailed description in the references where it was cited. However, the inclusion of the equation II.*18* might provide for the reader some insight for entrainment modelling.

$$E_{fg} = \frac{R}{1-R} \qquad \text{II.18}$$

With

$$R = 284\left(\frac{n_g 10^6}{\rho_g \Delta\rho}\right)^2 \left(\frac{j_g \rho_g}{3.23h^2 + 8.86h + 3.6}\right)$$

Azbel (Azbel, 1981) proposed an entrainment equation based on a stochastic approach by assuming the flowing: the velocities of droplets and their size at the interface of the pool are independent, and the distribution of droplet velocities and their size obey a Gaussian distribution.

$$E_{fg} = E_0\left(\frac{1}{\sqrt{2\pi}}\int_b^0 exp\left(\frac{-x^2}{2}\right)dx + \int_0^\infty exp\left(\frac{-x^2}{2}\right)dx\right) \qquad \text{II.19}$$

With $b = \frac{\sqrt{2gh}-V_0}{\sigma}$

The first integral term refers to the entrainment near the interface that corresponds to a specific height *h*, and the second integral term refers to the entrained droplet far from the surface, with velocity superior to the initial one at the time of the ejection. The equation II.*19* shows that with increasing height ***x***, the entrainment decreases. However, the Azbel model only indicates that the height above the water pool is important in entrainment modelling.

Kataoka and Ishii (Kataoka and Ishii, 1984) developed a set of correlations that includes three equations corresponding to three zones above the water pool, as shown in **Table II-3.**

The first zone and the second zone are controlled by the momentum of the droplets, and the third zone is controlled by the deposition.

These zones are determined by analysing the main parameters having notable effect on entrainment: superficial gas velocity and height above the water pool. Kataoka and Ishii's(Kataoka and Ishii, 1984) considerations on quantifying the entrainment are different from previous work (Sterman (Sterman, 1958), Panasenko and Antonov (Panasenko and Antonov, 1959), Styrikovich (Styrikovich et al., 1955) and Kruzhilin (Kruzhilin, 1951)). Assuming that the droplets travel in a vertical direction – from zone I to zone III – gives rise to another parameter affecting the entrainment, which is the height above the water surface. This parameter appear in previous correlation, however it has not been addressed explicitly. The height itself depends on the composition of the atmosphere and pool's thermal hydraulics(Cosandey, 1999).

The Kataoka and Ishii's (Kataoka and Ishii, 1984) correlations for different regions above the water pool from the surface to the uppermost part of the vessel are:

For the near surface region

$$E_{fg}(h, j_g) = 4{,}84.10^{-3}\left(\frac{\rho_g}{\Delta\rho}\right)^{-1{,}0} \quad \text{II.20}$$

Momentum controlled region

- Low gas flux

$$E_{fg}(h, j_g) = 2{,}213 N_{\mu g}^{1.5} D_H^{1{,}25} j_g^* h^{*-1}\left(\frac{\rho_g}{\Delta\rho}\right)^{-0{,}31} \quad \text{II.21}$$

- Intermediate gas flux

$$E_{fg}(h, j_g) = 5{,}417.10^{6} j_g^{3} h^{*-3} N_{\mu g}^{1.5} D_H^{1{,}25}\left(\frac{\rho_g}{\Delta\rho}\right)^{-0{,}31} \quad \text{II.22}$$

- High gas flux

$$E_{fg}(h, j_g) \propto \left(\frac{j_g^*}{h^*}\right)^{7\sim20} \quad \text{II.23}$$

Deposition controlled region

$$E_{fg}(h, j_g) = 7{,}13.10^{-4} j_g^{*3} N_{\mu g}^{0.5}\left(\frac{\rho_g}{\Delta\rho}\right)^{-1{,}0} e^{-0{,}205\left(\frac{h}{D_H}\right)} \quad \text{II.24}$$

Equations II.*20* through II.*24* was validated against data of Kolokoltsev (Styrikovich et al., 1964), Garner (Garner et al., 1954), Sterman et al. (Sterman et al., 1957)(Sterman, 1958), Styrikovich et al. (Styrikovich et al., 1964), Golub (Golub, 1970) and Rozen et al. (Rozen et al., 1976b).

The range of validity of the Kataoka and Ishii's (Kataoka and Ishii, 1984) for superficial gas velocity is $j_g \in$ [0.2 - 5] m/s, which correspond to churn turbulent flow regime.

Cosandey, (Cosandey, 1999)(Cosandey and Von Rohr, 2001) developed a correlation to quantify the re-entrained soluble and insoluble particle from droplets entrainment under very low gas flow rates as a consequence of vessel slow depressurization from 6 bar to 2 bar, using data from his own experiments. The correlation is based on the dimensional Buckingham theory, which leads to a group of dimensionless numbers.

$$E_{fg} = k_1 . x_{BP}^{k_2} We_{cont}^{k_3} Fr_{cont}^{k_4} (1 + Ra)^{k_5} \qquad \text{II.25}$$

The k_i, with $i = 1 \ldots 5$, are coefficients to be determined with experimental data (**Table II-5**).

Table II-5 *Coefficient k_i of the equation* II.25 *to predict the entrainment for soluble and solid particles*

	k_1	k_2	k_3	k_4	k_5
Soluble fission product	$2.954.10^{-9}$	0.3636	1.1968	-1.3057	-0.0216
Solid fission product	0.095	0.000	-0.0997	0.0153	0.0060

Cosandey's correlation indicated that the turbulent diffusivity is a relevant factor in analyzing the entrainment by considering the *Ra* number. However, this effect is manifested implicitly. To consider it explicitly, the concentration of the droplets needs to be established from the surface to the upper part of the vessel. Unfortunately, Cosandey did not measure this quantity.

Bagul (Bagul et al., 2018a) performed a CFD simulation to quantify the carryover through the exit of the steam drum using OpenFoam v2.3.1. Lagrangian method was used to track the droplet trajectories in the Eulerian phase (gas). The waving of the swell level (two-phase flow level) is expensive to simulate numerically, for this reason Bagul simulated only the gas space above the

water pool (Eulerian phase which is the distance between the swell level and the drum exit) by injecting droplets as Lagrangian discrete phase at different mass flow rates at the inlet. As the droplets are the main concern, the mesh was refined in the outlet zone and at the exit of the drum. It was found that, CFD simulation with high flow rates agrees with experimental data and Kataoka's model for low swell levels of up to 1.75 m. Beyond 1.8m, Kataoka's correlation is valid for the range of gas velocity as shown in **Figure II-10**. The results of Bagul experimental data (green triangles in **Figure II-10**) are far from being in agreement with CFD for gas flow rate of 3000 and 6000 litre per minute, and that might be due to the unrealistic conditions adopted during the simulation regarding the fixed swell level used instead of the oscillated one (realistic). In addition, the disagreement might be related to the initial conditions for droplet velocities, as this later is challenging to measure experimentally. Furthermore, the disagreement might be also due to the deposition of the droplet into the wall at the exit of the drum.

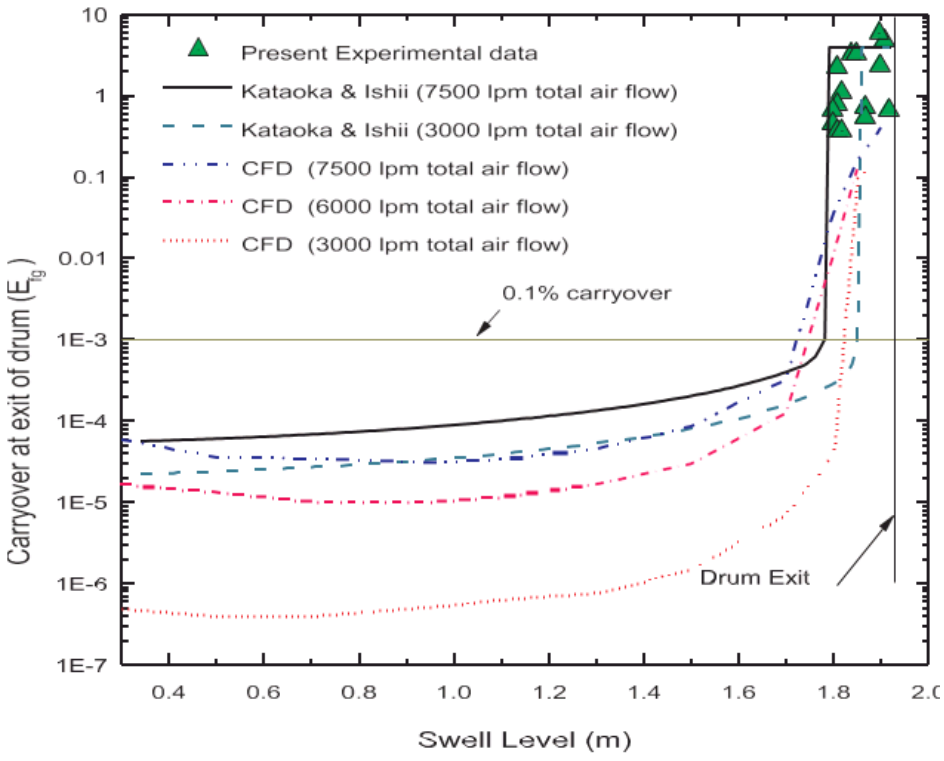

Figure II-10 *Comparison of prediction of carryover by E-L simulations, correlations and experimental data* (Bagul et al., 2018b).

Bagul et al. (Bagul et al., 2019) performed another numerical simulation of the carryover and the droplet motion above the water surface. A 1D code was used which adopts several assumptions applied to the droplets ejected from the water surface. These assumptions match those of the Stokes flow regime: 1) The droplets are perfect rigid spheres so the volume could be calculated easily, 2) it is a 1D code, which means the ejected droplets have one direction in which to travel: from normal to water surface, 3) droplets coalescence is not considered – because the superimposition of droplets will result in returning them to the water pool, 4) the evaporation of droplets is not considered (Kataoka, and Ishii also adopted the same assumption)), 5) droplets have the same size, and the gas has constant velocity.

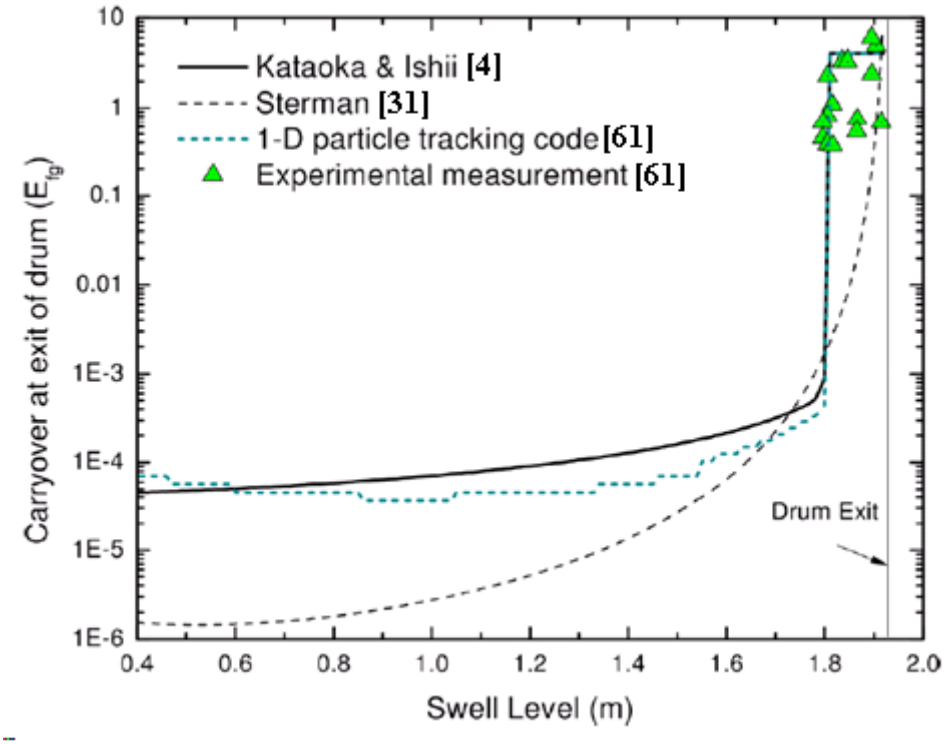

Figure II-11 *Prediction of entrainment using 1D code and comparison against* (Bagul et al., 2019) *data and* (Kataoka and Ishii, 1984) *and* (Sterman, 1958) *correlations.*

Bagul's data agree well with the correlation of Sterman (Sterman, 1958) and Kataoka and Ishii (Kataoka and Mamoru, 1983). The distance between the swell level and the drum exit is too small (<0.1m), and this corresponds to two zones (zone I and zone II in **Table II-3**, which means the

data agree with Kataoka's near surface entrainment equation (equation II.*20*) and momentum controlled region equation (equation II.*21* through equation II.*23*). As shown in **Figure II-11**, the entrainment consists of all droplets (Kataoka and Ishii, 1984). The movement of the droplets is accelerated at the exit of the drum, thus, the correlation developed by Kruzhilin (Kruzhilin, 1951) would agree as well with Bagul's data due to superficial gas velocity power 4 (equation II.*13*).

Lu and Xie (Lu and Xie, 2017a), (Lu and Xie, 2017b) investigated numerically the phenomena of the water carry-over based on Kim's experiments (Kim, Hyun and No, Cheon, 2005) with an emphasis on the effect of the exit using an upward and a side exits using Ansys 16 Fluent VOF method.

The mesh used in Lu and Xie's simulation was limited in terms of the number of elements. The entrainment of water consisted of all droplet sizes – from those measured in *microns* to *mm*-- and the elements have to be small enough to track such tiny droplets, (the element has to be one order of magnitude smaller than the droplet). Therefore, Lu and Xie (Lu and Xie, 2017b), did not consider small elements in the range of microns, since such simulation demands high computational performance as well as being time consuming. Therefore, the contribution of tiny droplets to the entrainment is neglected; however, it is not the case for different geometry where the height above the water pool is significantly large where tiny droplet stay volatile for long time. Obviously this statement is applicable to such geometries as investigated by Kim (Kim, Hyun and No, Cheon, 2005) where entrained water is dragged through the exit, the acceleration is substantial (Bernoulli's effect). Therefore, tiny droplets contribute less to the entrainment in such a case, meaning that some of them will be deposited onto the wall exit, and some of them will be added to the entrained water mass. Lu and Xie (Lu and Xie, 2017b) assumed this could be neglected and reduce the number of elements to speed up the simulation. Kim (Kim and No, 2003) used a cylindrical vessel in his experiments, while Lu and Xie (Lu and Xie, 2017b) used a rectangular vessel in order to increase mesh quality.

The carry over using a side-exit is greater than the carry over calculated by the upward-exit (**Figure II-12**).

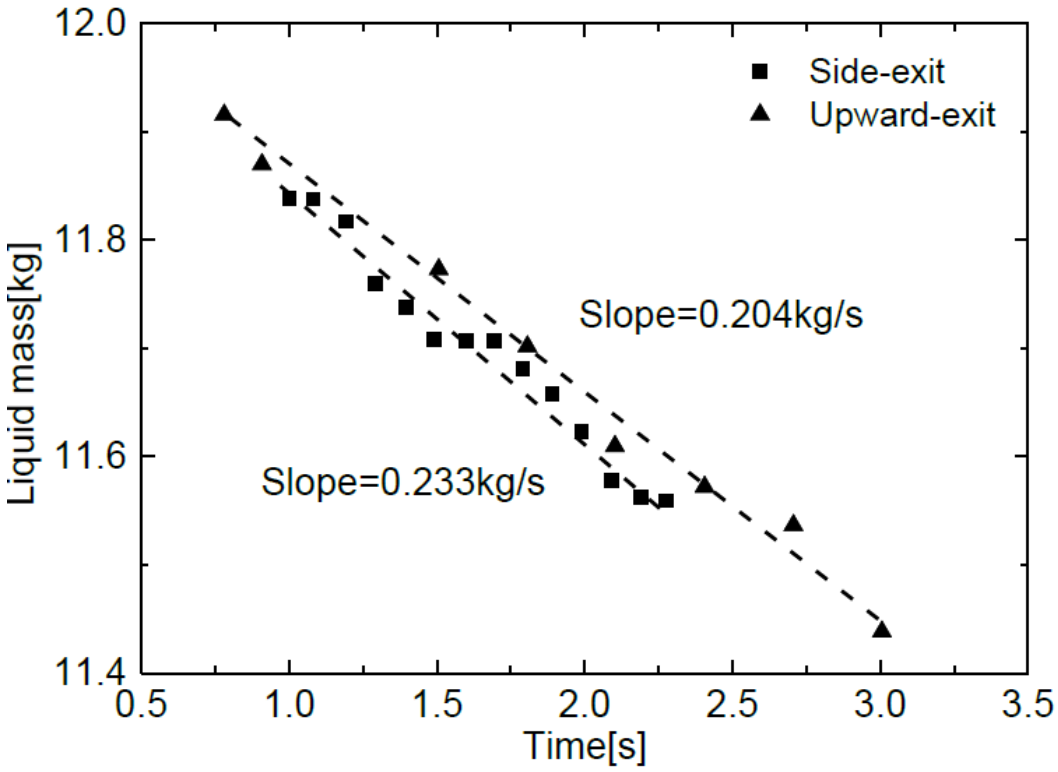

Figure II-12*Liquid mass loss rate for side exit and upward exit.*

On the one hand, for an upward exit, the water might accumulate at the exit, therefore due to gravity, it returns to the surface. On the other hand, this might not occur at the side exit, thus, even if the water accumulates at the exit, it will be deposited at a lower side of the exit, and eventually will be driven out due to the Bernoulli effect.

The analytical formulated by previous authors presented in this chapter attempted to give a prediction of the entrainment of water droplet, however, some formulation needed data to be validated, and others showed limitation in applicability.

The equation of Zenz and Weil(Zenz and Weil, 1958) is a satisfactory theoretical approach only if data on number of droplets per bubble size and initial velocity size distribution were available. Moreover, the initial velocity is a challenging magnitude to calculate from experiments since due to multiple bubble burst, the surface is highly agitated, and even complicated in churn turbulent flow regime where the droplets are generated by shear of water ligaments.

The equation developed by Andrews (Andrews, 1960) calculated the entrainment as a function of Boltzmann-Maxwell distribution of droplet velocities. However, Andrews's model does not give information on superficial gas velocity, which is necessary to entrain droplets. Supposing that the superficial gas velocity was considered, the model would be still limited as the Boltzmann-Maxwell function is applied to steady-state conditions. Kruzhilin (Kruzhilin, 1951) correlation considers only the gas kinetic energy. Yet, the information on height is not taken into account as the entrainment changes with height above the water surface.

The height above the water pool, the gas kinetic energy, gas void fraction in the pool and effect of pressure was analysed by Sterman (Sterman et al., 1957), however, the operating pressure used was up to 185 bar, which affects greatly the hydrodynamics of the pool as will be discussed in the third part of this chapter.

Golub (Golub, 1970) investigated the effect of height especially when the entrainment is dominated by deposition. The calculated entrainment decrease as the height increase for all gas velocities values. Golub's model is only applicable to deposition controlled region and low superficial gas velocity.

Kataoka and Ishii (Kataoka and Mamoru, 1983) analyzed the previous correlations and decided to decorticate the phenomena in detail. They subdivided the entrainment formulation as a function of height above the water pool as shown in equations II.*20* through II.*24*. The formulation of Kataoka and Ishii is of extreme precision in quantifying the entrainment comparing to previous correlations, nevertheless, their correlations are not applicable to low gas velocities (bubbly flow regime).

In large vessel diameter such as containment buildings, the effect of deposition is neglected. For instance, in Kataoka and Ishii and Golub's correlations, the term $e^{-\left(\frac{h}{D_H}\right)}$, which translate the droplet deposition onto vessel walls, does not contribute in the case of large vessel diameter, where $D_H \rightarrow \infty$, implies $e^{-\left(\frac{h}{D_H}\right)} \rightarrow 1$.

This effect is extensively investigated in THAI facility (Gupta et al., 2016) where experiments on re-entrainment of contaminants by water droplets are conducted in large vessels.

C. Factors affecting entrainment

The experiments are the key to unlock variables responsible for a specific phenomenon. The entrainment from water pools has been investigated for different scenarios: entrainment obtained by gas release from the surface of the pool by gas injection (downcomer, quencher, horizontal vent), (Freitag and Schmidt, 2017)(Kim, Hyun and No, Cheon, 2005)(Bagul et al., 2019) or heating plates, and entrainment measured by depressurization (Kudo et al., 1994)(Freitag and Schmidt, 2017).

The factors that affect the entrainment are achieved by analyzing the factor affecting the dynamics of the bubble in the water pool.

1. Effect of thermal-hydraulics and physical properties

The effect of thermal-hydraulics on the pool hydrodynamics, hence on the entrainment, could have been revealed in the experiment of Sterman (Sterman et al., 1957). The experiment was conducted under pressures up to 185 bar, and superficial gas velocity up to 0.555 m/s, while Kim et al. (Kim and No, 2003) used atmospheric condition with superficial gas velocities up to 0.35 m/s (**Figure II-2**). The churn turbulent flow regime begins from superficial gas velocities values of 0.1 m/s (Yan et al., 2019). Thus, for values higher than this value, the flow regime in the water pool is churn turbulent. Kim's experiments measured higher entrainment value than Sterman's knowing that in churn turbulent flow regime the entrainment increase exponentially with increasing superficial gas velocity (Kataoka and Mamoru, 1983). The effect of pressure might be the cause of this redundancy. The experiment of Sterman's might show the effect of pressure on entrainment, however, it did not explain how it affects the bubble dynamics.

Lin et al. (Lin et al., 1998) investigated the effect of thermal-hydraulics on the bubble size for different temperature up to 78°C and for pressure up to 152 bar, for superficial gas velocity up to 0.08 m/s. The pressure has a clear noticeable effect on bubble size as it decrease with increasing the pressure as can be seen in **Figure II-13**. From 1 bar to 152 bar, under superficial gas velocity up to 0.05 m/s, the bubble size distribution shifts from larger- to smaller-size bubbles. Even with higher superficial gas velocities up to 0.08 m/s, the effect of pressure could be seen clearly how

the bubble size changes. The experimental data used in this thesis to develop the empirical correlation did not used such higher pressures, since the maximum pressure in a containment building reaches 10 bar during accident scenarios. Moreover, the shift in bubble size distribution could be seen clearly in **Figure II-15**. The minimum dominant bubble size for all superficial gas velocities at 152 bar is 0.5 mm diameter. This size could be considered as an unbreakable hard sphere due to the substantial surface tension.

In case of containment applications when pressure can range from 1bar to 10 bar, some experiment have shown effect of pressure on the bubble diameter. In the experiment of THAI (Freitag and Schmidt, 2017), under 2.5 bar, the maximum bubble size measured is up to 3 mm. Whereas in the experiment of Cosandey (Cosandey, 1999), the bubble size was approximately no more than 2 mm diameter, under a pressure of 6 bar. This is 1 mm of difference, and shows that in this range of pressure, the change in bubble size is not as substantial as the case of very high pressures where bubble size decreases by one order of magnitude.

The shift from large to small bubble showed in **Figure II-15** is due to bubble breakup. This is due to the increase of density as the pressure increases, which decrease the capillary length of the bubble (the maximum stable bubble size). The inertial force become more relevant than surface forces, leading to bubble breakup, until the bubble reaches a size where surface force become more significant **Figure *II-16***.

Therefore, the entrainment in the experiment of Sterman et al. (Sterman et al., 1957) could be explained from the bubble size perspective as a function of pressure, where the film and jet droplet produced by such bubbles is limited (Lhuissier and Villermaux, 2012) comparing to the entrainment in the experiment of Kim et al. (Kim and No, 2003) where the surface is highly agitated producing large amount of droplets.

Lin (Lin et al., 1998) also found that the physical properties of the system affect the bubble size. For the range of pressure and temperature used, the density and viscosity increases by increasing pressure from 1 bar to 160 bar and the surface tension decrease for the same range. The density and viscosity decrease with increasing temperature from 293 K to 393 K, and the surface tension decreases with increasing temperature.

Newitt (Newitt, 1954) investigated the mechanism of droplet formation from gas bubbles as well as the physical properties affecting it. Unfortunately his works could not be found to asses this section with great detail, however some conclusion could be found in the work of (Santiago, 1991). Newitt investigated the effect of surface tension by increasing temperature, and found that by increasing this latter the surface tension decreases, and the bubble produces less film and jet droplets. The same conclusion later on was stated by (Lhuissier and Villermaux, 2012) and (Poulain et al., 2018), that decreasing the bubble size down to 1.2 mm diameter, its burst is limited to the production of jet droplets, and by increasing the bubble size up to 10 mm, few film droplets will be produced and no jet droplets. The peak of jet and film droplets production was found attributed to bubble of sizes between 2 mm and 2.5 mm (Blanchard and Syzdek, 1988). Lin (Lin et al., 1998) further noticed that at high temperature, the maximum stable bubble size decreases with increasing pressure due to increase of density and decrease of surface tension. As the temperature decreases, the increase of viscosity with increasing pressure would damp the fluctuation of liquid velocities, retarding the decrease of bubble size in comparison with high temperature.

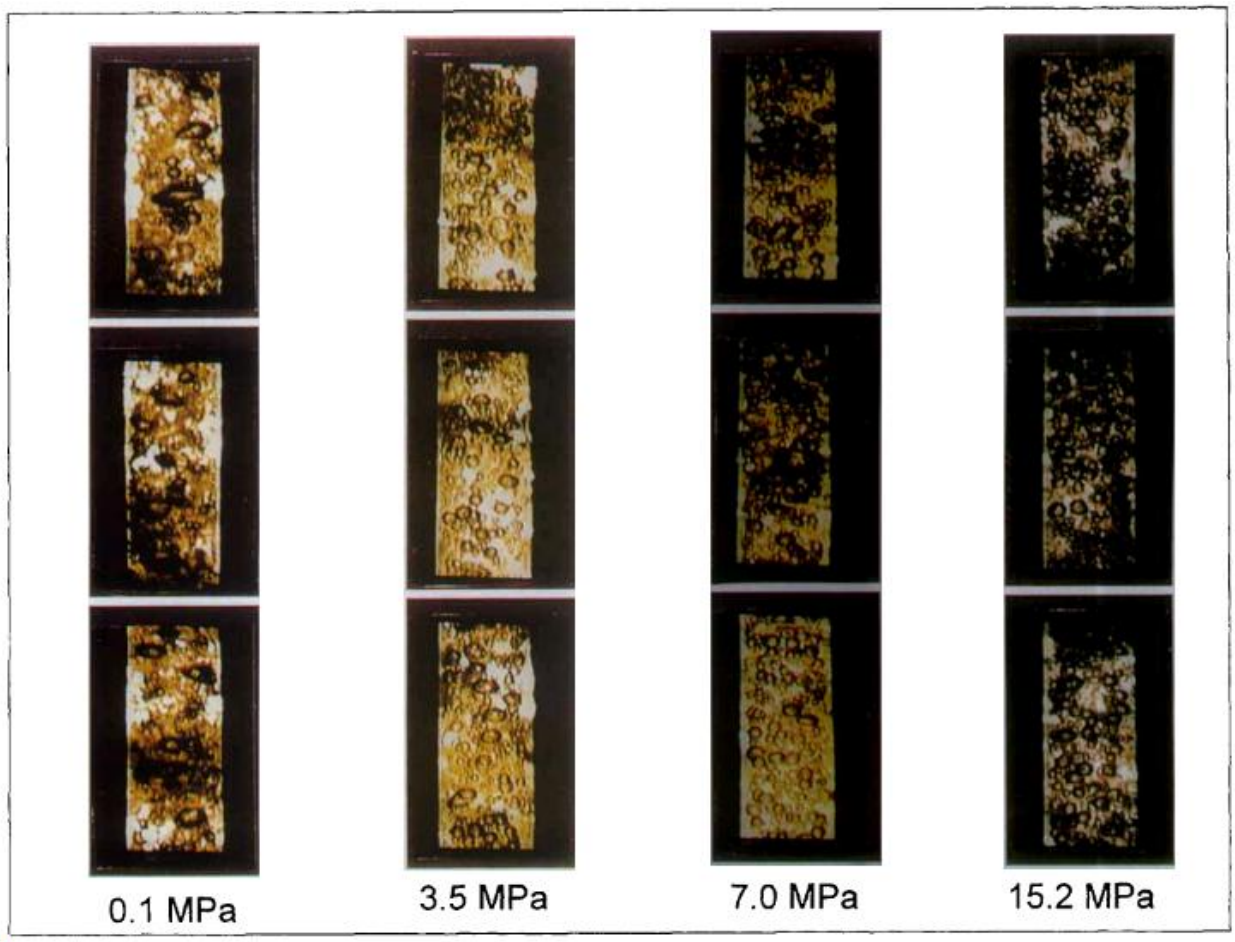

Figure II-13 *Bubble under various pressure at T=27 °C and j_g= 0.05 m/s* (Jamialahmadi and Muller-Steinhagen, 1990)

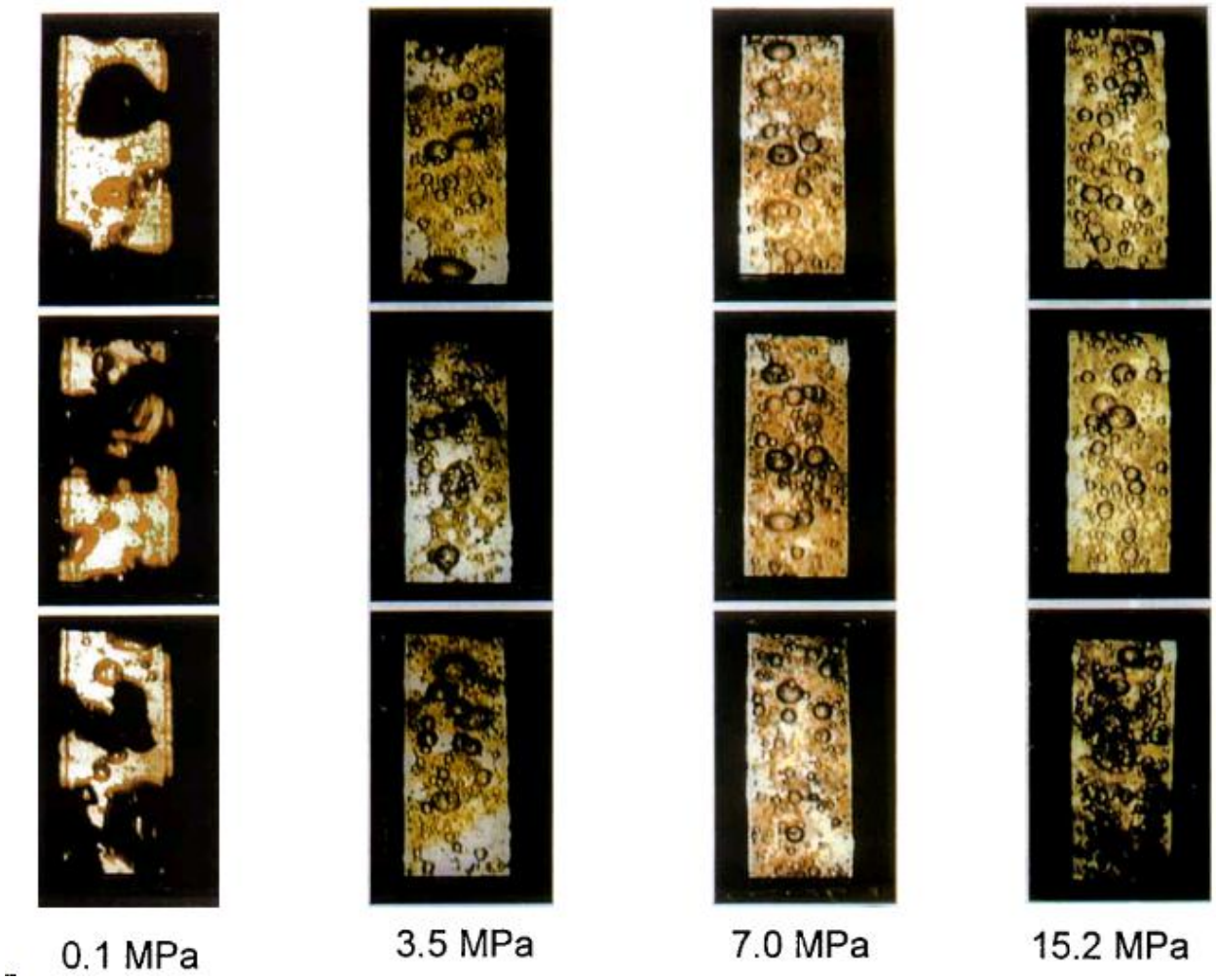

Figure II-14 *Bubble under various pressure at T=27 °C and j_g= 0.08 m/s* (Jamialahmadi and Muller-Steinhagen, 1990)

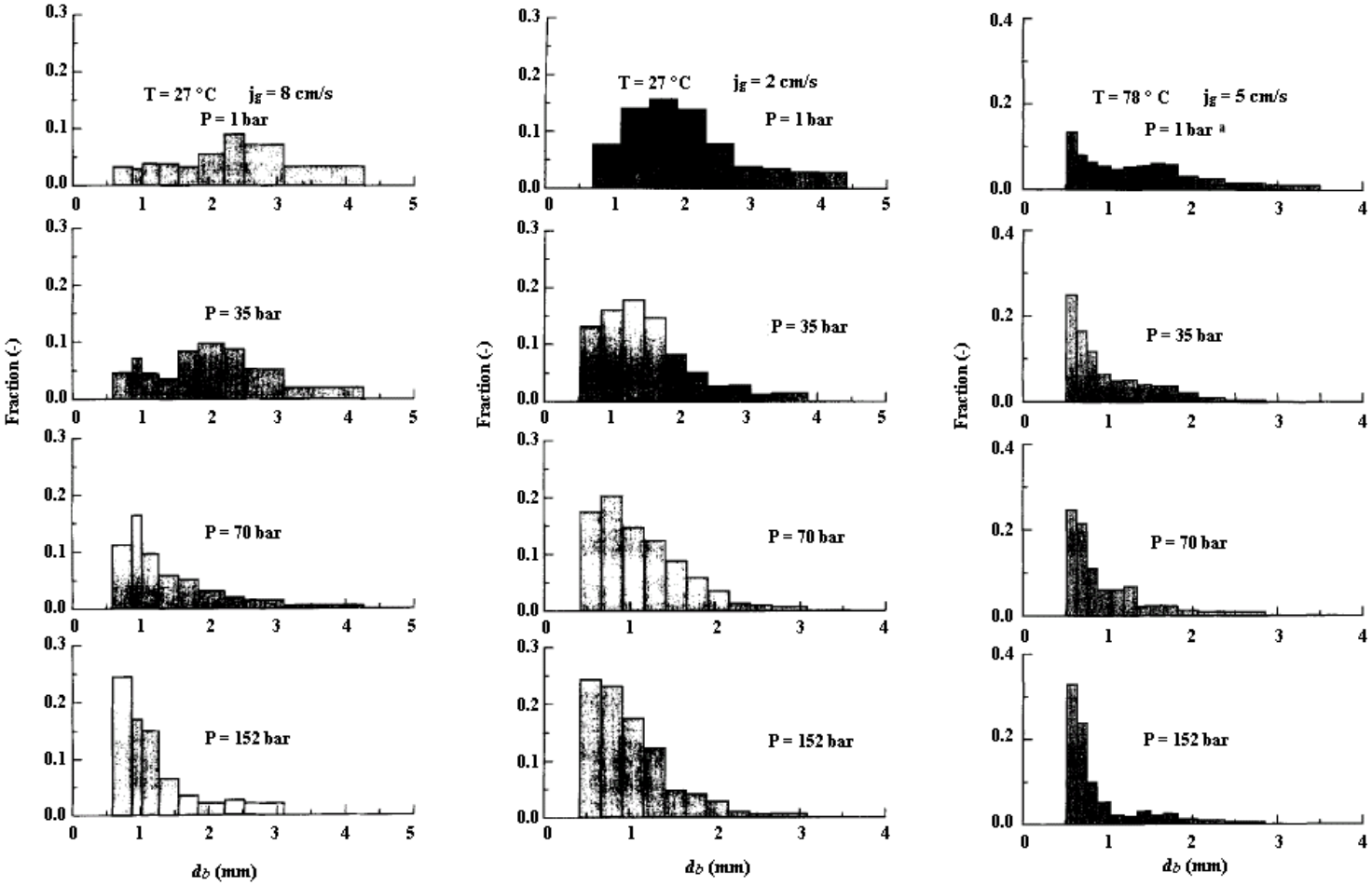

Figure II-15*Bubble size distribution for different pressure and superficial gas velocities*

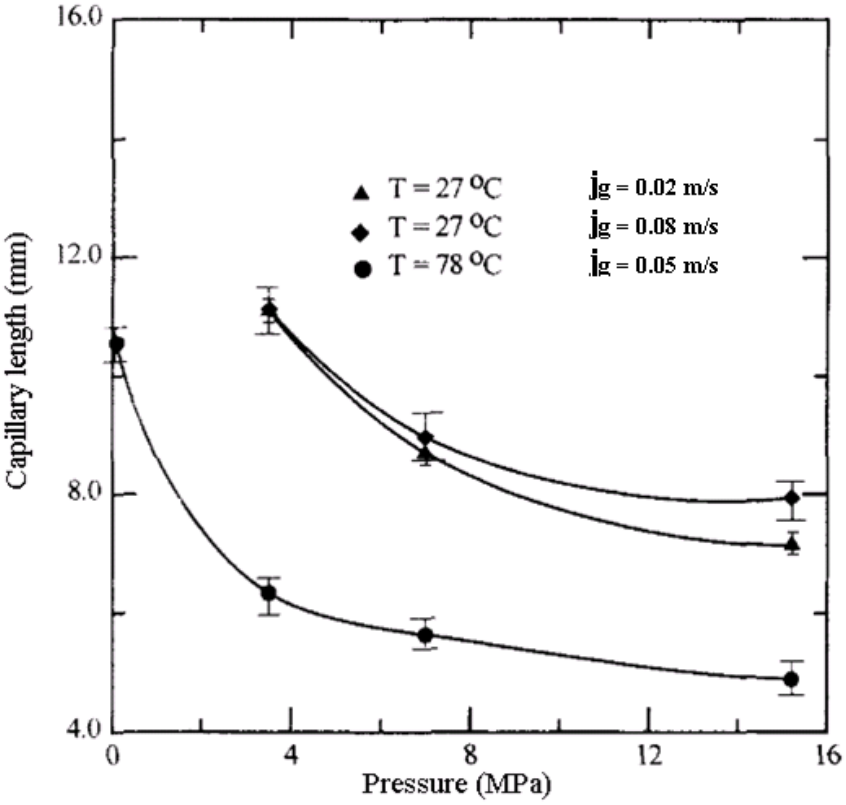

Figure II-16*Capillary length as a function of pressure and temperature*

The pool hydrodynamics might be affected by the existence of impurities such as aerosol, in turn, that might affect the terminal velocity and the bubble shape. Clift et al. (Clift et al., 1978) shows data on the terminal velocity of the gas bubble in pure and contaminated water depending on the bubble size. For pure water as for contaminated water, the terminal velocity of the bubble increase with the bubble size because of gravity. For contaminated water, the terminal velocity decrease with increasing the bubble size in ellipsoidal regime, due to the drag force. The contaminations in pool decrease the drag on the gas bubble, which decrease the terminal velocity. This effect decrease as the bubble increase in size in spherical cap regime corresponding to bubble of diameter higher than 18 mm (**Figure II-17**).

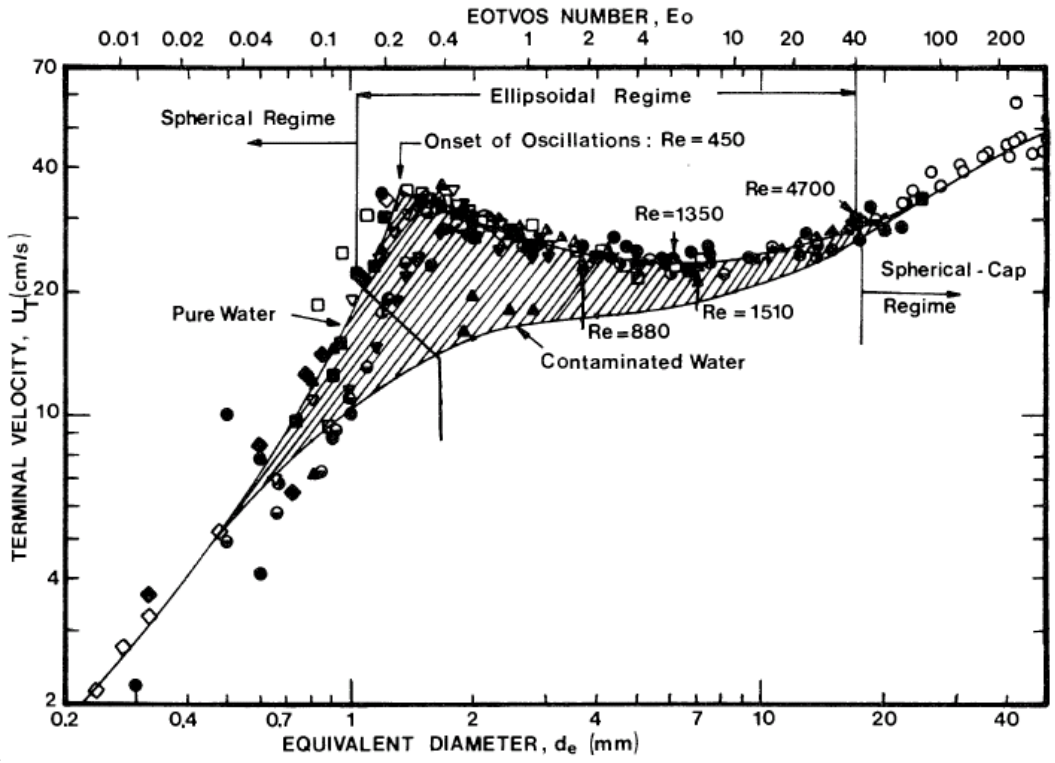

Figure II-17 *Terminal velocity of air bubble in water*(Clift et al., 1978)

According to Clift et al. (Clift et al., 1978) the contaminants affect the gas bubble of a certain size corresponding to an ellipsoidal regime. However, a question arises that if the impurities affect the droplets production, since the bubble will rise and burst eventually regardless its terminal velocity.

This effect was investigated by (Wei et al., 2020) as well as the effect bubble burst position. Wei et al. (Wei et al., 2020) investigated the bubble burst (9 mm to 16 mm) under low and high temperature (16 °C to 77 °C), and for different aerosol species (TiO_2 and $BaSO_4$) and concentrations (0 g/L to 0.2 g/L). They also investigated the speed of the rolling film cap after the burst. The bubble for the pure water case are more likely to burst at the edge of the film cap. The probability to burst at this position is about 47% for low liquid pool temperatures (16°C), and this probability increases with increasing temperature up to 60 % (**Figure II-18**). The increase of the temperature implies a decrease in surface tension eventually the bubble becomes instable. Moreover, the occurrence of the bubble to burst at that position is that the film is thinner at the

edge (Lhuissier and Villermaux, 2012)(Poulain et al., 2018), and the bubble tend to burst at the position where the cap film is thinner.

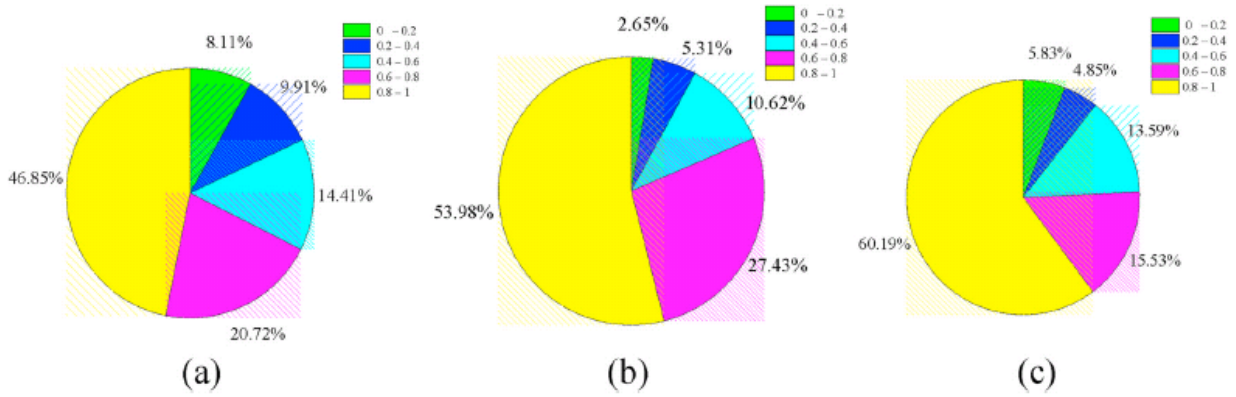

Figure II-18 *Puncture position distribution in distilled water at different temperatures:(a) 16 °C; (b) 40 °C; (c) 60 °C*(Wei et al., 2020).

The presence of aerosols increase the probability of the bubble burst at the edge of the bubble cap up to 83 %. It was shown that the concentration of the aerosol in the film cap at the edge is less than any other position, moreover the film is thinner at that position as well. The temperature showed no effect on the bubble burst position in the present of aerosol even with different concentrations and aerosol species (Wei et al., 2020).

After the burst, the film returns to the bulk water with a speed called film-rolling speed. This can be calculated by the Taylor-Culick velocity $V_{tc} = \sqrt{2\sigma}/\rho h_{film}$(Taylor, 1959)(Culick, 1960), where V_{tc} is the roll film velocity, σ surface tension , ρ density of the liquid and the film thickness h_{film}. As can be seen, the velocity of the film depends on the surface tension, density and the film thickness. The effect of temperature was investigated by (Wei et al., 2020) and found that the velocity of decrease with increasing temperature, due to the decrease of surface tension. Moreover, the velocity decrease when the film thickness increases, the droplet production is then affected.

In the presence of aerosols, the droplet production from the film might be influenced by agglomeration of aerosols at surface of pool as investigated by (Wei et al., 2020). The bubble has the ability to generate more droplet before agglomeration, and drastically decrease when aerosols agglomerate at the surface of the pool (**Figure II-19** and **Figure II-20**).

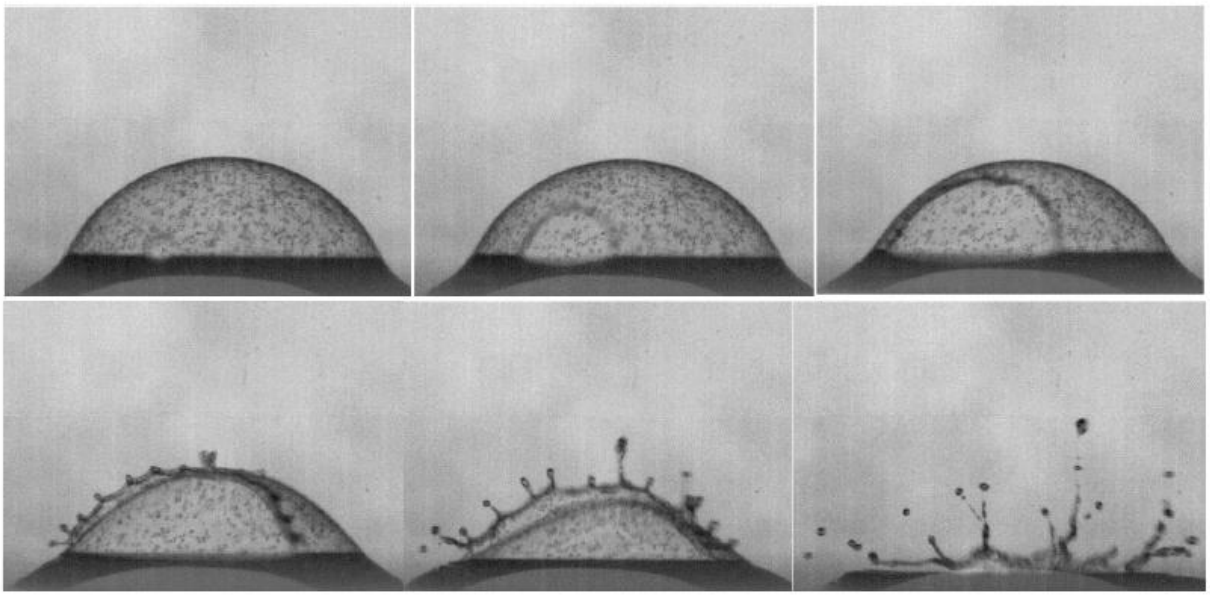

Figure II-19 *Bubble burst before aerosol agglomeration*

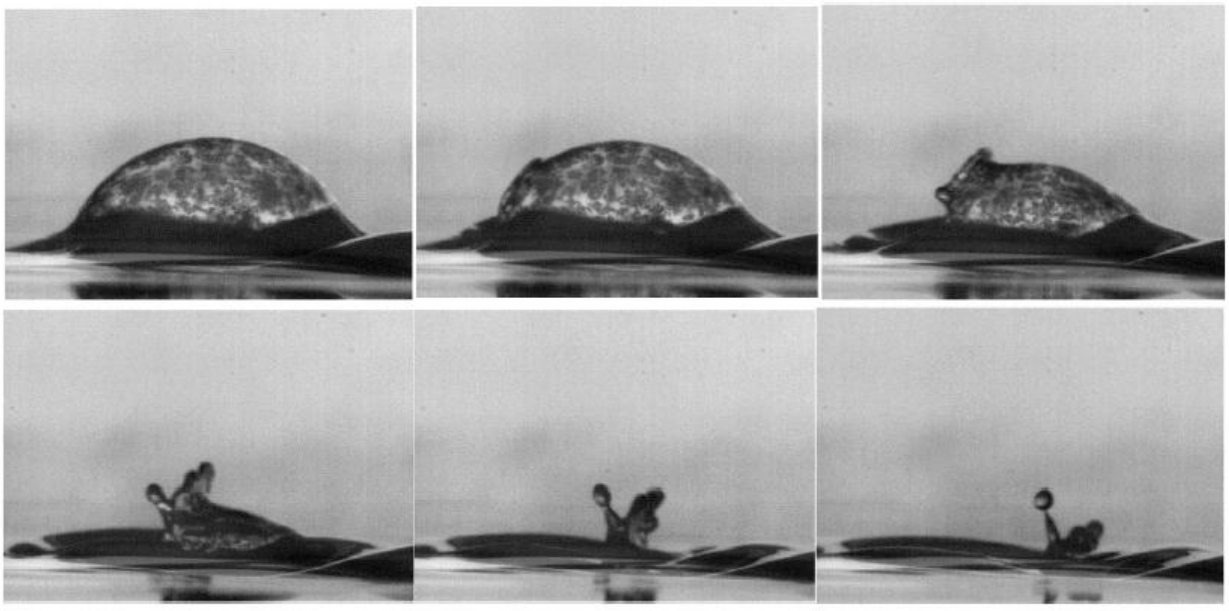

Figure II-20 *Bubble burst after aerosol agglomeration*

The agglomeration of aerosol particle increase with increasing the temperature as concluded by Wei et al. (Wei et al., 2020). In the experiments where tracers such as aerosol to quantify the entrainment are used (Freitag and Schmidt, 2017)(Schmidt et al., 2015)(Bunz et al., 1992), might

shows the effect of particle agglomeration, which in turn could have an effect on droplet production.

2. Effect of bubble size on droplets production

As for the analysis of the droplets generation, it was extensively investigated by (Spiel, 1992)(Poulain et al., 2018)(Koch et al., 2000)(Blanchard and Syzdek, 1988). Bubbles in bubbly flow regime, have the ability to produce film droplets and jet droplet. The film droplets are a consequence of the complete thinning of the bubble cap at the surface for small bubbles, and partial thinning for large bubbles. The jet droplets are consequence of the pressure inside the bubble after the burst, forming a crater to give birth to a jet. The bubbles have a limit size for producing jet droplets and film droplets (Lhuissier and Villermaux, 2012). Bubbles of 1.2 mm diameter and less, do not produce film droplet and tend more to produce jet droplets (Koch et al., 2000)(Donald E. Spiel, 1998)(Lhuissier and Villermaux, 2012), however, bubbles of 10 mm and above this value, produce very limited amount of jet and film droplets (equation II.*26*). The peak of the production of jet and film droplets together is associated to bubbles of 2 mm to 2.5 mm diameter **Figure II-21** (right). Zhan et al. (Zhang et al., 2012), found, by analysing the characteristics of bubble size in producing jet droplet, that the number of jet droplet decrease with increasing the bubble size **Figure II-21** (left).

$$R_0 \sim 3.8a \qquad \text{II.26}$$

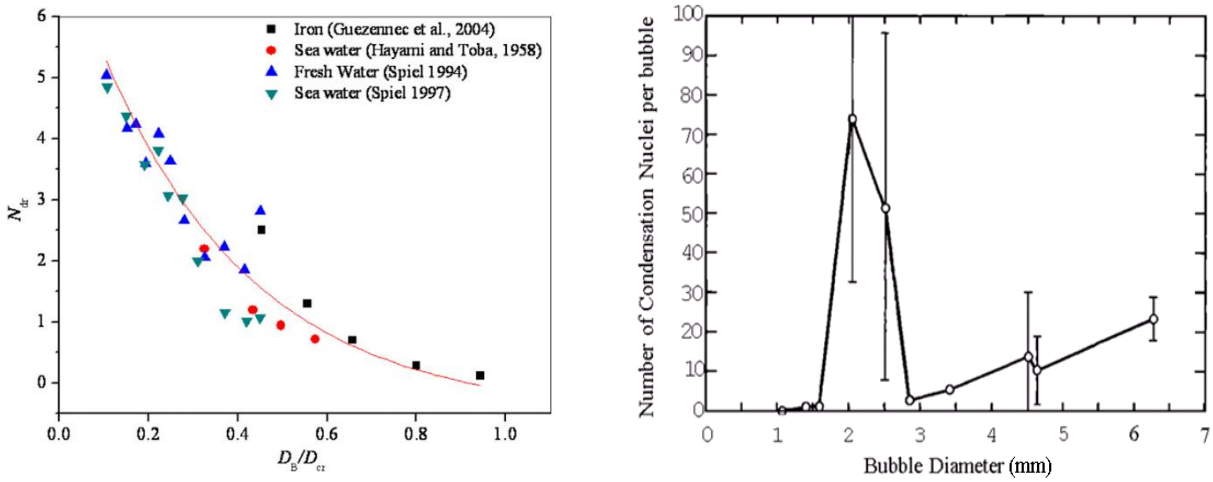

Figure II-21 *Number of jet droplets per bubble size (left)* (Zhang et al., 2012), *Number of film droplets production per bubble size* (Blanchard and Syzdek, 1988)

Koch et al. (Koch et al., 2000) earlier came to the same conclusion as (Zhang et al., 2012) (**Table II-6**). The number of jet droplets decreases with increasing bubble diameter. From Laplace equation II.*27*, the pressure inside the bubble P_i is higher than the pressure of the surrounding P_o.

$$P_i = \frac{4\sigma}{d_b} + P_o \qquad \text{II.27}$$

As the bubble diameter d_b increases, the pressure of the bubble is approximately comparable to the pressure of the surrounding, and as the bubble diameter decreases, the pressure inside the bubble becomes much higher than the pressure of the surrounding. This high pressure in the case of small bubbles, gives birth to a substantial jet that detaches into multiple droplets. While for larger bubbles, the surface tension is weak, becoming less stable, and they even burst before the complete drainage of the film cap. Eventually, these large bubbles end up producing less film droplets and practically no jet droplets.

Table II-6 *Number of droplet as function of bubble diameter* (Koch et al., 2000)

$D_b\ (mm)$	≤0.5	≤1	≤1.5	≤2	≤2.5	≤5.5	>5.5
N_d	6	5	4	3	2	1	0

3. Effect of vessel geometry

Furthermore, the geometry is one of the important factors affecting the entrainment. For instance, during depressurization, the position of the vent is of extreme relevance in determining the hydrodynamics of the pool. The depressurization rate also affects the hydrodynamics of the pool.

Figure *II-22* shows how the hydrodynamics are affected based on the analysis of experiments of (Kudo et al., 1994)(Freitag and Schmidt, 2017).

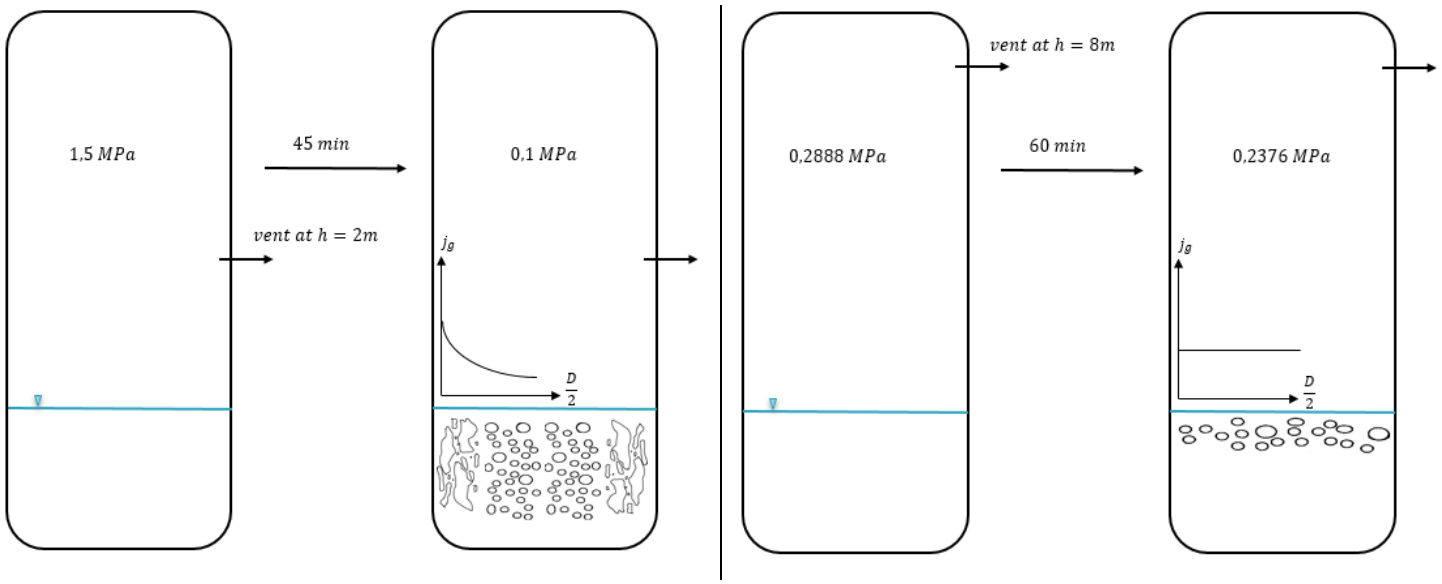

Figure II-22 *Pool depressurization of Kudo experiment* (Kudo et al., 1994) *(right) and THAI experiments* (Freitag and Schmidt, 2017) *(left)*

In **Figure II-22** (right), the pool was depressurized from 1.5 MPa to atmospheric pressure, and the vent was at 2*m* from the water surface. Under these conditions, the pool is highly agitated, and two flow regimes were observed according to Kudo et al. (Kudo et al., 1994): 1) churn turbulent flow near the walls and 2) bubbly flow away from the walls. That implies at least four mechanisms of droplet generation: bubble burst (bubbly flow regime), shear of ligament liquid (churn turbulent

flow regime), and roll waves (pool agitation) and liquid impingement. Therefore, the entrainment of droplets would be substantial.

In the experiments of THAI (Freitag and Schmidt, 2017), on the other hand, the vent was placed at 8*m* from the water surface, and the pool was depressurized from 0.2888 MPa to 0.2376 in 1 hour. As a result, only the surface was bubbling. Slow depressurization of the containment is to be expected during the late phase of severe accident in order to conserve the containment integrity. Whereas leakage might also occurs as consequence of containment failure. Kudo et al. (Kudo et al., 1994) experiment shows the consequence of rapid depressurization.

Another factor that affects the entrainment is the Bernoulli's effect. This latter was notable in many experiments (Bagul et al., 2019), (Bagul et al., 2018a),(Bagul et al., 2018b) and (Kim and No, 2003), (Kim, Hyun and No, Cheon, 2005), (Sun et al., 2014), (Qiu et al., 2015), (Sun et al., 2015), (Xiang et al., 2016), and simulated numerically (Lu and Xie, 2017a), (Lu and Xie, 2017b), (Bagul et al., 2019), (Bagul et al., 2018b).

Figure II-23 shows the Bernoulli effect for different scenarios, side exit, upward exit and the break that occurs during a SBLOCA scenario in a PWR. An important amount of entrainment could be measured from these scenarios due to the important momentum at each exit type. The variable that translates the Bernoulli effect in this case is the ratio of the dimensionless superficial gas velocity to dimensionless height above the pool $\left(\frac{j_g^*}{h^*}\right)^n$ power *n* corresponding to zone II and III (**Table II-3**).

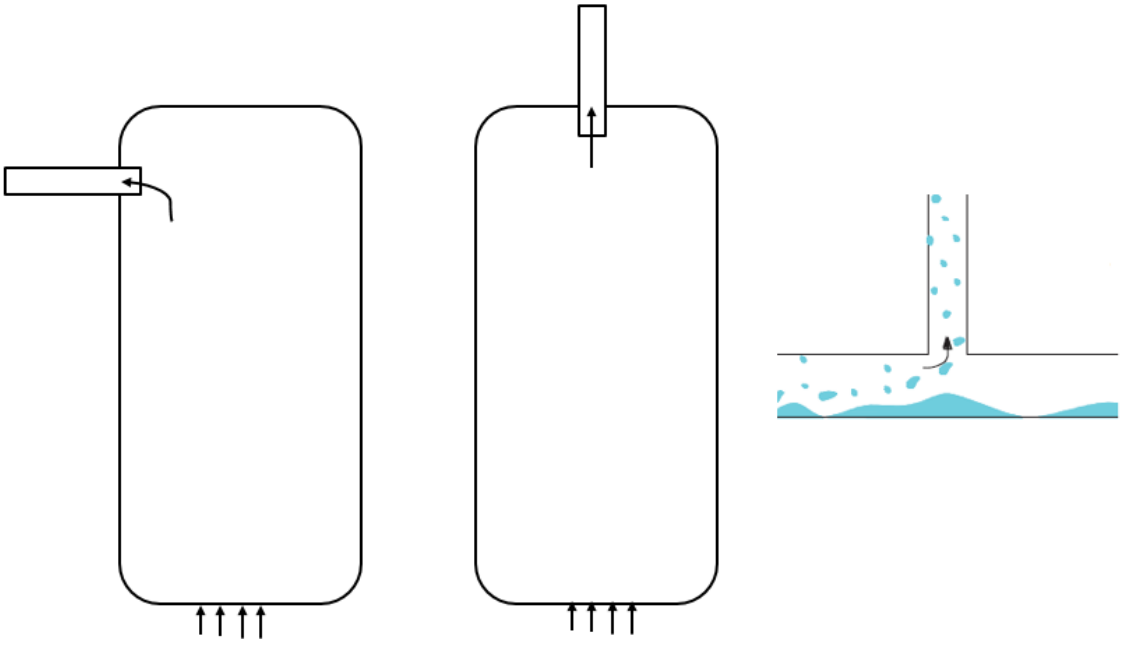

Figure II-23 *Simulation of a SBLOCA scenario conducted by Lu and Xie* (Lu and Xie, 2017a) *and Sun et al.* (Sun et al., 2014)

The diameter of the pool is the most important factor when analysing the entrainment phenomena as it defines the regime of two-phase flow. The carryover phenomena in pool are different from pipes. The two-phase flow regime in pipes are well defined due to the small domains (small diameter), so as the superficial gas velocity increases we observe transition from one flow regime to another. Whereas the flow regime in a water pool (infinite diameter), are limited to two flow regime, bubbly flow and churn turbulent flow regimes. The Bond number in a pipe is much smaller than in a pool, which means, for an air-water system, the gravitational force is more significant in a pool, which implies that more droplets will fall back to the water surface comparing to a pipe.

The maximum entrainment is 4 in **Figure *II-10*** was measured from the experiment of Bagul et al. (Bagul et al., 2019). Kim and No (Kim and No, 2003) measured a maximum entrainment of 5.10^{-2} (**Figure *II-24*)** and maximum off-take of 7. Wallis (Wallis, 1962) measured a maximum entrainment of 20 (**Figure *II-25***). In THAI experiments, the highest value of measured entrainment was 6.10^{-4} (**Figure *II-26***). From these experiments, despite the pool diameter, the entrainment depend mainly on the height. It is shown that the entrainment decrease with increasing height above the water pool (**Table *II-7***).

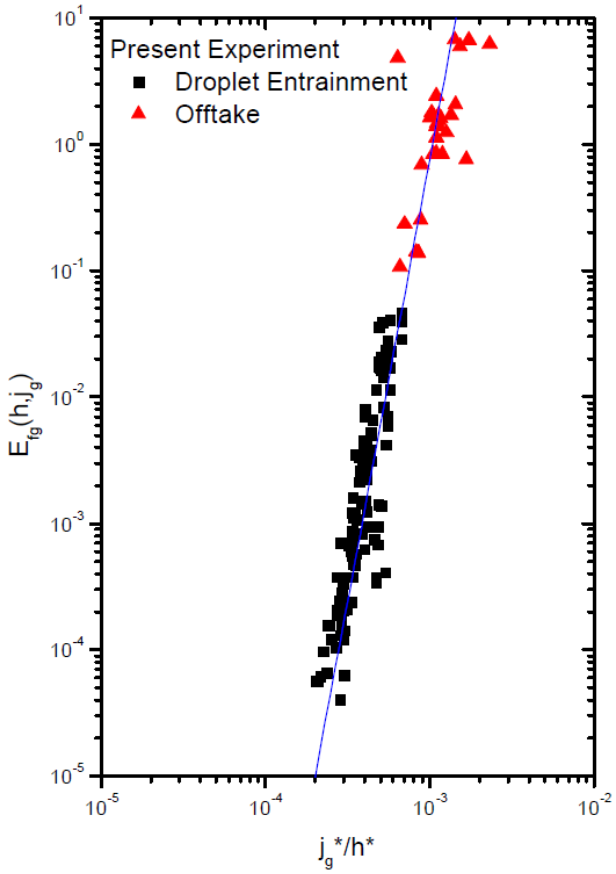

Figure II-24 *Pool entrainment (TLOFW in PWR) Kim and No* (Kim and No, 2003)

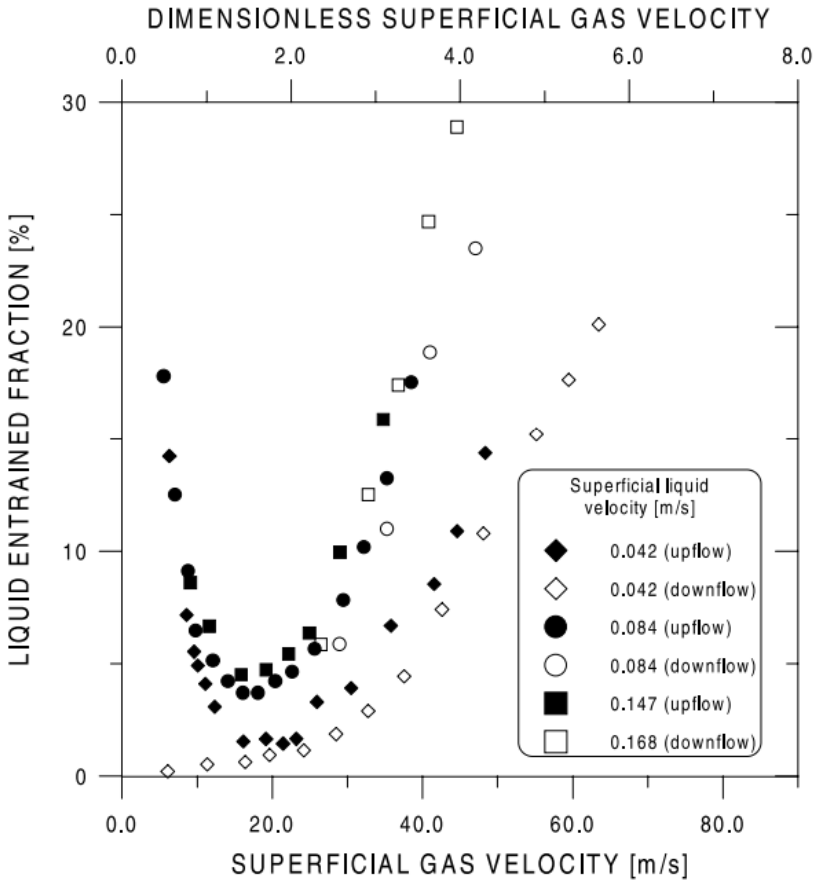

Figure II-25 *Pipe entrainment Wallis* (Wallis, 1962) *(figure taken from Barbosa et al.* (Barbosa et al., 2002)*)*

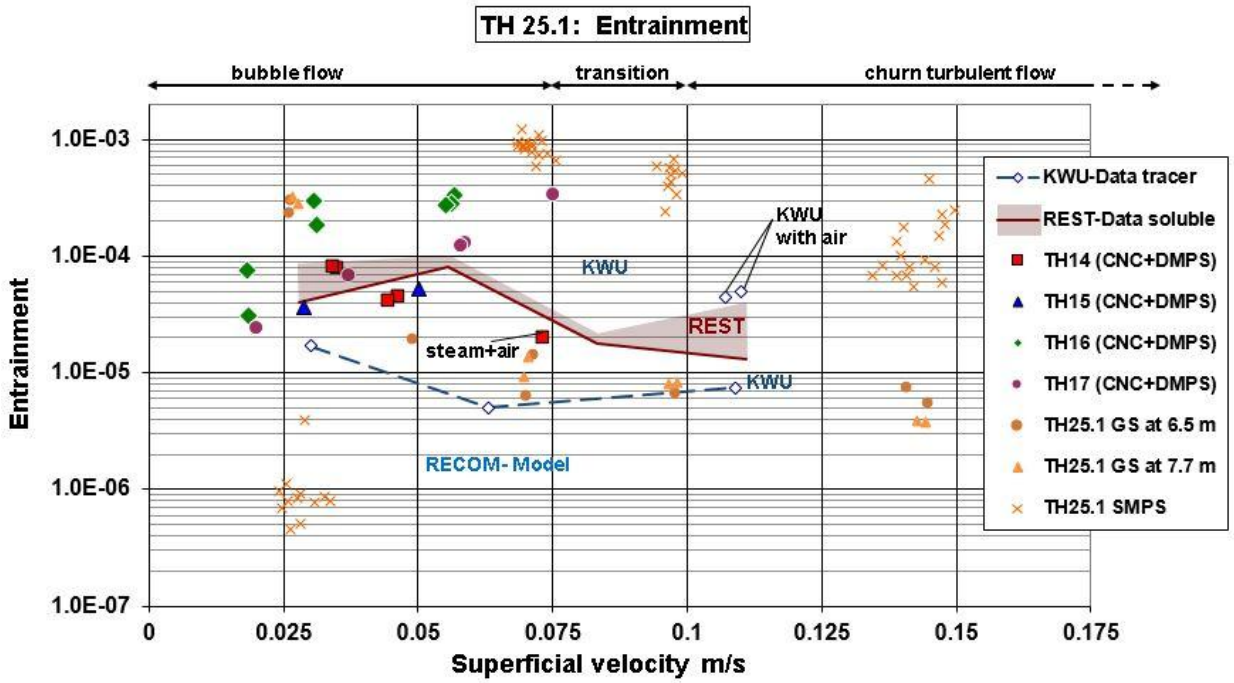

Figure II-26 *Pool entrainment in THAI experiments* (Schmidt et al., 2015)

Table II-7 *The effect of vessel diameter and the height above pool surface on Entrainment*

	THAI (Schmidt et al., 2015)	Bagul et al. (Bagul et al., 2019)	Kim and No (Kim, Hyun and No, Cheon, 2005)	Wallis (Wallis, 1962)
Pool diameter (m)	1.4	1.93	0.3	12.10^{-3}
Bond number	575.454	744.2	118.97	-
Height above pool surface (m)	8	0.1	1.0 - 0.1	-
Superficial gas velocity (m/s)	0.0287 to 0.0688	0.09 to 0.277	0.09 – 0.33	50
Entrainment	6.10^{-4}	0.371 – 4.900	0.01 - 0.1	20
Type of geometry	Large vessel	Small vessel	Small vessel	Pipe

The potential energy in terms of pressure $\left(e_{pot} = \rho g h\right)$ is also an important factor. This could be translated to the height above the water surface h. The entrainment near the surface consists of all droplets as stated by Kataoka (Kataoka and Ishii, 1984) and decreases as h increases. The effect of pressure in the dimensionless height $h^* = h/\sqrt{\frac{g\Delta\rho}{\sigma}}$ was not considered in the correlation of Kruzhilin (Kruzhilin, 1951).

This review provided experimental and analytical works on entrainment phenomena. It also provides the main shortcoming of the developed correlations by previous authors. It was identified that some correlation are either limited to a specific flow regime, or a specific zone above the water pool. Furthermore, explanations on discrepancies between some experimental data within the same superficial gas velocity range related to thermal-hydraulics and physical properties of the system was given. Therefore, based on these findings, it is substantial to give a correlation that englobes flow regimes in pools (bubbly flow and churn turbulent flow regimes) applicable to large and small scale facilities, which defines the main objective of this thesis.

III. Entrainment analysis with COCOSYS

The simulation of severe accident propagation in containments of nuclear power plants is required for the analysis of the potential consequences of severe accidents and possible counter measures under conditions as realistic as possible. Therefore, at GRS the **co**ntainment **co**de **sys**tem (COCOSYS) has been developed. The main objective is to provide a code system on the basis of mechanistic models for the comprehensive simulation of all relevant phenomena processes and plant states during severe accidents in the containment of light water reactors, also covering the design basis accidents (Arndt et al., 2015). First, a description of the code is given including the main modules used in the simulations.

The data used to simulate the entrainment with COCOSYS are provided by THAI experimental program (Freitag and Schmidt, 2017)(Schmidt et al., 2015). These data do not provide information on droplet size distribution. The technique used to quantify entrainment in the experiments of THAI (Freitag and Schmidt, 2017) was based on the use of tracers such as aerosols and their concentrations.

Additionally, this chapter includes the experiments conducted in THAI facility on entrainment, including matrix for each test, and the apparatus used to quantify the entrainment. The report of THAI experiments (Freitag and Schmidt, 2017)(Schmidt et al., 2015)(Freitag et al., 2016) give a great detail description of the measurement technique. Finally, the results obtained by COCOSYS are compared to the experimental data, in order to identify the main shortcomings of the code.

A. Entrainment of water droplets

The entrainment is calculated experimentally by using materials such as aerosol in water pool, these materials are called tracers. The tracers serve mainly in such approach to quantify the entrainment by measuring their concentration in the water pool and in the instrument used for sampling (e.g. gas scrubber, filters). The entrainment is determined theoretically by considering

distribution functions of bubbles and droplets. Some assumptions need to be adopted for bubble distribution. Under bubbly flow regime, a uniform bubble size could be considered, while in churn turbulent flow regime, the bubbles cannot be considered uniformly distributed. The entrainment then could be calculated as follows (equation *III.1*) (Cosandey, 1999):

$$E_{fg} = \frac{\iint_0^{d_{dr,crit}} \rho_l \Phi_{\mathrm{b}}(d_b).n_{dr}.\overline{\Phi_{\mathrm{dr}}}(d_{dr}).d_{dr}^3.dd_{dr}.dd_b}{\int_0^{\infty} \rho_g \Phi_b(d_b).d_b^3.dd_b} \qquad \text{III.1}$$

For a single bubble size, the equation above can be reduced to equation *III.2*:

$$E_{fg} = \frac{\mathrm{V}_{dr}}{V_b}.F(d_{dr,crit}).\frac{\rho_l}{\rho_g} \qquad \text{III.2}$$

Where V_{dr} is the total volume of liquid droplets ejected for each bubble of volume V_b. $F(d_{dr,crit})$ is the fraction of the ejected volatile droplet (diameter smaller than $d_{dr,crit}$).

The total volume of liquid droplets from a single bubble is calculated considering film and jet droplets. As for film droplet, their volume is calculated assuming that the film cap totally disintegrates into droplet (Koch et al., 2000). Several works have been carried out to determine the ratio $\frac{\mathrm{V}_{dr}}{V_b}$ in order to calculate the amount and size distribution of droplets for a single bubble (Donald E Spiel, 1998)(Poulain et al., 2018)(Zhang et al., 2012)(Cosandey, 1999) (**Figure II-21**).

The composition of the atmosphere affect the entrainment. For the pure steam case(Cosandey, 1999), a sample of the atmosphere is taken and steam and droplets are condensed and collected in a sampling instrument such as gas scrubbers. The entrainment is then calculated:

$$E = \frac{\mathrm{C}_{\mathrm{cond}}}{C_{BP}} = \frac{\dot{m}_l}{\dot{m}_g} \qquad \text{III.3}$$

For gas-steam atmosphere, and assuming that condensation at the walls is neglected, the equation *III.3* is multiplied by the ratio of non-condensable x_{ncg} gas in the venting pipe. Therefore:

$$E = \frac{\mathrm{C_{cond}}}{C_{BP}} . (1 - x_{ncg}) \qquad \text{III.4}$$

When x_{cond} is set to zero, then the equation *III.4* reduces to equation *III.3* for pure steam atmosphere.

Now if the condensation at the walls is taken into account, the equation *III.4* becomes:

$$E = \frac{\mathrm{C_{cond}}}{C_{BP}} . \frac{\dot{m}_{st,cond} + \dot{m}_{st,w}}{\dot{m}_{st,cond} + \dot{m}_{st,w} + \dot{m}_{ncg}} \qquad \text{III.5}$$

If the mass flow rate of the condensed steam at the wall is neglected ($\dot{m}_{st,w} = 0$), then equation *III.5* becomes equation *III.4*.

B. COCOSYS

COCOSYS provides a code system on the basis of mechanistic models for the comprehensive simulation of all relevant processes and plant states during severe accidents in the containments of light water reactors, also covering the design basis accidents. One of the main aspects of this code system is the consideration of the interactions between the different processes. The code system can be used for:

- The identification of possible deficits in plant safety
- The quantification of the safety reserves of the entire system
- Assessment of damage limiting or mitigating accident management measures
- Safety evaluation of new plant concepts.

The inner part of the code system consists of three main modules:

- The thermal hydraulic main module for the simulation of the thermodynamic behaviour and transient processes like hydrogen deflagration, simulation of safety systems
- The aerosol fission product main module for the simulation of the fission product behaviour and chemical reactions
- The core concrete interaction main module for the simulation of the core melt behaviour, concrete erosion, releases from core melt and chemical processes inside the core melt.

1. Thermal-hydraulics

In this module, the compartments of the considered power plant, test facility or other building types have to be subdivided into control volumes (zones). The thermodynamic state of a zone is defined by its temperature(s) and masses of the specified components.

These control volumes or zones are attributed to 2 models, an equilibrium zone model and non-equilibrium zone model.

In the Equilibrium zone model, all components (liquid water, vapour and other non-condensable gases) are assumed to be mixed homogeneously, resulting in a homogeneous distributed temperature in the zone (only one value). Superheated as well as saturated conditions are considered. Superheated atmospheres cannot contain liquid water. In these cases the water is drained immediately into other zones (Arndt et al., 2015).

a) Equilibrium zone

The governing equations which are solved in the equilibrium zone for energy and mass are given below:

- ***Energy equation***

$$V\,\frac{dP}{dt} = \sum_{k=1}^{m}\left[\sum_{j=1}^{p} G_{kj}^{a} i_k - \sum_{j=1}^{n} G_{kj}^{e} i_{kj}^{e}\right] - \frac{dQ^{e}}{dt} + \frac{dQ^{a}}{dt} \qquad \text{III.6}$$

V is the time dependent volume, *P* is the pressure, *G* is the mass flow rate, *i* is the specific enthalpy of the component *k* (water, steam or non-condensable gases), and *Q* is the heat exchange with the surroundings. The sum over *k* includes all components (water, steam and non-condensable gases) and *n* or *p* the number of inlet or outlet mass flow rates (junctions, injections and so on) respectively.

- ***Mass equation***
    - For non-condensable gases

$$\frac{dM_i}{dt} = \sum_{j=1}^{n} G_{ij}^{e} - \sum_{j=1}^{p} G_{ij}^{a} \qquad \text{III.7}$$

    - For water

$$\frac{dM_W}{dt} = \sum_{j=1}^{n} G_{Wj}^{e} - \sum_{j=1}^{p} G_{Wj}^{a} - G_{VD}^{vol} \qquad \text{III.8}$$

    - For steam

$$\frac{dM_D}{dt} = \sum_{j=1}^{n} G_{Dj}^{e} - \sum_{j=1}^{p} G_{Dj}^{a} + G_{VD}^{vol} \qquad \text{III.9}$$

G_{VD}^{vol} in equations III.8 and III.9 is the volume evaporation rate describing the phase change.

b) Non-equilibrium zone

In some cases the thermodynamics behavior in a containment can't be assumed in equilibrium only. The atmospheric temperature is a basic boundary condition for aspects like suspended water droplets, aerosols and heat transfer to structure. Therefore, a zone model which can distinguish temperature for the gas phase and the liquid phase is mandatory. For this purpose, the concept of non-equilibrium zone needs to be implemented.

In the non-equilibrium module, the energy and mass are solved for a given control volume (zone).

- ***Energy equation***

The energy balance for the gas phase is:

$$H_D = \frac{d}{dt}\sum_{k=1}^{m}[M_i i_i] - V_{gas}\frac{dp}{dt} \qquad \text{III.10}$$

The energy balance for the liquid phase (water) is:

$$H_W = \frac{d}{dt}[M_W i_W] - V_W\frac{dp}{dt} \qquad \text{III.11}$$

With H_D and H_W is total enthalpy of the gas components and water respectively, i_i and i_W is the specific enthalpies for gas components and water respectively, V_{gas} and V_W is the time dependent volume of the gas and water respectively. The second term of equation III.10 and III.11 is attributed to the work done by the system on the surroundings.

- ***Mass equation***

The mass balance in the non-equilibrium zone is solved by means of:

$$\frac{d}{dt}M_D = G_D + G_{VN} \qquad \text{III.12}$$

$$\frac{d}{dt}M_N = G_N - G_{VN} \qquad \text{III.13}$$

$$\frac{d}{dt}M_W = G_W \qquad \text{III.14}$$

Where, G_D, G_N and G_W are the sum of all inlet and outlets mass flow rates. G_{VN} is the total evaporation rate in the zone.

The shortcoming of the present thermal-hydraulics module is the subcooled conditions. Until now, it is an extensive area of research at GRS, in order to provide a model able to predict thermal hydraulic for scenarios under subcooled conditions.

The control volume are connected via junctions, therefore, the momentum conservation is manages by the simulation of junction between these control volume and injection scenarios.

$$\frac{d}{dt}G_j = \frac{A_j}{l_j}\left[\left(p_{j_s} - p_{j_t}\right) + w_j - K_j G_j\left|G_j\right|\right] \qquad \text{III.15}$$

Equation III.15 is valid for incompressible flow in the junction of a cross section A_j and length l_j, neglecting the kinetic part. w_j is attributed to the weight. *s* and *t* indicate the source and the target zone of the junction *j* respectively.

c) Re-entrainment module - RUB

This module works along with thermal-hydraulic module. To simulate this phenomena in a boiling sump, a correlation (so called RUB) (Dapper, 2009) based on THAI experiments (TH14 to TH17) have been implemented in COCOSYS. This correlation works by triggering the fission product transport module.

The RUB correlation (**Figure III-1**) depends on the cross section of the bubbling pool, the droplets diameter and the superficial gas velocity.

$$r = \frac{\dot{V}_{dr}\rho_{pool}}{M_{pool}} \qquad \text{III.16}$$

With the suspended droplet volume flow rate

$$\dot{V}_{dr} = A.j.e^{f.d_{dr}} \qquad \text{III.17}$$

The droplet diameter is assumed to be:

$$d_{dr} = \frac{a'}{j_g^{b'}}\sqrt{\left(\frac{\mu_g}{\rho_l}\right)} \qquad \text{III.18}$$

The droplet diameter was obtained from forces acting on it in the buoyancy region (Dapper, 2009), which are the weight and the drag.

Table III-1 shows the RUB correlation constants as function of superficial gas velocity. The case where $j_g \leq j_t$ corresponds to bubbly flow regime with j_t = 0.05 m/s. the case where $j_g \geq j_t$corresponds to the transition regime to churn turbulent flow regime.

Table III-1 *RUB model constants correlation*

	a'	b'	j	f
$j_g \leq j_t$	$6.20.10^{-4}$	0.62	$1.734079.10^{-7}$	$-8.042443.10^{6}$
$j_g \geq j_t$	$3.36.10^{-3}$	0.28	$1.27701.10^{-12}$	$9.625573.10^{6}$

The RUB model is limited to superficial gas velocity beyond the transition region (Dapper, 2009), and cannot predict the entrainment in churn turbulent flow regime which is characterized by the ejection of large drops resulting from the ligaments of water.

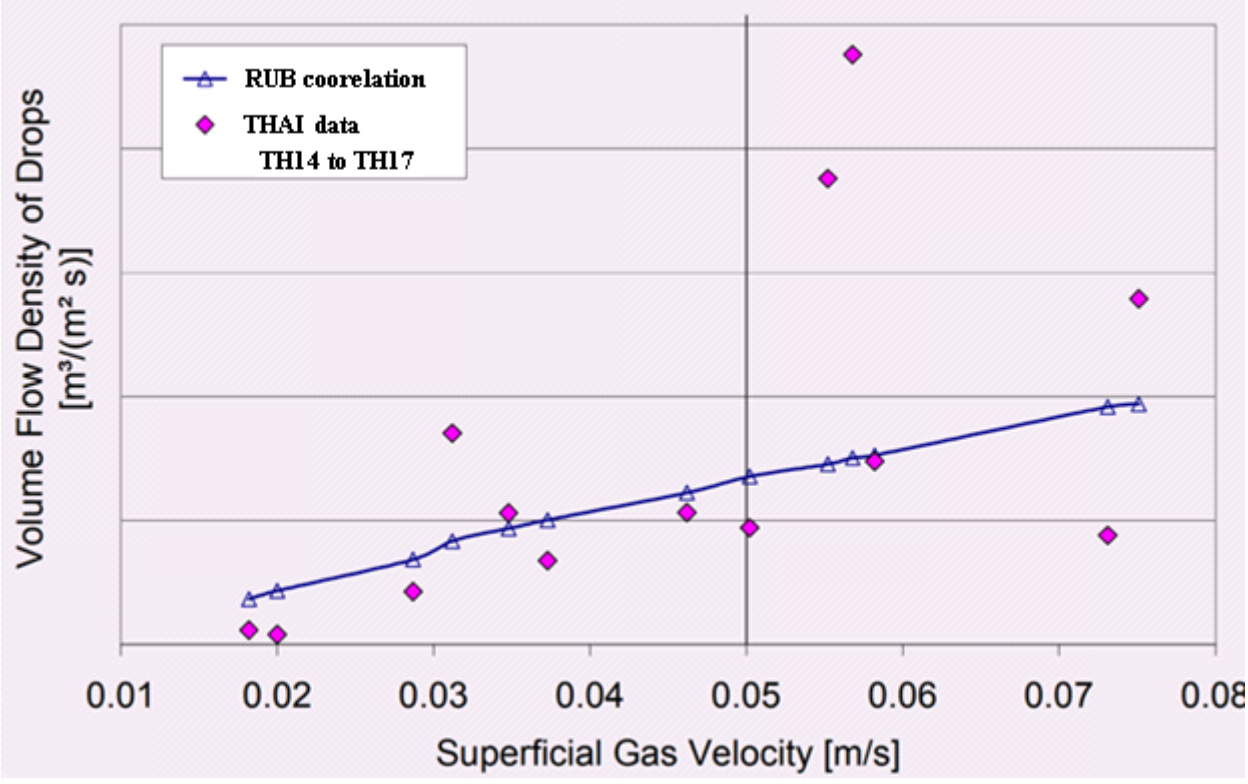

Figure III-1 *COCOSYS entrainment correlation - RUB*

C. THAI facility

THAI (Thermal-hydraulic, Hydrogen, Aerosol, Iodine) is a technical-scale containment test facility designed and built to address hydrogen and fission product issues under design basis accident and severe accident condition (Gupta et al., 2015). The main component of the facility is a 60 m^3 stainless steel vessel, 9.2 m high and 3.2 m in diameter, with exchangeable internals for multi-compartment investigations. The vessel structures are made of stainless steel (AISI316Ti). The vessel is designed for a maximum overpressure of 1.4 MPa at 180 °C and can withstand moderate hydrogen deflagrations. The cylindrical part of the THAI vessel wall consists of a 22 mm thick inner wall and 6 mm thick outer wall, with thermal oil in between forming three independent heating/cooling jackets over the height for controlled wall temperature conditioning by means of external thermal oil circuits. The heating/cooling power of each jacket is determined from measurements of oil mass flow and inlet/outlet temperature difference. The sump water basin at the bottom of the THAI vessel has a diameter of 1.4 m and is equipped with a 20 KW electrical heating coil. The outer sides of the vessel including the heating/cooling jackets are thermally well insulated by wool. Operation of the three heating/cooling jackets and/or controlled injection of steam and gas allow arranging either a stratified atmosphere within the vessel volume or atmosphere mixing by natural convection (NEA/CSNI, 2010)(Freitag et al., 2016)(Ouallal et al., 2017).

The THAI vessel is connected to Parallel Attachable Drum PAD vessel (1.556 m of diameter,10.294 m height and a volume of17.7 m^3) by an upper pipe. Three oil-filled mantles heat the PAD vessel walls (**Figure III-2**). Several tests was conducted at the THAI facility (TH14-17 and TH25) and at THAI+ (WH24). The supply system is different for each test.

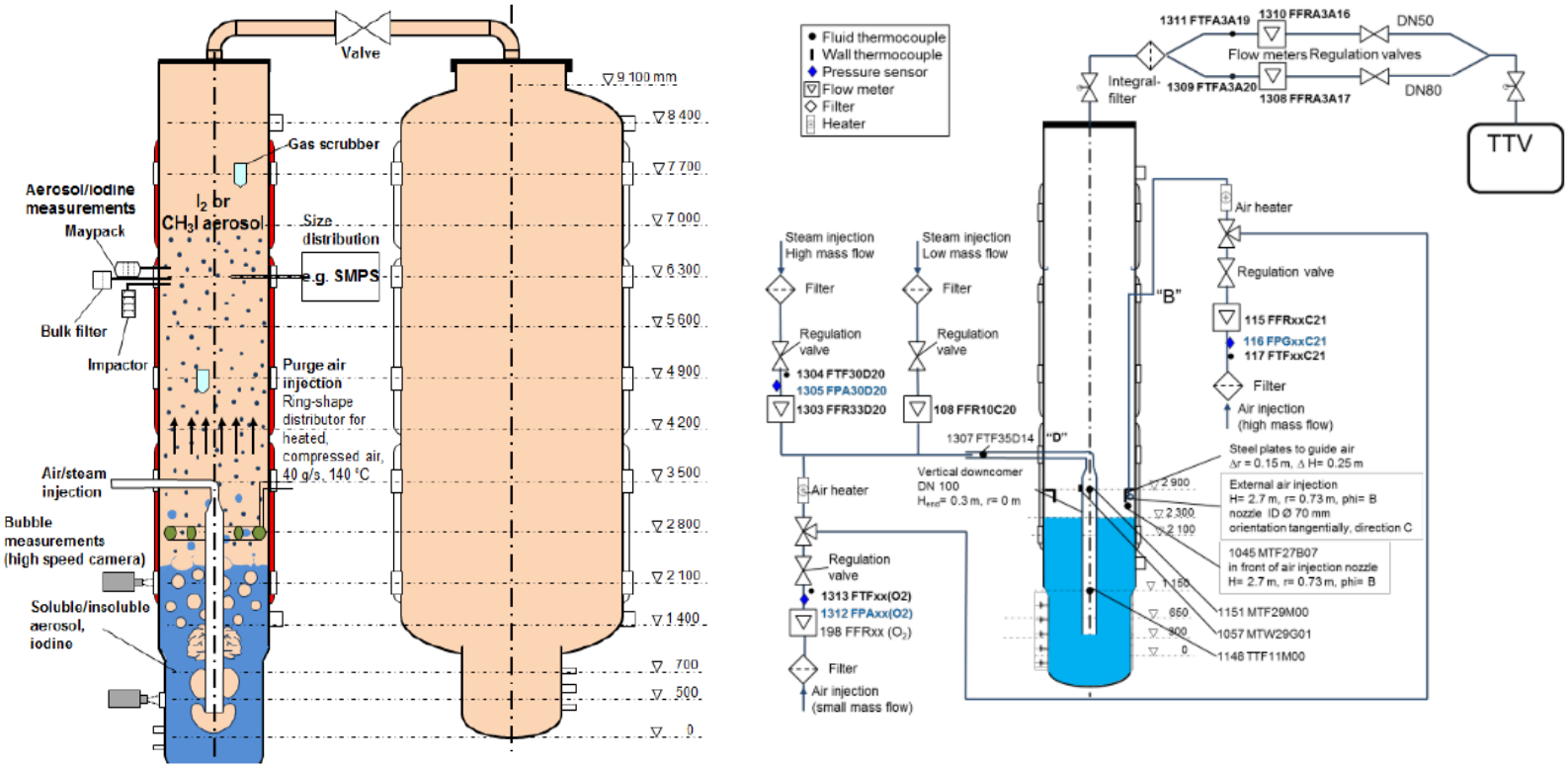

Figure III-2 *THAI+ test facility (left), experimental set up (right)*

1. Experimental configuration TH14 to TH17, TH25 and WH24

These test series were conducted in the THAI test vessel (**Figure III-2**, left), before the extension of the facility. The sump compartment (Ø 1.4 m) was divided by bulkheads, so the boiling range will be 1.03m x 0.54m (**Figure III-3**). the heating power required for sump boiling was provided by supplying heating steam at the bottom of the sump (up to 75kW) while a smaller part was supplied by electric heating elements (heating capacity range from 13.5kW to 15.2 kW).

In the test phases, TH14 to TH17 tests, pure steam and/or steam-air mixture was injected via a quencher through two horizontal pipes containing 58 holes with 2 mm of diameter each. The main differences between the tests are the boundary and the initial conditions as shown in **Table III-2** to **Table III-5**.

The test TH25 is an extension of the TH14 to TH17 tests series (**Table III-6**). To measure the entrainment, soluble, non-soluble aerosols are used as tracers. High gas flow rate was simulated to investigate the entrainment at high superficial gas velocity compared to TH14-17 (Schmidt et al., 2015). Identically to TH14 to TH17, as can be seen in **Figure III-3**, the pool is partly covered and not used entirely for TH25.

The WH24(Freitag and Schmidt, 2017) tests are conducted in the extension of the THAI facility, namely the parallel attachable drum (PAD) as shown in the right hand side of **Figure III-2**. The THAI Test Vessel (TTV) is connected to the PAD vessel via 80mm pipe DN80, and is used as a reservoir. The re-entrainment test consists of a large water pool, where a gas mixture of steam and non-condensable gases is injected into it via a 100 mm diameter downcomer pipe DN100. Similarly, to previous THAI tests, purging air is injected above the water pool in order to allow superheated conditions inside the vessel, so eventually to measure the aerosol concentration in the atmosphere by drying out the droplets that carry them. Thermocouples was installed in the water pool and in the vessel gas space at multiple height. As for the boundary condition of the system, the wall of the vessel are heated to prevent steam condensation. Pure steam or steam-air mixture is injected at different flow rate through the DN100 pipe into water pool. The exhaust gas is released from the PAD vessel to TTV vessel at the top. During the entire experiment, the pressure was kept constant for subcooled and boiling water pool conditions, except for the depressurization tests (Freitag and Schmidt, 2017). **Table III-7** shows the matrix for the WH24 test phases. The operating pressure during the WH24 test phase a1 through a5, and b1 through b4 is 2.5 bar.

Table III-2 TH14 test boundary conditions

TH14	Phase 1	Phase 2	Phase 3
Bubble released at the surface	Steam	Steam	Steam+air
Duration (min)	80	65	30
Steam mass flow rate (g/s)	18	27	15
Air mass flow rate (g/s)	-	-	48
Electric Heating sump (Kw)	13.5	13.7	13.4
Pressure vessel (bar)	2.11	2.35	2.4
Initial water temperature (°C)	122	126	105 (subcooled)

Table III-3 TH15 test boundary conditions

TH15	Phase D	Phase D1	Phase E1	Phase F	Phase G	Phase H	Phase I
Bubble released	Steam	Steam	Steam	Steam	air	Steam	Steam
Duration (min)	16	29	49	20	58	20	23
Steam mass flow rate (g/s)	19	33	26	21	-	27	10
Air mass flow rate (g/s)	-	-	-	-	40	-	-
El. Heating sump (Kw)	13.5	13.5	13.5	-	13.5	13.7	13.4
Pressure vessel (bar)	1.67	1.95	1.97	1.74	1.63	1.91	1.82
Initial water temperature (°C)	113.41	117.73	119.99	115.94	92.11	117.84	117.99

Table III-4 *TH16 test boundary conditions (subcooled conditions)*

TH16	**Phase 1A**	**Phase 1B**	**Phase 2A**	**Phase 2B**	**Phase 3A**	**Phase 3B**	**Phase 4**
Bubble released	Steam	Steam	Steam	steam	Steam	Steam	Steam
Duration (min)	12	31	19	33	40	35	74
Steam mass flow rate (g/s)	32.9	33.3	18.5	10.4	10.4	10.6	31.5
El. Heating sump	-	-	-	-	-	-	-
Pressure vessel (bar)	1.79	1.86	1.82	1.85	1.79	1.79	1.78
Initial water temperature (°C)	112.35	115.67	112.83	112.64	110.79	110.58	114.56

Table III-5 *TH17 test boundary conditions and initial conditions (subcooled)*

TH17	**Phase 1A**	**Phase 1B**	**Phase 2**	**Phase 3**	**Phase 4**
Bubble released	Steam	Steam	Steam	Steam	Steam
Duration (min)	27	57	59	70	72
Steam mass flow rate (g/s)	29.8	23.1	28.2	18.9	10.3
El. Heating sump (Kw)	18.9	19.0	19.2	9.7	4.8

Pressure vessel (bar)	1.56	1.62	1.99	1.97	1.96
Initial water temperature (°C)	106.6	112.5	117.3	115.8	111.4

Table III-6 *TH25 test phases boundary conditions*

TH25 (boiling)	**Phase 1**	**Phase 2**	**Phase 3**	**Phase 4**
Bubble released	Steam	Steam	Steam	Steam
Duration (min)	20	42	47	55
Steam mass flow rate (g/s)	14.5	49.6	68	96.6
El. Heating sump (Kw)	0	0	0	0
Pressure vessel (bar)	2.22	2.21	2.21	2.24

Table III-7*WH24 test phases boundary condition*

Test phases	Air injection flow rates (kg/h)	Steam injection flow rates (kg/s)	Water temperature (°C)	Purge air flow rates (kg/s)	Depressurization rates
a1	78.7	0	57.2	0	
a2	81.2	0	61.8	0	
a3	19.6	54.1	72.4	143.2	
a4	19.4	64.1	92.1	143.2	
a5	19.4	69.5	114.8	146.2	
b1	0	70.8	124	145.8	

b2	0	217.2	128	145.4	
b3	0	363.3	128.2	145.5	
b4	18.4	224.1	124.1	145.6	
c1	0	0	132	0	1 bar/4.9 min
c2	0	0	128.4	0	1 bar/12.9 min
c3	0	0	127.9	0	0.1 bar/11.4 min

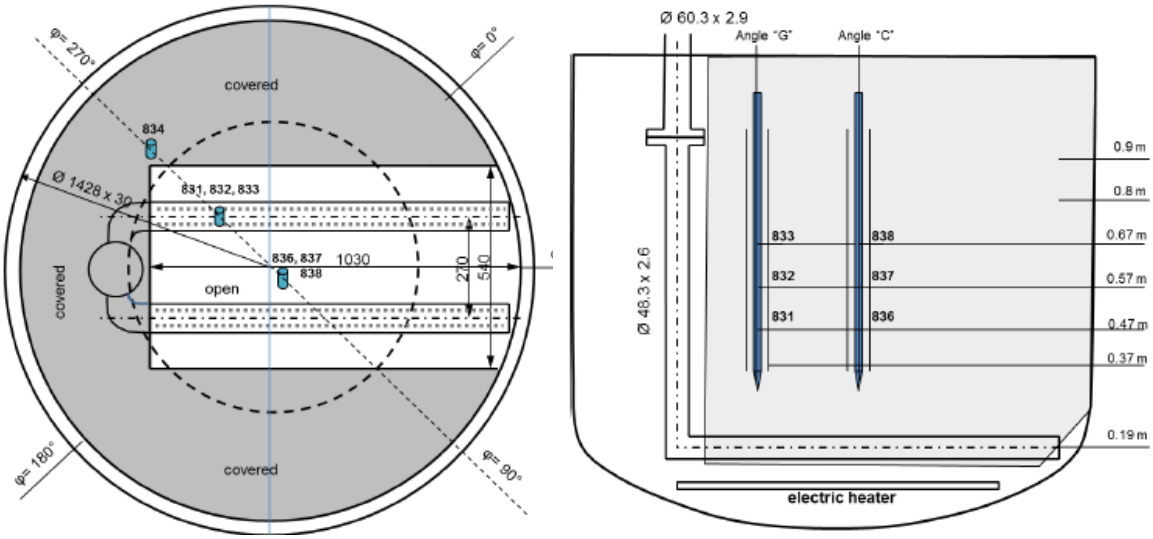

Figure III-3 *: Left, TTV sump cross section. Right, TTV sump pipe submergence*

Soluble and non-soluble tracers was used to quantify the entrainment, by measuring their concentrations. The entrainment in THAI experiments is calculated from the concentration of the tracers by equation *III.3***.**

During the experiments, for the calculation of entrainment, the fluid samples were taken from a steam air mixture(Freitag and Schmidt, 2017).

2. Entrainment measurement

a) Scanning mobility particle sizer

The entrainment of water droplet in the experiments of THAI was calculated from the concentration of the tracers used in the water pool (soluble or non-soluble aerosols) via equation *III.4*. The measurement of aerosol concentration were conducted using a scanning mobility particle sizer (SMPS) which is comprised of a differential mobility analyser (DMA) and a condensation particle counter (CPC). The principle of the measurement system is to classify aerosol particles by equivalent electrical mobility diameter using a variable electrical field. For a given electrical field, particles of small size range are separated from the particle population and directed to CPC. The particles that pass through the DMA are too small to be counted optically, thus the CPC forces a working fluid (typically water or butanol) to condensate the particles creating large droplets with the particle at their centre. From these droplet the concentration of aerosol is then measured.(Schmidt et al., 2015). The SMPS provides data on aerosol size distribution mainly (**Figure III-4**).

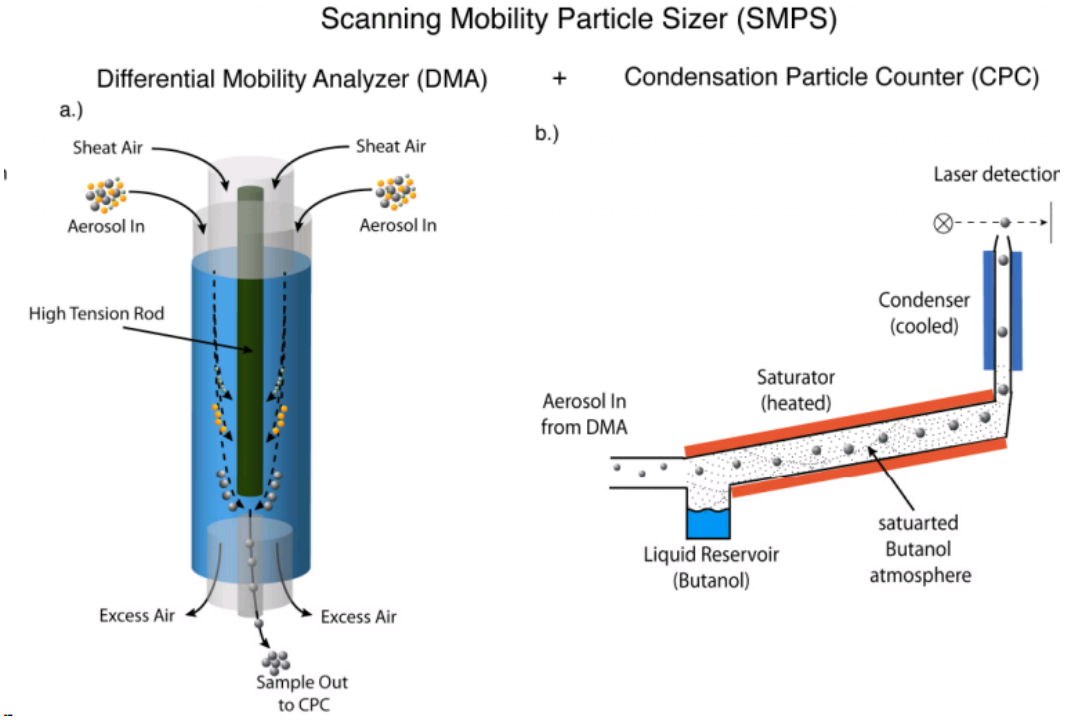

Figure III-4 *Scheme of a Scanning Mobility Particle Sizer (SMPS)* (Hagendorfer, 2011)

b) Gas scrubbers

Gas scrubbers (GS) are mainly used to measure the aerosol concentration. In the experiments of THAI (Schmidt et al., 2015) the gas scrubber was located at elevations h=7.7 m and h=6.5 m in the gas space. During the sampling operation, the gas scrubbers are filled with 180 ml of purified water for the absorption of contaminants. The extracted measurement liquid is diluted using additional absorption liquid to 200 ml by the help of graduated flasks. The absorption liquid is mixed and split into 2 sampling vials. Then the chemical analysis yield the concentration of the tracers (**Figure III-5**).

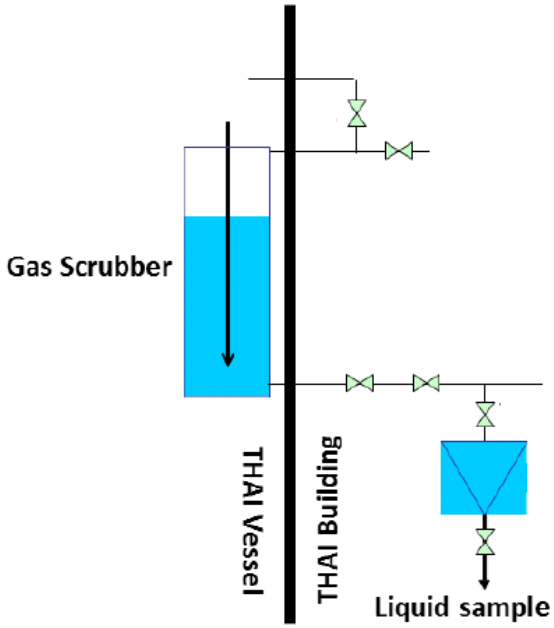

Figure III-5 *Gas scrubber principle(adapted from* (Schmidt-Naujok et al., 2013)*)*

c) Integral filters

In WH24 experiments (Freitag and Schmidt, 2017), the aerosol concentration was measured in the PAD vessel. In order to collect all aerosols leaving the vessel, a metal fibre filter is installed at the exhaust line (**Figure III-2**, right). These fibres are heated up to 200°C before they are placed in the exhaust line to capture only aerosols, and after a test phase is finished, the filter is leached into 5

L of decalcified water after dismantling. The resulting solute is then analysed for aerosol concentration measurement.

The three mentioned measurement techniques allow calculating the entrainment of water droplets based on the concentration of the solute. It was reported (Schmidt et al., 2015) that the GS and Integral filter show lower entrainment value than those obtained by SMPS. The reason might be related to the fact that SMPS is not designed to give results on the solute concentration mainly. GS and Integral filter allow calculating the entrainment directly from the concentration of the solute from equation **III.*4*** for steam air mixture.

D. COCOSYS nodalisation

COCOSYS nodalisation principle provide the possibility to discretise the most complex geometry to a much simpler one. The code recommends, for the accuracy of results to use lower spatial resolution and a smaller number of nodes.

The Thai Test Vessel (TTV) is simulated in COCOSYS by subdividing the vessel into 4 control volumes, 1 control volume for sump (R2_fluid) and 3 control volumes for the atmospheric part (R2_gas, R3 and R4). A control volume for steam or air-steam generation is also simulated for injection into the water pool (R1) and a control volume (R5) to simulate the off-gas and to keep a constant pressure as was the case in THAI experiments TH14 to TH17 and TH25 (**Figure *III-6***). The same nodalisation principle is applied to the PAD vessel for the WH24 tests.

The injection scenario depends on the tests. In THAI tests TH14 to TH17 and TH25, a quencher was used (**Figure *III-6***). In WH24, a downcomer pipe was used to inject gas into water pool (**Figure III-7**).

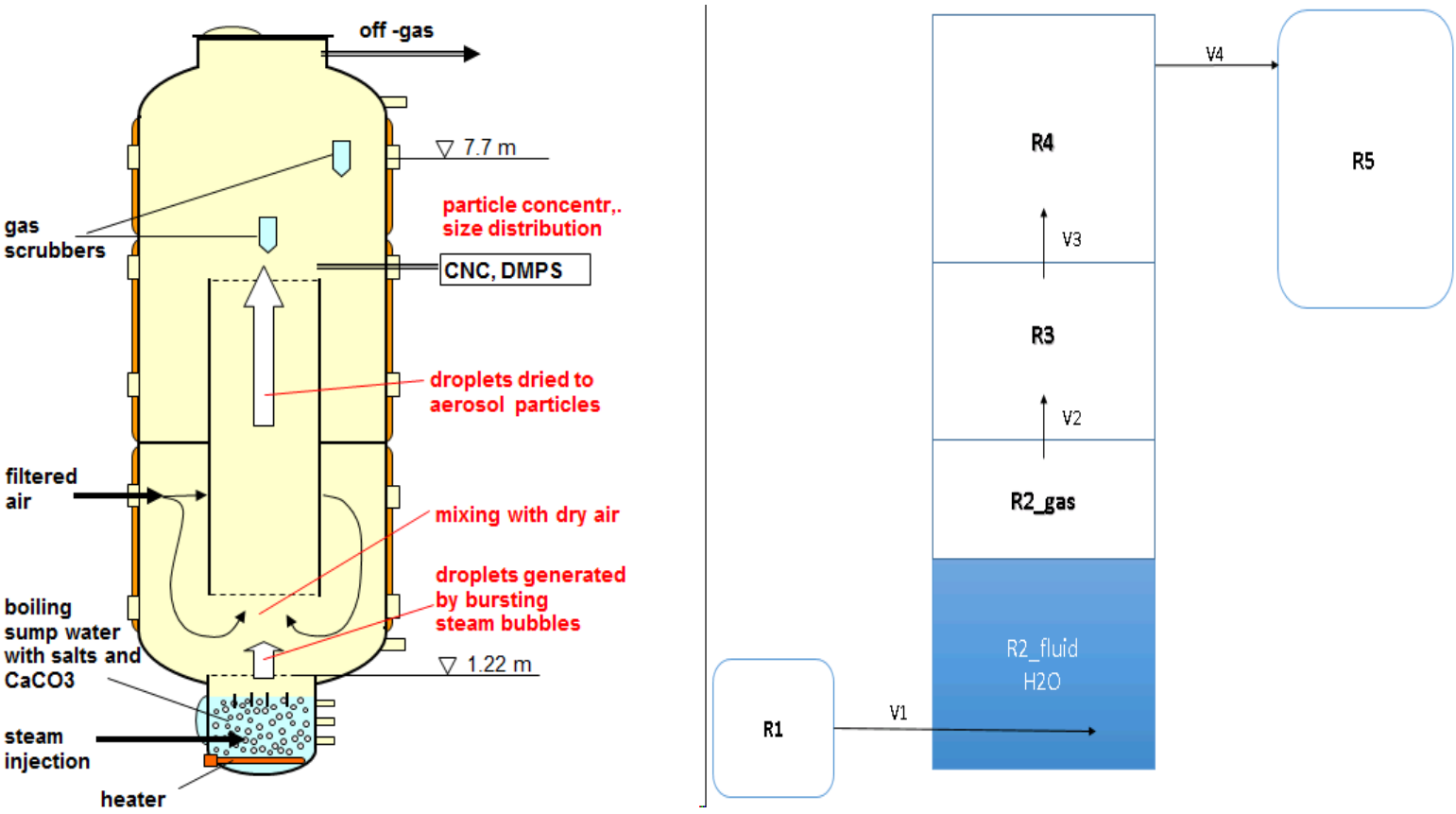

Figure III-6 *TTV vessel (left)*(Schmidt et al., 2015), *COCOSYS discretization of TTV (right)*

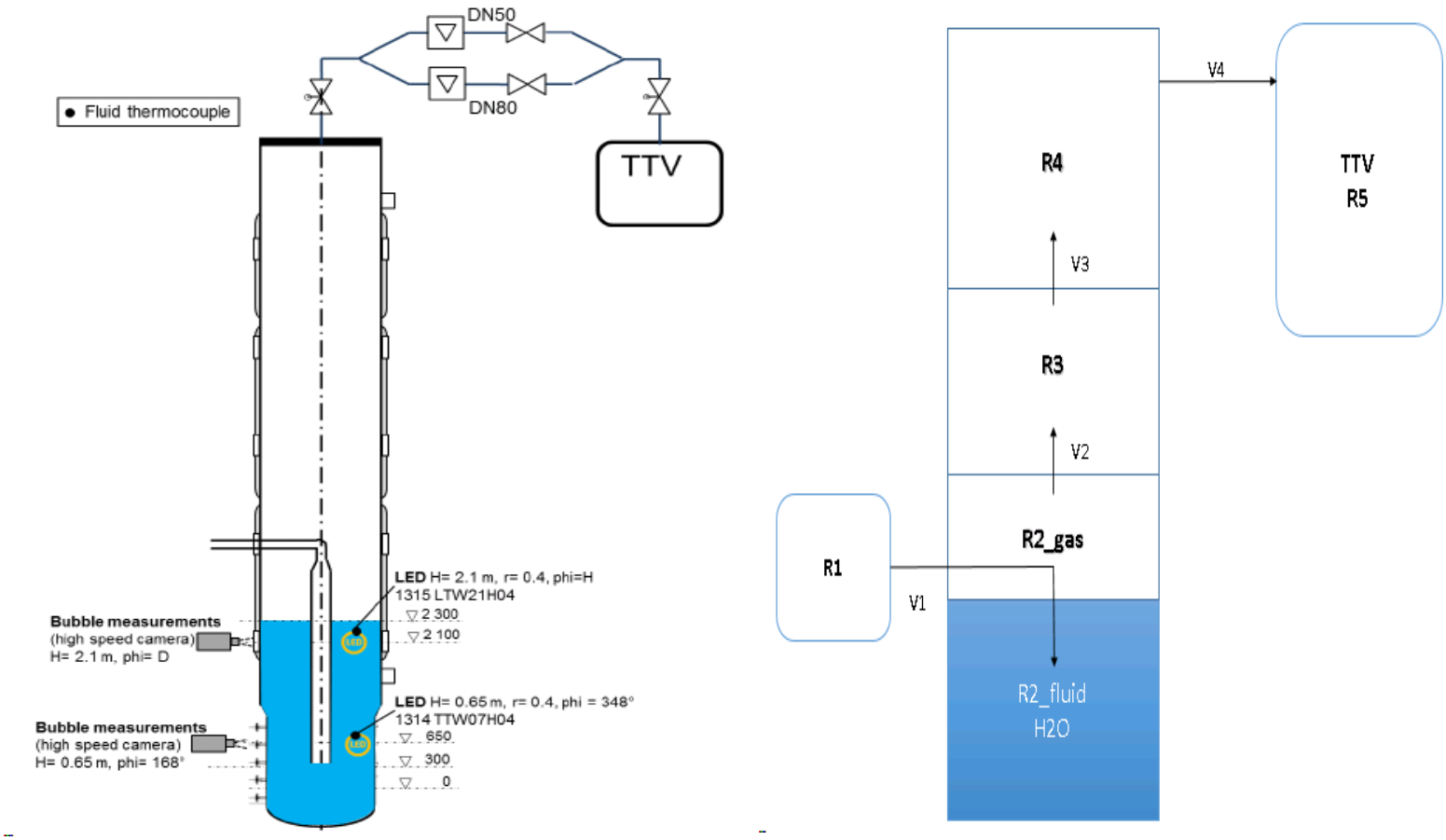

Figure III-7 *PAD vessel (left)*(Freitag and Schmidt, 2017),*COCOSYS discretization of PAD (right)*

The input and out parameters for the test phase TH14 through TH17, TH25 and WH24 are given below:

Table III-8 Input and Output parameter of COCOSYS simulations

COCOSYS Input parameter	COCOSYS output parameter
Water mass in the pool ***M*** **[Kg]** Water temperature ***T*** **[°C]** Gas composition (condensable or steam or mixture) Pressure and Temperature of the gas mixture ***P*** **[bar],** ***T*** **[°C]** Relative humidity **[%]** Gas or gas mixture mass flow rate $\dot{m}$ **[Kg/s]** Injection type (quencher or downcomer) Area of bubbling part of the pool ***A*** **[m^2]**	Entrainment factor ***E*** **[-]** Superficial gas velocity j_g **[m/s]**

For the depressurisation simulation, a valve was used to between R4 and R5 **(Figure III-7**) coupled with the junction.

E. Simulation results

The post calculation of the steady-state experiments have been done based on data from THAI (Schmidt et al., 2015), as well as the transient calculation (Freitag and Schmidt, 2017). The objective of this simulation is, first, to show the ability of COCOSYS in predicting the thermal-hydraulic of THAI tests, and second to show at what extent the RUB correlation is able to predict the entrainment.

The thermal hydraulics and aerosol fission product (RUB) works together as main modules, hence the first results to be presented are the thermal hydraulics, followed by the RUB results. As for thermal hydraulics code, only superheated condition are implemented, due to thermal-hydraulics module shortcoming to not being able to simulate the subcooled conditions.

Test phases TH14 through TH17, TH25, WH24a and WH24b have been conducted under boiling conditions and superheated atmosphere, thus the result of one test is sufficient for thermal-hydraulics (**Figure III-8**). Transient simulation (depressurization WH24 c) are presented in **Figure III-9**.

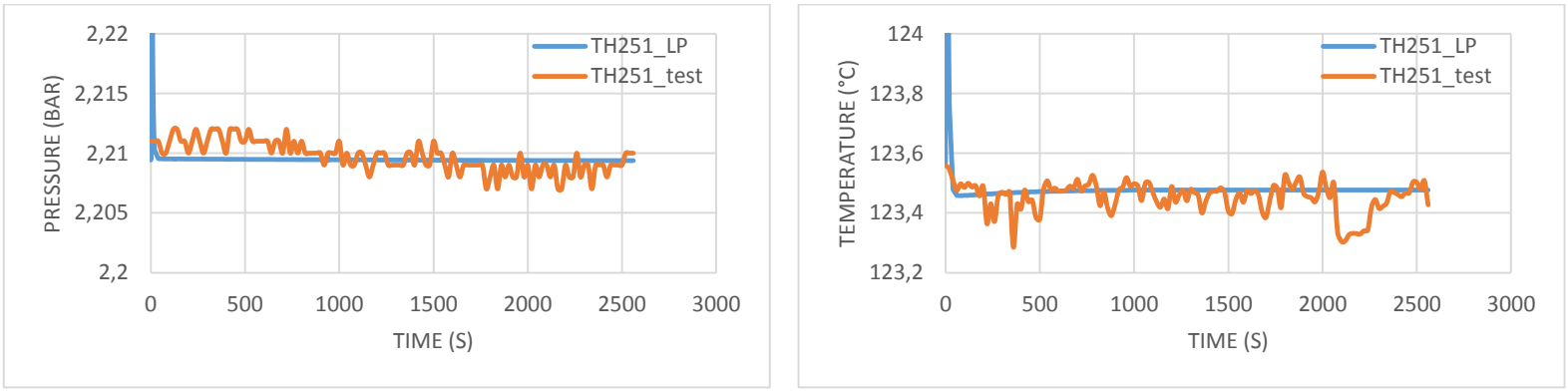

Figure III-8*Steady state simulation: Comparison between COCOSYS results and THAI data of vessel pressure and pool temperature*

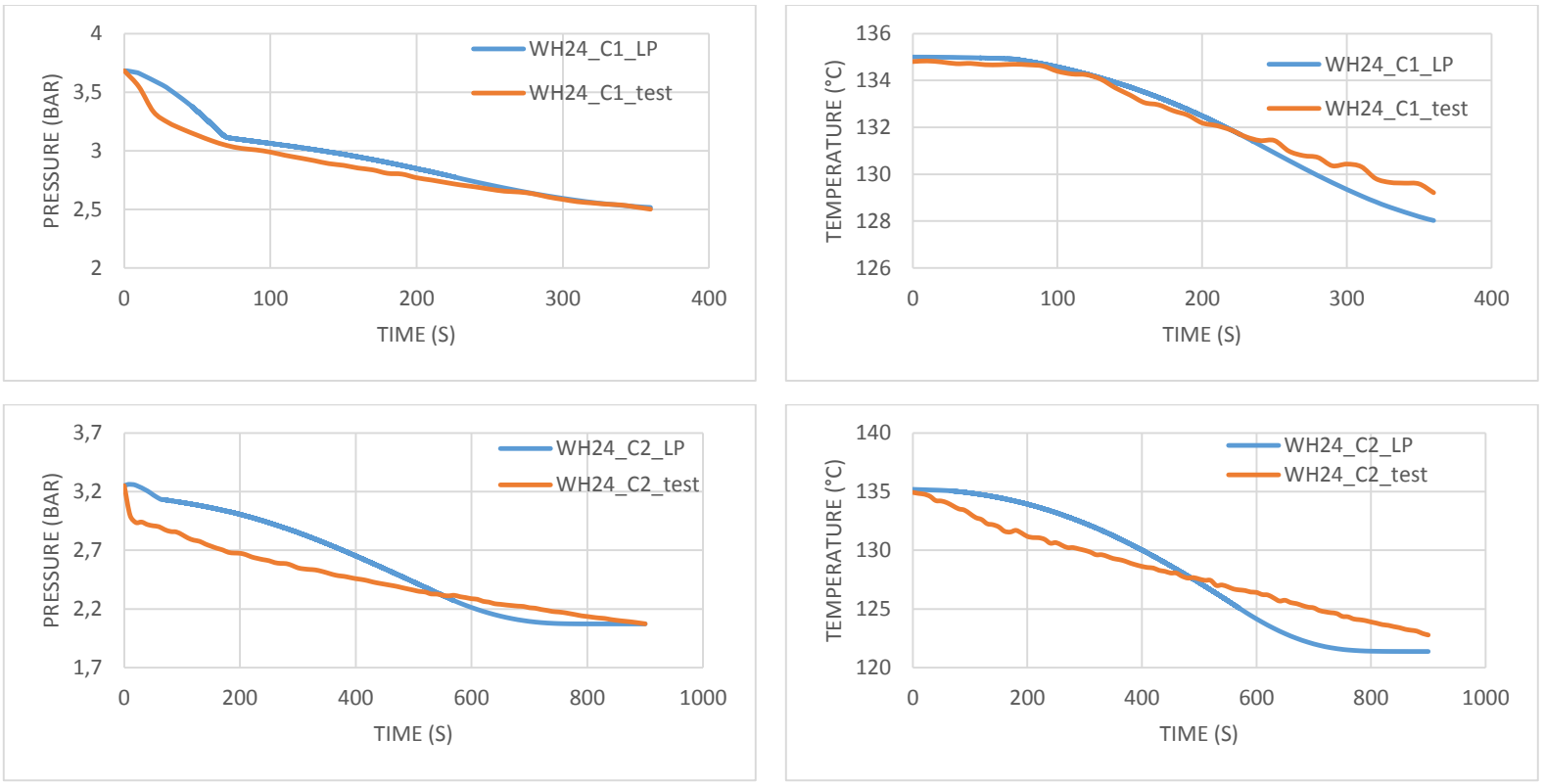

Figure III-9*Transient simulation results: Comparison between COCOSYS results and THAI data of vessel pressure and pool temperature*

Figure III-10 to **Figure III-14** show the entrainment measured from TH14, TH15, TH25 and WH24 tests data, and plotted against COCOSYS correlation (Dapper, 2009). THAI experimental data agree with COCOSYS results for steady state conditions, and the entrainment generally has the same order of magnitude that ranges from 10^{-6} to 10^{-4}, except for transient simulation (depressurization).

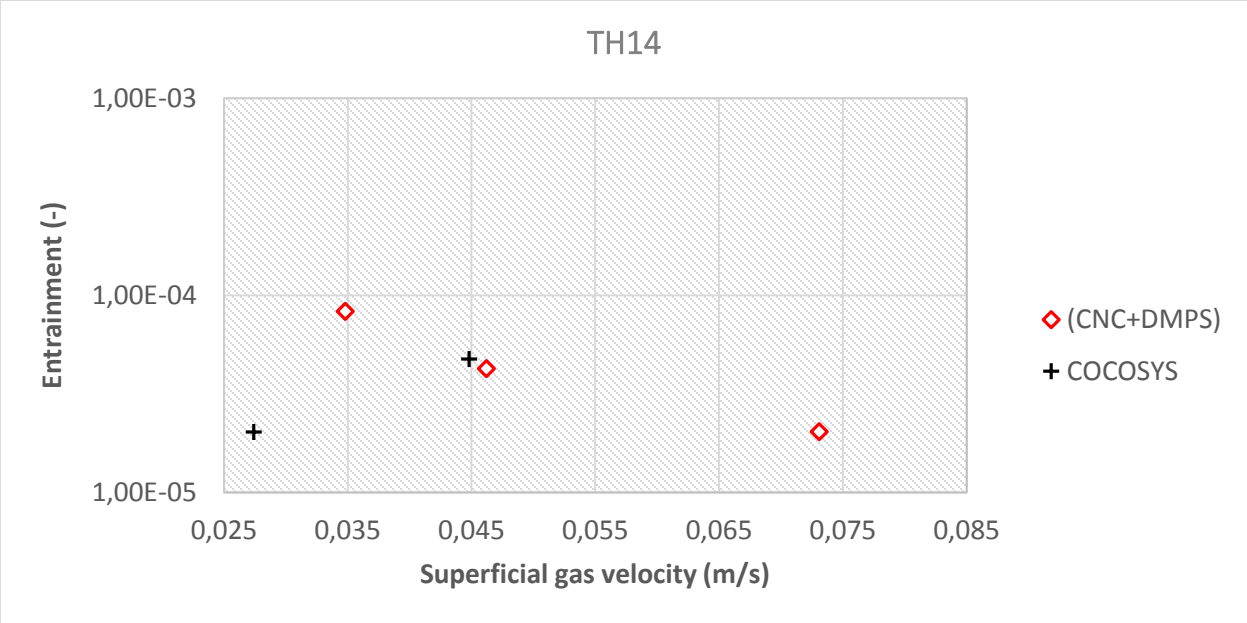

Figure III-10*Entrainment THAI TH14 test comparison with COCOSYS correlation*

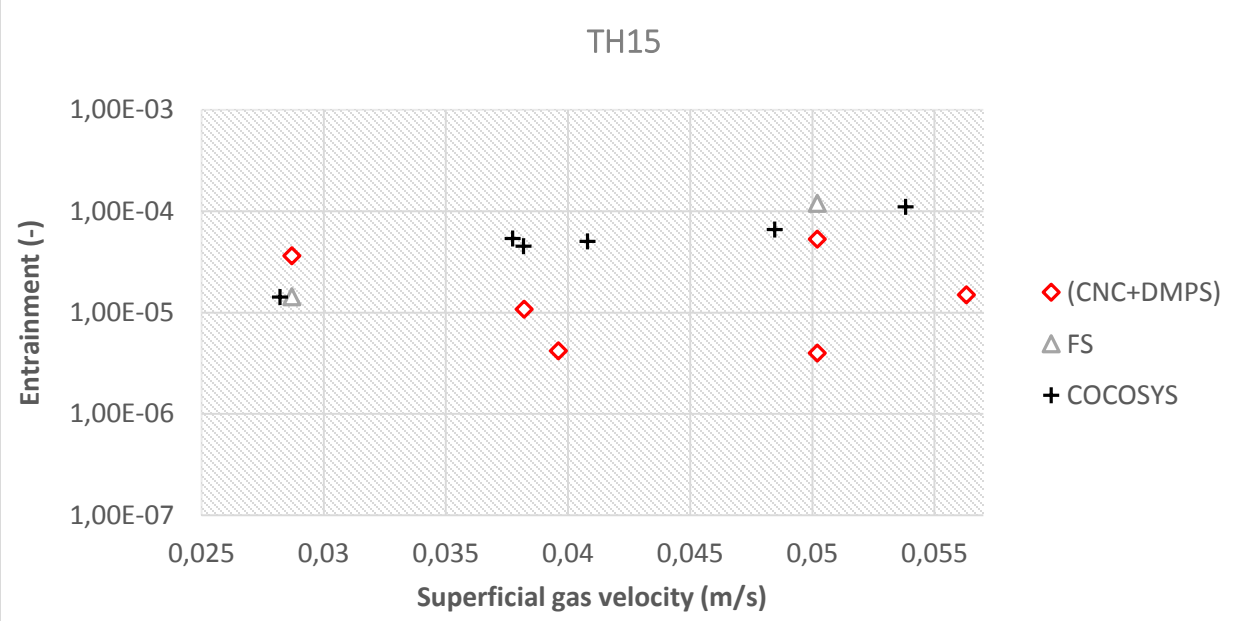

Figure III-11*Entrainment THAI TH15 test comparison with COCOSYS correlation*

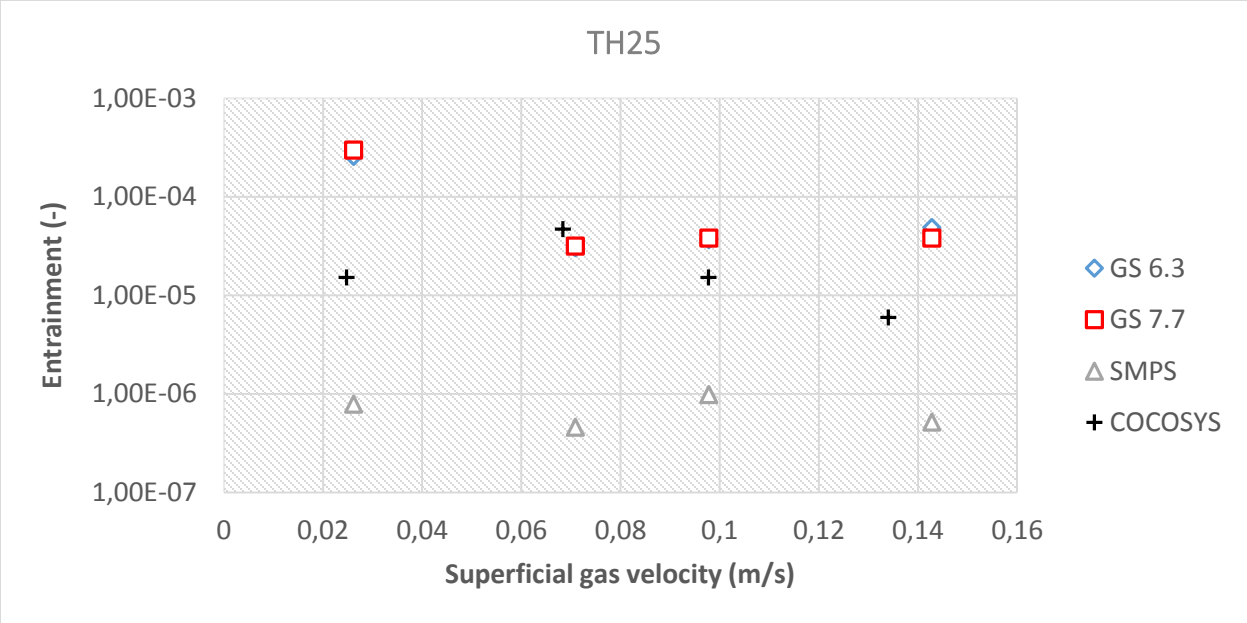

Figure III-12*Entrainment THAI TH25 test comparison with COCOSYS correlation*

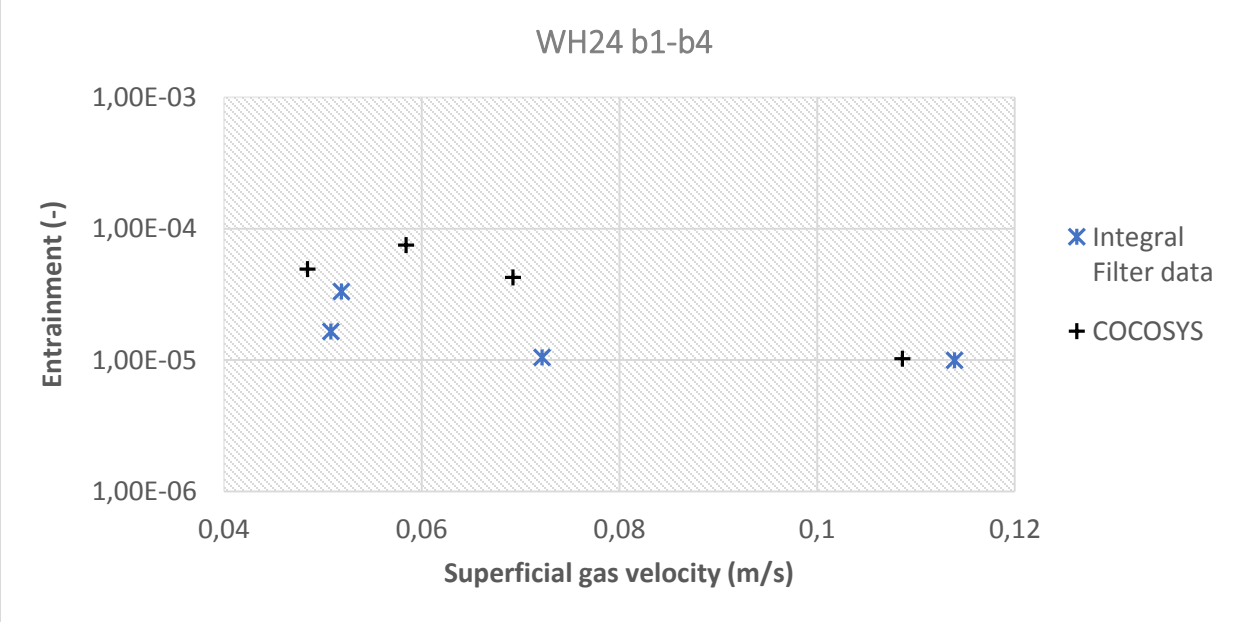

Figure III-13*Entrainment THAI WH24 b1 to b4 test comparison with COCOSYS correlation*

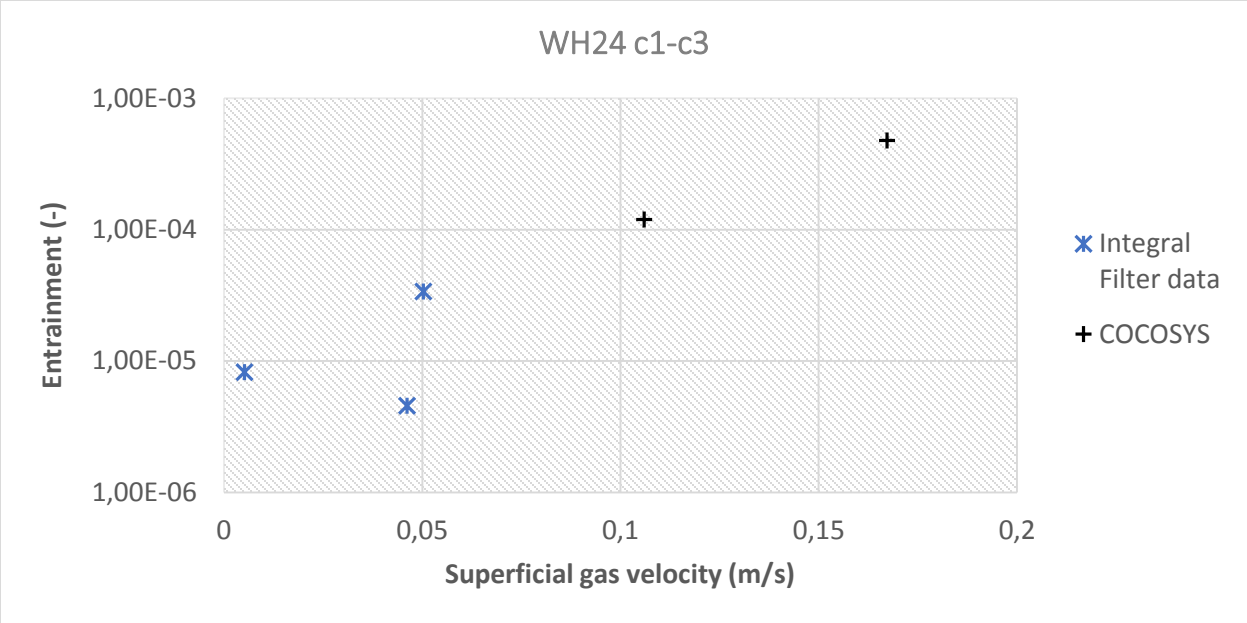

Figure III-14*Entrainment THAI WH24 c1 to c3depressurization test comparison with COCOSYS correlation*

As mentioned in Chapter 3, the superficial gas velocity is an output value, thus, the obtained value (numerical) is approximated to the exact value (experimental). In general, the error is small, and the uncertainty is a factor of one.

The entrainment in the experiments of THAI (Freitag and Schmidt, 2017), (Schmidt et al., 2015) TH14 through TH17, TH25 and WH24 take into account an uncertainty of factor of 2 to 5. The COCOSYS entrainment correlation showed efficiency in predicting the entrainment in TH14, TH15, TH25 and WH24 b1 through WH24 b4. In the experiment TH14 and TH15 (**Figure III-10** and **Figure III-11**), COCOSYS results have the same order of magnitude as THAI data. In the TH25 experiment (**Figure III-12**), COCOSYS results agree with the measurement conducted with the gas scrubber place at the locations 6.3 m and 7.7 m. However, SMPS measurements recorded entrainment values lower by 1 order of magnitude comparing to COCOSYS results. This disagreement might be related to the different functionalities of SMPS and GSs. As mentioned earlier in the entrainment measurement technique, the SMPS is designed mainly to record particle size distribution. Furthermore, the lower value might be due to low concentration obtained by CNC used to condensate the particle inside the SMPS. In the experiments WH24b1 through WH24b4,

agreement could be observed between COCOSYS results and the data from Integral filters, and the entrainment is 4.92E-5 for a superficial gas velocity of 0.048 m/s, increases to reach a maximum value of 7.52E-5 corresponding to superficial gas velocity of 0.058 m/s, and decreases to 1.03E-5 for superficial gas velocity of 0.108 m/s (**Figure III-13**).

COCOSYS correlation over predicts the entrainment under depressurization conditions (**Figure III-14**), and the entrainment tends toward 1E-3, while the Integral filters showed lower values by 2 to 3 order of magnitude from 7E-6 to 5E-5. The reason might be related to the fact that COCOSYS correlation does not include the effect of depressurization, since the correlation was developed using TH14 through TH17 data. These experiments was conducted under steady state conditions (constant pressure).

In **Figure III-15**, the entire set of THAI data and COCOSYS simulation results are plotted. Regarding the THAI data, it is reported (Freitag and Schmidt, 2017)(Schmidt et al., 2015) that even though large spreading between the measurements was identified within each of the test phases, two main trends can be identified:1) The entrainment increases for increasing superficial gas velocities as long as the two-phase flow can be attributed to the bubbly flow regime and the entrainment rate is constant, 2) or even slightly decreasing within the transition regime. Moreover, based on test data of WH-24 and literature findings(Bunz et al., 1992)(Freitag and Schmidt, 2017) a noticeable uncertainty should be considered with respect to the entrainment rate value at given superficial gas velocity.

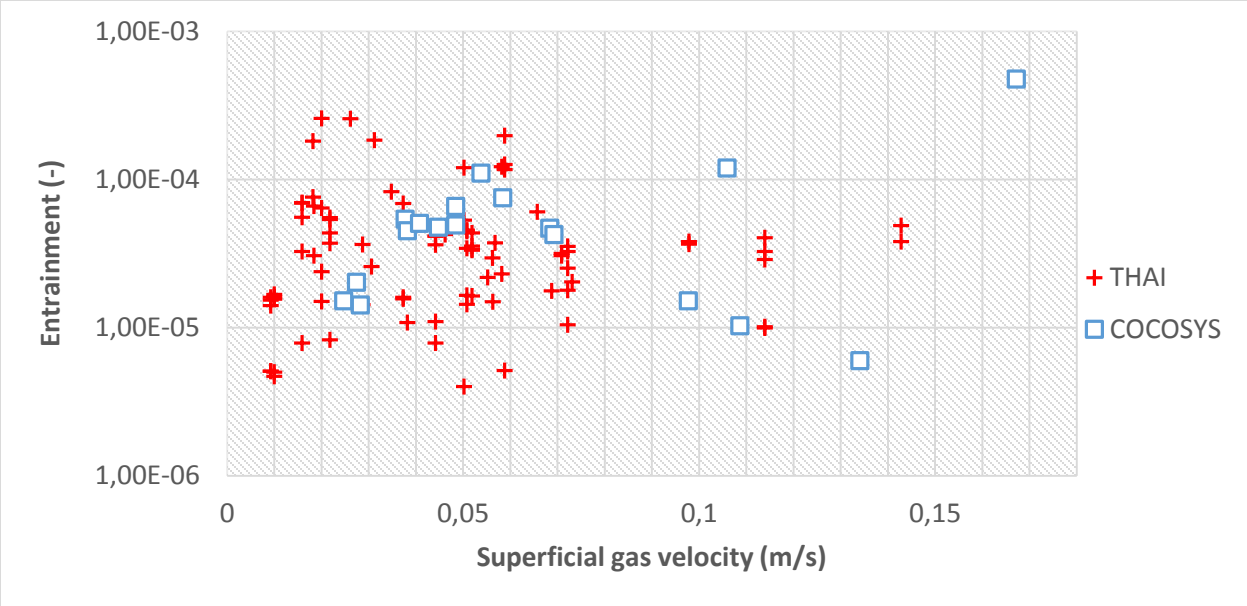

Figure III-15*THAI data (TH14, TH15, TH16, TH17, TH25 and WH24) and COCOSYS results*

As could be noticed, the entrainment in **Figure III-15** only covers short range of superficial gas velocity from 0 to 0.14 m/s conforming to a bubbly flow regime and the transition regime to churn turbulent flow regime. Which defines the main shortcoming of the COCOSYS correlation, plus the effect of depressurization. Churn turbulent flow regime was unachievable in the experiments series of THAI, however, it exist large amount of data in the open literature that covers entrainment as a function of superficial gas velocities in churn turbulent flow regime. Nevertheless, in the experiment conducted by different authors, the entrainment was quantified at different height, and different vessel geometries. As for the vessel diameter, from 0.19 m diameter is the value where only two flow regimes could be observed as a function of superficial gas velocity, which are bubble flow regime and churn turbulent flow regime. Less than 0.15 m pool diameter, which is attributed to the categories of small diameters, at high gas flow rates, bubble slugs begin to appear (Shah et al., 1982). The height above the water pool affect the entrainment noticeably as discussed in Chapter 2. The entrainment decrease as the distance above the water pool increase due to turbulent diffusion. In the next section, an empirical correlation that includes the bubbly flow, transition and churn turbulent flow regimes using data from the open literature is proposed.

IV. Current correlation development

In this section, we provide an empirical correlation that predicts the entrainment using data from the open literature for bubbly flow regime, transition regime and churn turbulent flow regime. Soluble and insoluble tracers was used in the experiments used to develop the present correlation.

Figure IV-1 represent the entrainment as a function of the ratio (j_g^*/h^*) for various vessel diameter. At the first sight, it can be noticed that the entrainment increases as the ratio increases. The redundancy on data could be explained as follows: Garner (Garner et al., 1954), Golub (Rozen et al., 1970), Kim (Kim, Hyun and No, Cheon, 2005) and Zhang (Zhang et al., 2016) and Lebel et al. (Lebel et al., 2020) conducted experiments at small heights above the water pool while the experiments of THAI (Freitag and Schmidt, 2017), Cosandey (Cosandey, 1999), REST (Bunz et al., 1992), REVENT (Müller and von Rohr, 1997) and ALPHA (Kudo et al., 1994), where the entrainment was measure at least at 1.3 m above the water pool (Kudo et al., 1994) to approximately 8 m (Freitag and Schmidt, 2017). The experiments of Golub used low superficial gas velocity and high swell level (two phase flow level), while Kim, Zhang, Garner used high superficial gas velocity and low swell level. To plot these data only as a function of superficial gas velocity will not be as accurate as including the height above the water pool. For this purpose, the entrainment is plotted against the ratio (j_g^*/h^*) .

With $j_g^* = j_g/\left(\frac{\sigma g \Delta\rho}{\rho_g^2}\right)^{1/4}$ and $h^* = h/\sqrt{\frac{g\Delta\rho}{\sigma}}$.

The dimensionless form of the superficial gas velocity and the distance above the water surface are used to take into account the thermal hydraulics condition of the system. Therefore, a reference value is set for a specific thermal hydraulics condition. For the dimensionless superficial gas velocity, the reference value is define as $j_{g,c} = \left(\frac{\sigma g \Delta\rho}{\rho_g^2}\right)^{1/4}$ (Wallis, 1970). Similarly for the distance above the water pool, the reference value is $h_c = \sqrt{\frac{g\Delta\rho}{\sigma}}$.

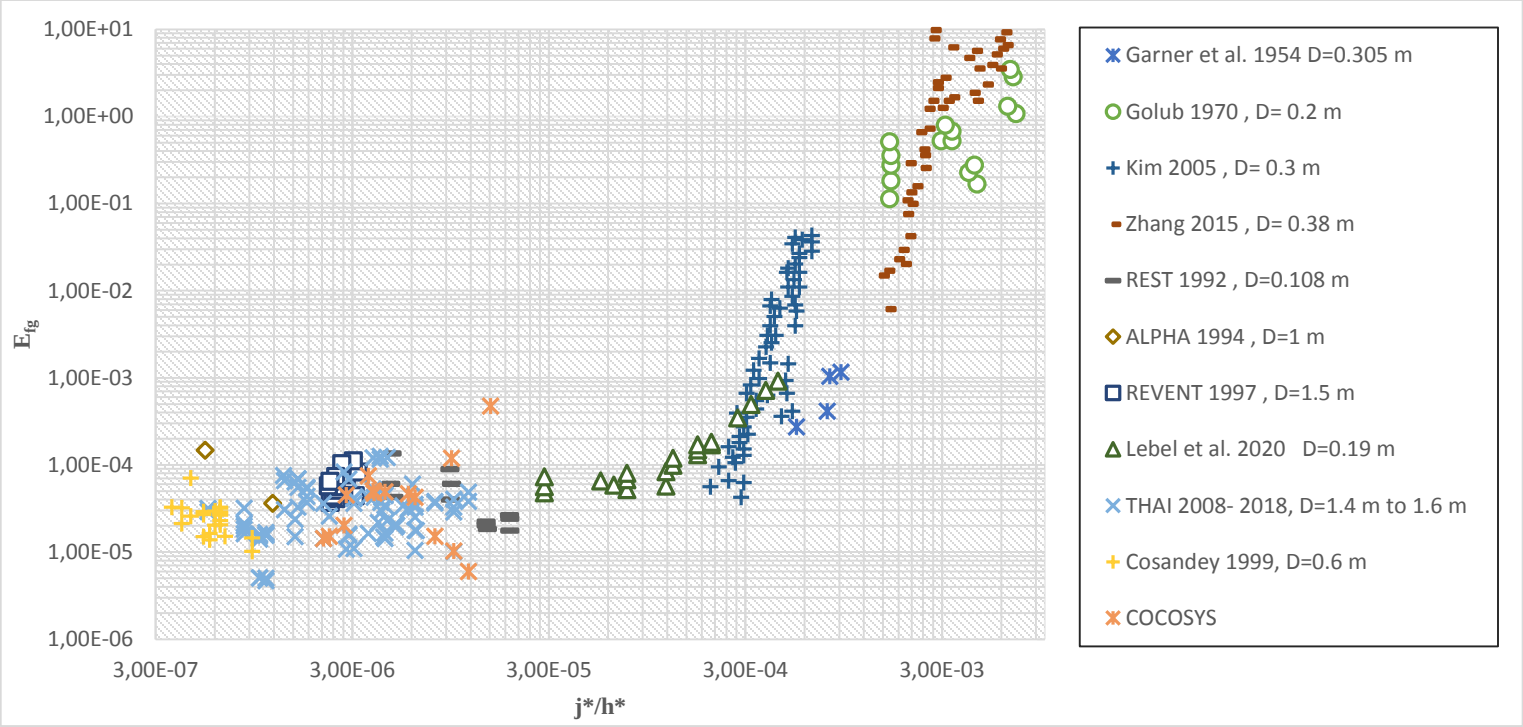

Figure IV-1 *Comparison of Entrainment data for different geometries*

The scatter of data in **Figure IV-1** could be attributed to differences in the experimental setups used by various authors, including the pool diameter and measurement techniques. In the experiments of THAI (Freitag and Schmidt, 2017), the scatter might be due to the used of several measurement technique that included GSs, SMPS, Integral filters and Cascade Impactors. Each of these measurement methods have different principle, which might yield different entrainment measurements. Even though, the trend as mentioned earlier could defined (Freitag and Schmidt, 2017).

Differences of the condition of the sump where some experiments did not use tracers to calculate the entrainment (Kim and No, 2005)(Golub, 1970)(Zhang et al., 2016). Garner (Garner et al., 1954) for instance used steam to inject gas into water pool and a 0.3 m vessel diameter. In order to calculate the entrainment, he used high concentrations of Potassium Nitrate of about 165 g/L as well as pure water, and gas velocity up to 1.2 m/s (churn turbulent flow regime). Even though the entrainment was in the same order of magnitude as the entrainment calculated by (Lebel et al., 2020). This might be related to the high pool concentration with limit the ability to produce droplet, due to particles agglomeration at the surface of the pool(Wei et al., 2020). Moreover, the use of

steam as gas to produce bubble might influence the bubble size by condensing or evaporating. Furthermore, the scatter might be related to the bias from how the measurements of the aerosol concentrations were carried out (Lebel et al., 2020).

In water pools, the entrainment is a strong function of the hydrodynamics. As long as the flow regime is bubbly, the entrainment increase with increasing gas velocity, and begin gradually to decrease as the gas velocity increases in the transition regime to the churn turbulent flow. As can be noticed, the entrainment in the experiment of (Freitag and Schmidt, 2017), (Bunz et al., 1992), (Müller and von Rohr, 1997), (Kudo et al., 1994) and (Cosandey, 1999) begins from 9E-6 to a maximum of 1.5E-4 and decrease to approximately 2E-5. This increase and decrease is strongly related to the behaviour of the bubbles at the surface. In order to describe this effect, an empirical correlation is introduced to calculate the entrainment as function of the ratio j_g^*/h^*.

A. Bubbly flow regime

This flow regime is characterized by the formation of quasi-uniform bubbles of typical size of 2 mm in the water pool. As they rise toward the surface, coalescence might occur between bubbles to form bigger one (**Figure IV-2**). Bubble coalescence is not a common phenomenon in bubbly flow regime at the surface, however it might occur occasionally.

The gas velocity to create such bubbles is 0.05 m/s (Shah et al., 1982).

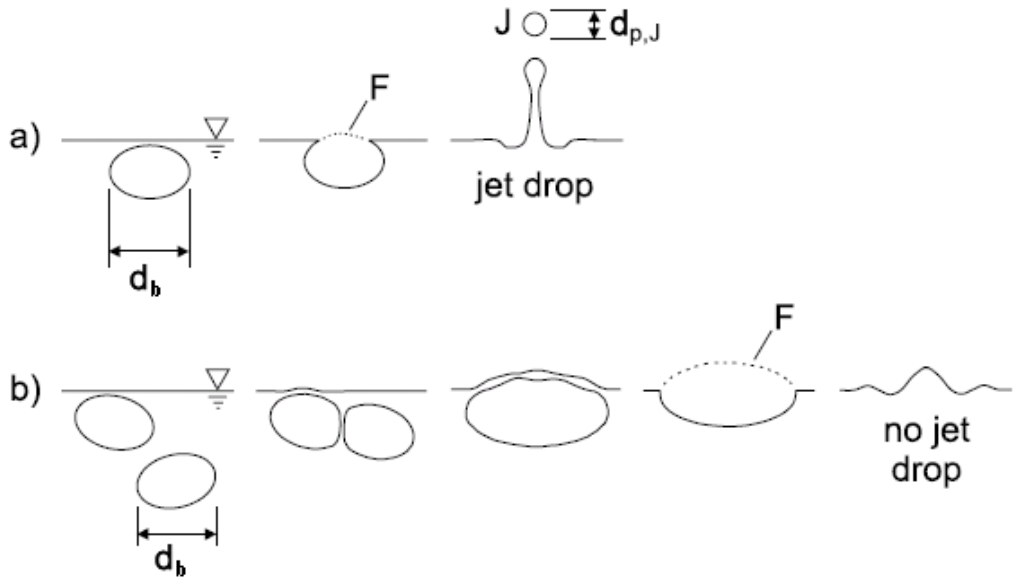

Figure IV-2 *Difference in the breakup mechanism for a single (a) and multiple (b) bubbles due to coalescence (figure adapted from* (Günther et al., 2003)*)*

The experiments of THAI (Freitag and Schmidt, 2017) , Cosandey (Cosandey, 1999), and REVENT (Müller and von Rohr, 1997) provide data for this range of superficial gas velocity. As shown in the figure below, the entrainment increase slightly with an exponential fit to reach a maximum value of 1.2E-04 which corresponds to a ratio j^*/h^* =3.4E-6.

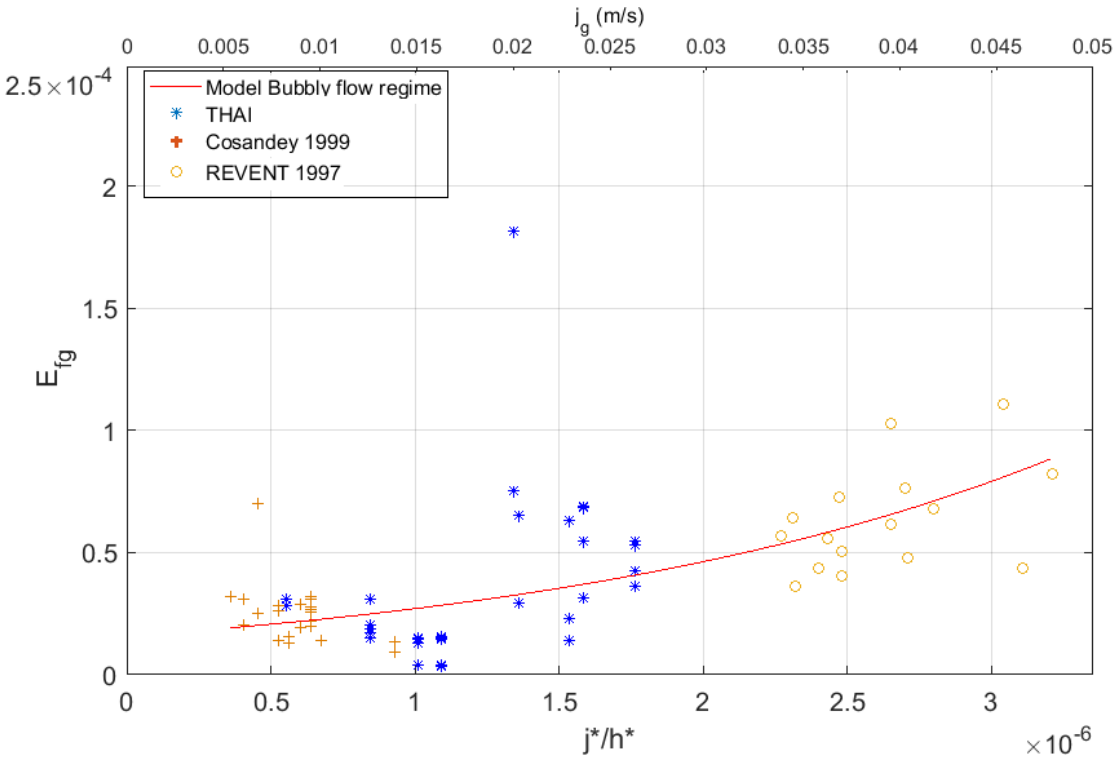

Figure IV-3*Entrainment correlation for Bubbly flow regime*

The correlation for this flow regime has the following form:

$$E_{fg} = \gamma_1 . \exp(\gamma_2 . \frac{j^*}{h^*}) \qquad \text{IV.1}$$

For superficial gas velocity values less than 0.05 *m/s*, corresponding to a ratio j^*/h^*=3.4E-6 and a height from *h*=3 m to *h*=8 m above the water surface, the coefficients of equation *IV.1* (**Table IV-1**) are calculated via nonlinear regression analysis, with the goodness of fit of R^2=0.525. The scatter of data has an impact on the R^2 value, with a value 1 denoting a perfect fit without scatter:

Table IV-1 *Correlation constants for bubbly flow regime*

condition	γ_1	γ_2
j< 0.05 m/s and j^*/h^*=3.4e-6	1.576e-5	5.353e+5

The entrainment in the THAI facility was measured at h = 8 m, while Cosandey (Cosandey, 1999) measured the entrainment at h = 3 m. At such heights, the entrainment corresponds to the entrainment in the "deposition region"(Kataoka and Ishii, 1984).

B. Transition regime

This flow regime is the transition from bubbly flow to churn turbulent flow regime. It is also referred as the heterogeneous flow regime due to the formation of bubble of different sizes. Such bubbles can reach a size of 5 mm in the water pool, and when reaching the surface, larger bubble might be formed due to coalescence(Shah et al., 1982)(Ruzicka et al., 2001). Coalescence might also occur inside the pool.

The data used to develop the correlation is from REST (Bunz et al., 1992) and THAI (Freitag and Schmidt, 2017)(Schmidt et al., 2015).

The entrainment decreases smoothly from 1.4e-4 (j^*/h^*=3.4E-6) to a minimum value of 2.5e-5 (j^*/h^*=1.9E-5) which corresponds to superficial gas velocity of 0.1 m/s (**Figure IV-4**).

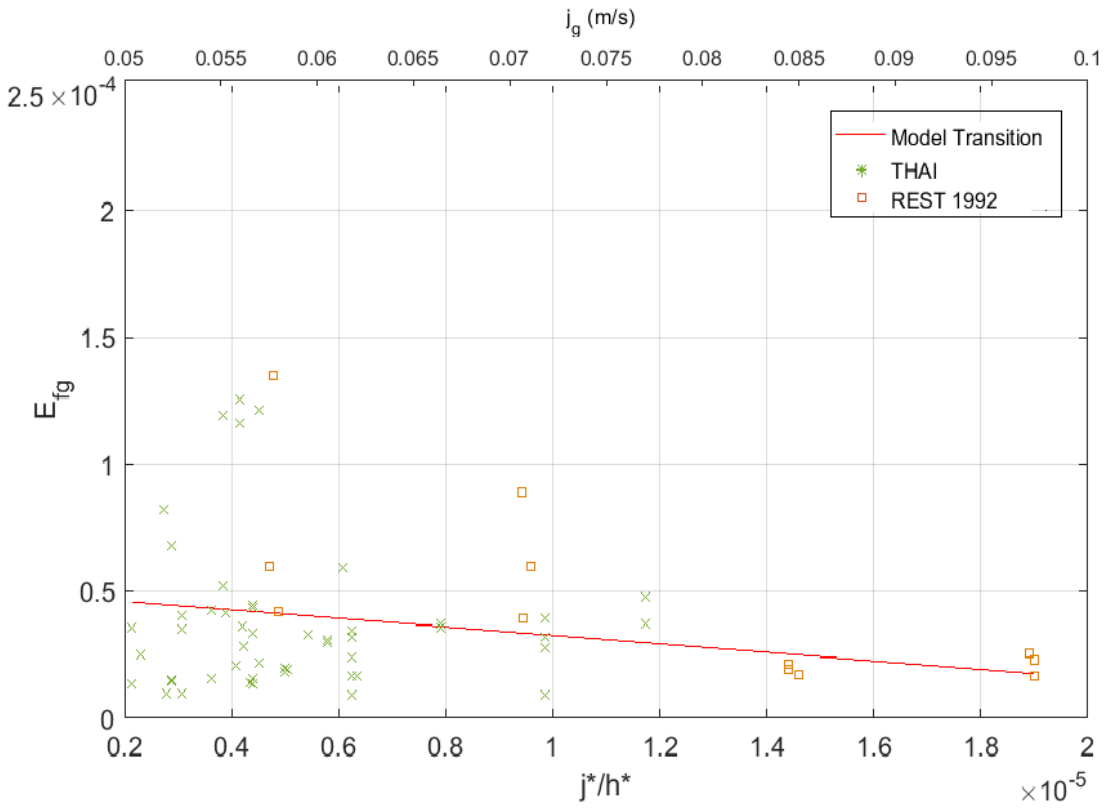

Figure IV-4 *Entrainment correlation for Transition regime*

The correlation for this flow regime is described by a linear function with a negative slope:

$$E_{fg} = \gamma_3 . \frac{j^*}{h^*} + \gamma_4 \qquad \text{IV.2}$$

For superficial gas velocity 0.05 *m/s*< j_g < 0.1 *m/s* corresponding to a ratio 3.4E-6 <j^*/h^*< 1.9E-5, the coefficients of equation IV.2 are calculated with the goodness of fit of R^2 = 0.570 (**Table IV-2**):

Table IV-2 *Correlation constants for Transition regime*

condition	γ_3	γ_4
0.05 m/s <j_g < 0.08 m/s 3.3e-6 < j^*/h^*< 1.9e-5,	-6.666E-6	4.019E-5

Based on test data of WH-24 and literature findings(Bunt et al., 2015), a noticeable uncertainty should be considered with respect to the entrainment rate value at given superficial velocity. In THAI experiments, this uncertainty was a factor of 2 to 5.

C. Churn turbulent flow regime

This regime occurs after the transition regime, with superficial gas velocity value above 0.1 *m/s*. Unsteady flow pattern with channelling occurs in the water pool and the main characteristics of this regime is the formation of large pockets of gas accompanied by small bubbles. Also, this flow regime is marked by the extreme high agitation of the surface of the pool (Shah et al., 1982)(Ruzicka et al., 2001).

The data supporting this flow regime was obtained from the open literature, and are up to date (Lebel et al., 2020),(Kim and No, 2005),(Zhang et al., 2016),(Garner et al., 1954),(Golub, 1970). **Figure IV-5** shows the correlation for churn turbulent flow.

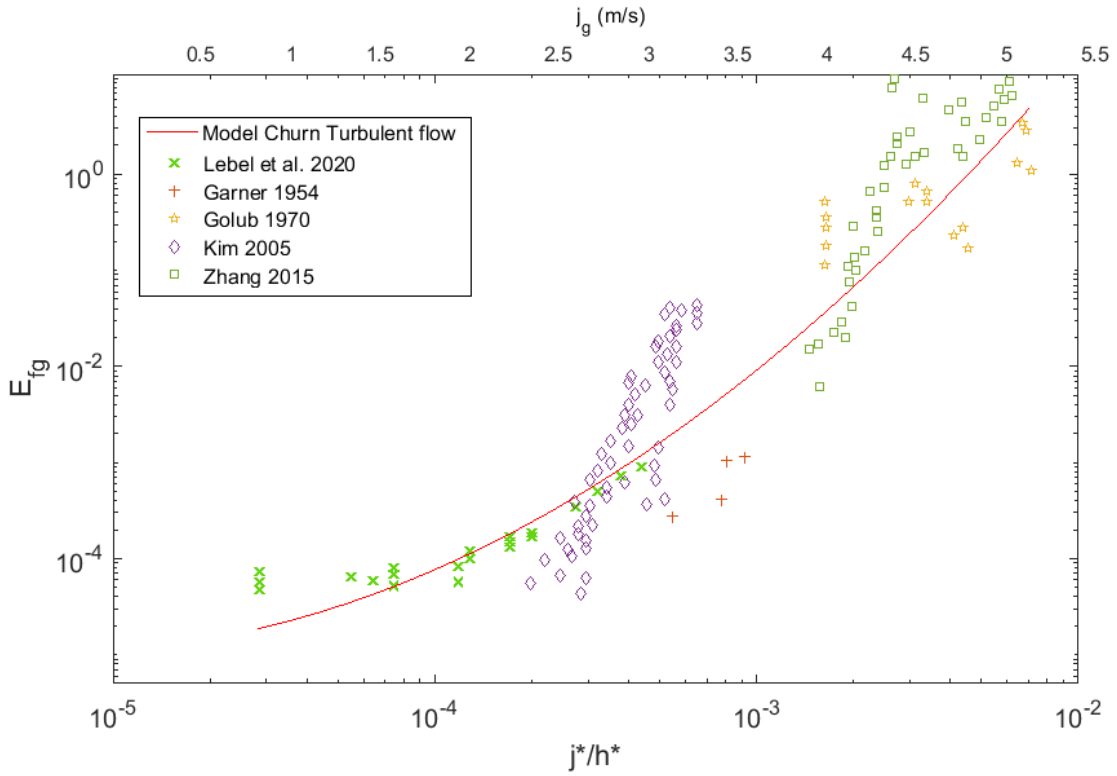

Figure IV-5 *Entrainment correlation for Churn Turbulent flow regime*

In **Figure IV-5**, as the entrainment ranges from 4E-5 to 10, a double logarithmic scale has to be used to cover the complete range in this flow regime. As shown in the figure, the entrainment increase sharply as a function of the ratio j^*/h^*, and the correlation follows the trend of the data. The correlation is described by a nonlinear function and has the following form:

$$E_{fg} = \gamma_5 * \left(\frac{j^*}{h^*}\right)^{\gamma_6} \qquad \text{IV.3}$$

For superficial gas velocity above 0.1 *m/s* corresponding to a ratio j^*/h^*=2E-5, the coefficients of equation IV.*3* are calculated with the goodness of fit of R^2=0.874 (**Table IV-3**):

Table IV-3*Correlation constants for Churn Turbulent flow regime*

Condition	γ_5	γ_6
0.1m/s <j_g 2E-5 <j^*/h^*	1.22e+7	4.748 to 7.838

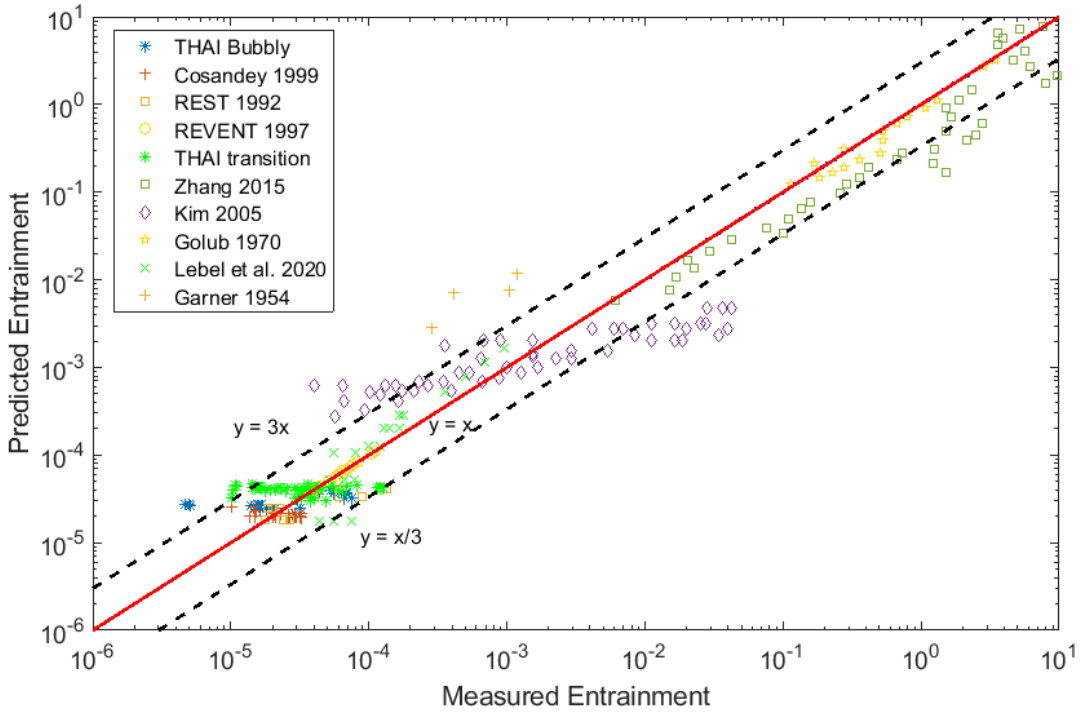

Figure IV-6 *Comparison of the calculated (current correlation) and measured entrainment* ((Lebel et al., 2020),(Kim and No, 2005),(Zhang et al., 2016),(Garner et al., 1954),(Golub, 1970),(Bunz et al., 1992)(Müller and von Rohr, 1997),(Cosandey, 1999))

In

Figure IV-6 the predicted and measured entrainments are compared for the complete range of regimes. As it shows, there is a fair agreement between the predictions and the experimental data (Lebel et al., 2020),(Kim and No, 2005),(Zhang et al., 2016),(Garner et al., 1954),(Golub, 1970),(Bunz et al., 1992),(Freitag and Schmidt, 2017) ,(Müller and von Rohr, 1997),(Cosandey, 1999). The scatter on both sides of the y=x line can be explained by the large standard deviation of the entrainment from experimental data.

In conclusion, the empirical correlations obtained by equations IV.*1* through IV.*3* allows the prediction of entrainment for bubbly flow regime, the transition regime and churn turbulent flow regime for heights above the water pool up to 8 m (Freitag and Schmidt, 2017). The correlation could be summarized as follows:

$$E_{fg} = \begin{cases} \gamma_1 . \exp\left(\gamma_2 . \frac{j^*}{h^*}\right) & 0 < j_g \leq 0.05\ m/s \\ \gamma_3 . \frac{j^*}{h^*} + \gamma_4 & 0.05 m/s < j_g \leq 0.1\ m/s \\ \gamma_5 * \left(\frac{j^*}{h^*}\right)^{\gamma_6} & j_g > 0.1\ m/s \end{cases} \quad \text{IV.4}$$

In the next section, a discussion follows in support of the current empirical correlation by analysing the dynamics of the bubbles, and the ability of such bubbles to produce droplets.

D. Discussion

In this section, the present empirical correlation is discussed as a function of the trends against experimental data. Large amount of data to validate the model are available as mentioned in the previous section on entrainment of droplets for bubbly flow, transition and churn turbulent flow regime.

In this work, in order to calculate the entrainment and compare different results from previous data set, it was found that the ratio of the dimensionless superficial gas velocity to the dimensionless height above the water pool is the adequate independent variable that can be used to take into account the flow regime and the geometry effect.

The main objective of this section is to show the order of magnitude of different results and to support the current model by physical facts.

1. Experiments with Bubbly flow regime

Figure IV-3 shows the entrainment correlation using data of THAI, Cosandey, and REVENT experiments for bubbly flow regime. The entrainment varies between a minimum value of 1E-6 and a maximum value of 1.2E-4. The range of gas velocity used by Cosandey is from 0.0008 m/s to 0.0044 m/s, whereas THAI covered the full range of gas velocity for bubbly flow regime (from

0 to 0.05 m/s). The Cosandey's experiments (Cosandey, 1999) were conducted under slow depressurization conditions from 6 bar to 2 bar. The bubble size measured in such conditions was about 2 mm. Similarly, the bubble size was about 2 mm in the REVENT experiments where a small range of superficial gas velocity from 0.009 m/s to 0.01 m/s was imposed. The characteristics of such flow regime is that the bubbles in the water pool could be assumed to be uniformly sized (Shah et al., 1982). When reaching the surface, these bubbles produce two families of droplets which eventually could be entrained by the gas coming out: film droplets coming from the cap, and jet drops coming from the crater formed after the bubble burst (Donald E Spiel, 1998). The film droplets size (order of 10 micron) is much smaller than the jet drops (order of 100 micron). These two families of droplets contributes noticeably to the entrainment (Garner et al., 1954)(Donald E. Spiel, 1998)(Blanchard and Syzdek, 1988).

It is reported (Freitag and Schmidt, 2017) that large scatter between the measurements was identified and two main trends could be identified: 1) The entrainment increases for increasing gas velocity as long as the two phase flow in the water pool can be attributed to the bubbly flow regime, and 2) the entrainment is constant or even slightly decreases within the transition regime. The trend of the model for the transition regime is presented below this subsection.

For an air-water system, the bubble size increase with increasing gas velocity as investigated by (Jamialahmadi and Muller-Steinhagen, 1990) as shown in **Figure IV-7**. The bubble size is constant for superficial gas velocity up to approximately 4 cm/s, and then the bubble size increases as the superficial gas velocity increases further. Expect the correlation of Akita and Yoshida (Akita and Yoshida, 1974), it contradicts the this trend (**Figure IV-7**). The reason given by (Jamialahmadi and Muller-Steinhagen, 1990), is that the correlation of Akita and Yoshida is limited to single orifice spargers (Shah et al., 1982).

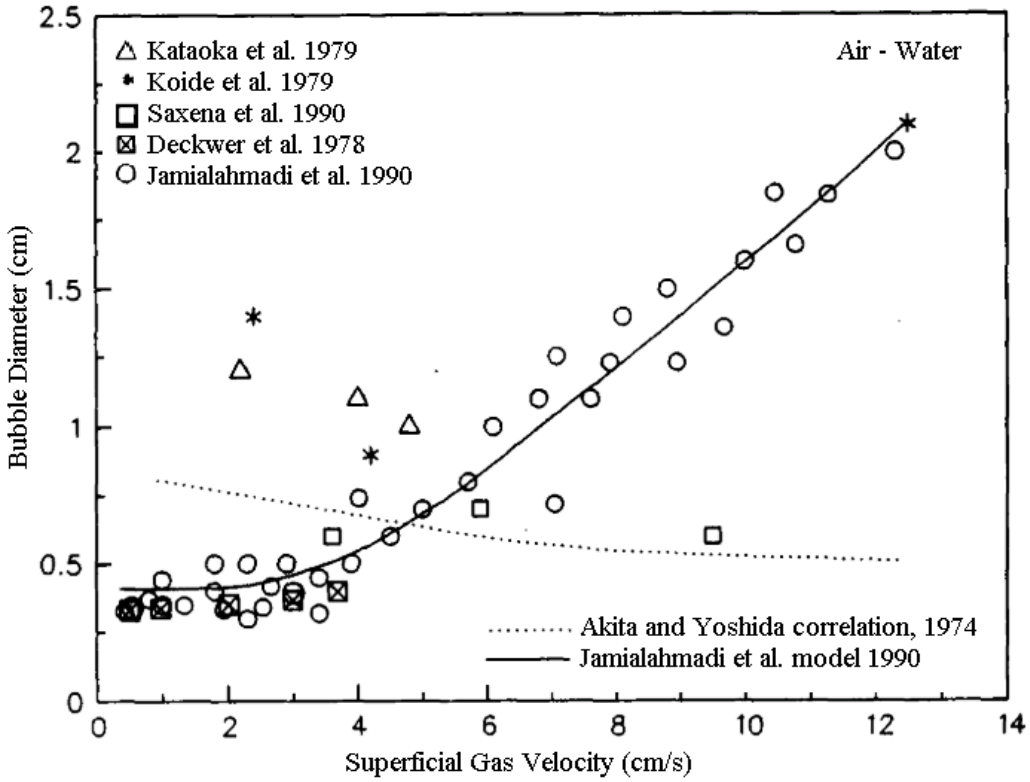

Figure IV-7 *Bubble size as a function of Superficial gas velocity* (Jamialahmadi and Muller-Steinhagen, 1990)

In the experiments of THAI (Freitag and Schmidt, 2017), for low gas velocity range from 0 to 0.05 m/s (bubbly flow regime), the bubble average bubble size was from 1.5 mm to 3 mm, which is consistent with values in **Figure IV-7**. It is necessary to know at what extent this bubbles size – superficial gas velocity dependence should be applied. Therefore, the effect of thermal-hydraulics, and physical properties of the gas-fluid should be taking into account.

The pressure in the experiments used to develop the current correlation for bubbly flow regime is from 2 bar to 6 bar. At this range of pressure, the bubble size distribution is affected slightly compared to bubbles submitted to very high pressure (Cosandey, 1999). Cosandey (Cosandey, 1999) noticed a decrease in entrainment measurement by a factor of 2 when decreasing the pressure from 6 bar to 2 bar, however this decrease is in the range of uncertainty. Nevertheless, the effect of pressure on bubbly size distribution is substantial at very high pressures as discussed earlier (Lin et al., 1998). In bubbly flow regime (j_g< 0.05 m/s), at pressure up to 6 bar (Cosandey, 1999),

bubbles have the ability to produce film and jet droplets. The production of film droplets is at its peak (Blanchard and Syzdek, 1988) (**Figure II-21**, right), however, fewer jet droplet are produced comparing to smaller bubble size (Koch et al., 2000) (**Table II-6**) (**Figure II-21**, left).

The production of droplet from film cap and the jet were also investigated by (Günther et al., 2003) for low superficial gas velocity similar to bubble flow condition of (Cosandey, 1999) producing bubble of around 2.98 mm diameter, from a sparger in a 100 mm diameter pool. The investigation mainly conducted by (Günther et al., 2003) aimed to compare the droplets production from single bubble against multiple bubbles (bubbly flow regime). The main outcome of their experiments was that the number of droplets (jet and film) produced by multiple bubbles was less than the number produced by a single rising bubble (discrete bubbles one after another) as shown in **Figure IV-8**.

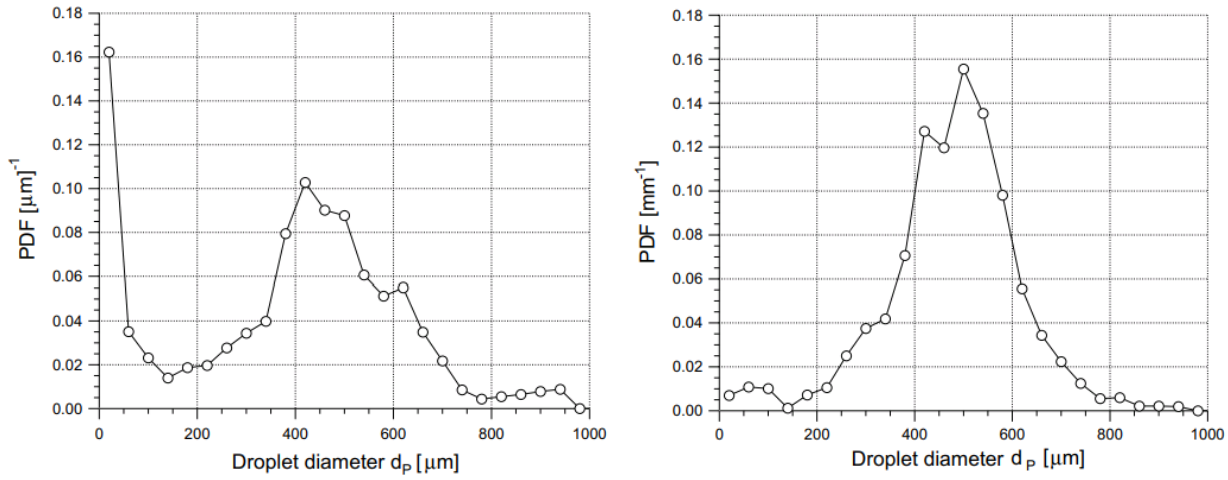

Figure IV-8 *Probability density function PDF for droplet diameter for (left) multiple bubble and (right) single bubble* (Günther et al., 2003)

As it shows in

Figure IV-8, the probability of multiple bubbles case to produce droplet is less than the probability for single bubble case. Bubbles tend to merge at the surface of the pool to form large ones (Günther

et al., 2003). Eventually bigger bubbles produces limited number of droplet, and sometime having the tendency to not produce them (Koch et al., 2000). Spiel (Donald E. Spiel, 1998) stated that the film opening speed S_f, caused by the bubble burst, decrease with increasing bubble size as $S_f = 27.\exp(-d_b/7.862)$, and that the film thickness increase with decreasing the film opening speed (film thickness could be calculated by Taylor-Culick velocity $S_f = V_{tc} = \sqrt{2\sigma}/\rho h_{film}$). Then, considering the film Weber number, $We_{film} = \frac{\rho S_f^2 l_{film}}{\sigma}$ with l_{film} being the film length, and according to Spiel (Donald E. Spiel, 1998), as the bubble size increases, the film velocity decreases and the We_{film} decreases too. The surface tension will become substantial and the film will find difficulties to break up, therefore the number of the film droplets decreases.

The presence of impurities, according to Clift et al. (Clift et al., 1978) (**Figure II-17**) have a slight effect on this class of bubble size, and could be comparable to pure water. In general, the entrainment in bubbly flow regime consists of jet droplets and film droplets, which explain the slight exponential increase.

2. Experiment with Transition regime

Figure IV-4 presents experiments supporting the transition regime to predict the entrainment. In the experiment of REST (Bunz et al., 1992) the range of superficial gas velocity was from 0.05 m/s corresponding to an entrainment of 1.4E-4 to a superficial gas velocity of 0.08 m/s corresponding to an entrainment of 3E-5. In the THAI experiments, most of the entrainment is scattered around 3E-5 as reported by (Freitag and Schmidt, 2017). Under such range of superficial gas velocities, the bubble cannot be considered uniformly sized (Shah et al., 1982). Large bubbles up to 1 cm are formed in the water pool with tendency of coalescence to occur (Ruzicka et al., 2001) inside the pool and at the surface to eventually form even larger bubbles. Consequently, the presence of these large bubbles at the surface tends to reduce the entrainment (Cosandey, 1999).

The arguments given for the bubbly flow regime is applicable for the transition regime, since the bubble is always define in shape and size.

In the experiments of THAI (Freitag and Schmidt, 2017) and REST (Bunz et al., 1992), the pressure imposed was from 1 bar to 2.5 bar and superficial gas velocity from 0.05 m/s to 0.1 m/s.

The size of the bubbles in the transition regime, tend to produce only film droplets (Zhang et al., 2012)(Koch et al., 2000). As for jet droplets, bubbles of diameter larger than 5 mm, practically do not produce jet droplets (**Table II-6** (Koch et al., 2000)), because bubbles of this size contain low energy comparing to smaller ones (Cosandey, 1999).

As for the droplet produced by the film, their number are reduced with increasing bubble size after a typical size of 2.5 mm as investigated by (Blanchard and Syzdek, 1988)(Donald E. Spiel, 1998)(Resch and Afeti, 1992) (**Figure II-21**, right). The slight increase of the number of film droplet after bubble size of 3 mm diameter in right hand side of **Figure II-21** might be due to the puncture position. Bubbles bursting at the edge produce more droplet than bubbles bursting at the centre of their cap (Donald E. Spiel, 1998).

Moreover, (Lhuissier and Villermaux, 2012) demonstrated experimentally that the maximum bubble size from which the number of film droplets begins to decrease could be calculated by equation II.*26* which gives a value of around 10 mm.

Additionally, the reason behind this lack of film droplet production might also be related to the drainage of film cap at the surface. In general, bubbles burst occur due film thinning, but the burst occurs as well due to instabilities. Large bubbles loses their stability before the complete film drainage, eventually, very few droplet will be produced (Lhuissier and Villermaux, 2012).

The capillary length, which is the maximum stable bubble size, could be calculated as a function of pressure as shown in **Table IV-4**. The capillary length decreases as the pressure increase as explained earlier on the effect of pressure on bubble size. In bubbly flow regime, the bubble size compete against the capillary length, thus, sometimes they will have enough time to drain the film cap and entrain more droplets, and sometimes they burst immediately due to bubble instabilities by the formation of large bubbles because of coalescence as mentioned earlier . In the transition regime, and as the bubble swarm reach the surface, the tendency to form larger bubbles than the capillary length is elevated, therefore, they lose their stability and burst quite immediately. In addition, these large bubbles will not have the required time to drain the film cap, resulting in entraining very few droplets.

Table IV-4 Capillary length as a function of pressure

Pressure (bar)	2	4	6
Capillary length (mm)	2.5	2.35	2.24

The impurities might affect as well the film droplets production to a very small amount. **Figure II-19** and **Figure II-20** show photos taken from (Wei et al., 2020) of bubble burst before and after aerosol (non-soluble) agglomeration respectively. The bubble is able to produce droplets before aerosol agglomeration at the surface, and the agglomeration occurs with increasing temperature (Wei et al., 2020).

In transition regime, the main characteristic is the formation of large bubbles inside the pool and at the surface by coalescence. Such bubbles are extremely instable, and tend to produce less droplet, thus, less entrainment. However, the situation changes when the gas velocity increase further in churn turbulent flow regime, where the information about bubble size is lost.

3. Experiment with Churn Turbulent flow regime

Superficial gas velocity superior to 0.1 m/s characterizes this flow regime. Lebel et al. (Lebel et al., 2020) used high superficial gas velocity from 0.1m/s, which corresponds to a minimum entrainment of 1E-4 to a superficial gas velocity of 0.4 m/s with a maximum entrainment of 1E-3. Garner et al. (Garner et al., 1954) obtained entrainment values from 4E-5 to 1E-3 corresponding to superficial gas velocity of 0.46 m/s to 1.4 m/s. Kim (Kim and No, 2005) measured an entrainment value of 5E-2 for superficial gas velocity of 0.35 m/s , Zhang (Zhang et al., 2016) recorded a minimum entrainment of 6E-3 for j_g = 0.98 m/s to a maximum value of 4 for j_g= 5.41 m/s. The values obtained by Golub (Rozen et al., 1976a) lies between the values obtained by Zhang (

data	H (m)	D_H(m)	h (m)	D_p (m)	P (bar)	j_g (m/s)	E_{fg}	*Tracer*

THAI (Freitag and Schmidt, 2017)	9	3.2 or 1.9	5.9 to 8.2	1.4 or 1.6	2.5	0 to 0.1	8e-5 – 1.2e-4	CsI, NaCl
Cosandey (Cosandey, 1999)	3	1.5	2	0.6	2 to 6	0 to 0.0044	2.5e-5 – 8e-5	KI, CsI
ALPHA (Kudo et al., 1994)	5.7	3.9	1.2	0.305	1 to 15	0.04	7e-5	Na_2SO_4
REVENT (Müller and von Rohr, 1997)	3	1.5	2	0.6 to 1.5	4	0.01	6.5e-5 – 1.3e-4	KI, CsI, $BaSO_4$, SiC
REST (Bunz et al., 1992)	1.5	1.5	0.14	0.108	1	0.08	1.3e-4 – 2e-5	$BaSO_4$
Lebel et al. (Lebel et al., 2020)	1.49	0.19	0.6	0.19	1	0.37	9e-4 – 1e-3	NaCl
Zhang et al. (Zhang et al., 2016)	2.2	0.38	0.187 to 1.53	0.38	1	0.98 to 5.41	6e-3 - 10	-
Kim et al. (Kim and No, 2005)	2	0.3	1.9	0.3	1	0.35	4e-5 – 5e-2	-
Garner et al. (Garner et al., 1954)	1.37	0.3	0.61	0.61	1	1.2	2e-4 – 1.1e-3	KNO_3
Golub et al. (Golub, 1970)	0.1 to 2.2	0.2	-	0.2	1	0.5 to 2	1e-1 - 3	-

Table IV-5 shows a comparison between experimental data). It is clear that the entrainment increase exponentially with increasing superficial gas velocity. In this flow regime, the main characteristic is the creation of large irregular pockets of gas surrounded by small bubbles in the water pool. The droplets production mechanism is excessively different from the bubbly flow regime and the transition regime. The increase of superficial gas velocity in such flow regime has

two consequences, both of which enhance entrainment: on the one hand, increasing superficial gas velocity creates more ligaments of water at the surface, implying the generation of large droplets. On the other hand, increased velocity offers the possibility to lift these larger droplets (Kataoka and Ishii, 1984)(Cosandey, 1999). Eventually the regenerated droplets contribute substantially more to the entrainment than in bubbly flow and transition regimes.

The effect of pressure on this flow regime as mentioned earlier is substantial especially at very high pressure. The paper of Sterman et al. (Sterman et al., 1957) could not be found to analyze effect of thermal-hydraulic in churn turbulent flow regime. Sterman used gas velocity up to 1.2 m/s and pressure up to 185 bar for a water steam system (appendix section of (Yeh and Zuber, 1960)). The entrainment decreases as the pressure increase in the experiment of (Sterman et al., 1957), from an entrainment of 2e-2 corresponding to a 1 bar, to 4e-4 corresponding to a pressure of 185 bar. This is a decrease by 2 order of magnitude, and the reason could be related the decrease in bubble to a much smaller size which eventually entrained less droplets relatively to churn turbulent flow regime.

In the experiment of (Zhang et al., 2016), the surface of the pool at the simulated superficial gas velocity up to 5 m/s, illustrate the enhancement of entrainment in this flow regime, as shown in **Figure IV-9**.

It can be seen that at such gas flow rates, the two-phase flow mixture is very agitated and could be assimilated to a jet/fountain type flow, which makes difficult to differentiate the overflow from entrainment.

In this flow regime, droplets are generated only by detachment. The liquid ligaments lose the stability due the high gas momentum exchange, which lead to the creation of droplet of multiple sizes quickly. Surface tension forces cease to be important, thus even with the presence of impurities in the liquid pool, it does not affect the droplet formation process nor their stability (**Figure II-17**) (Clift et al., 1978).

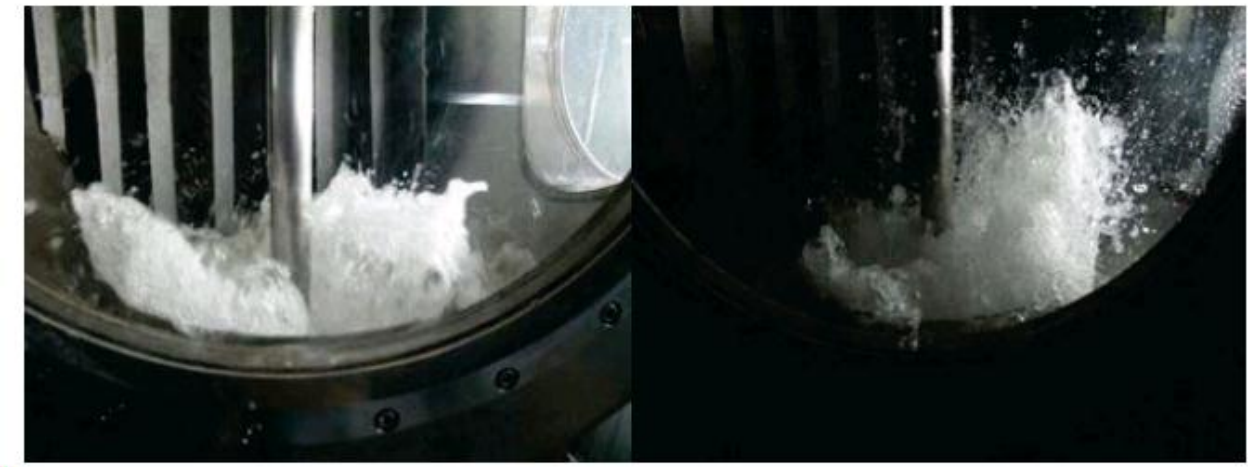

Figure IV-9 *Pool surface condition at high gas flux condition (5 m/s)* (Zhang et al., 2016)

The weber number We, which is the suitable quantity to study the liquid sheets dynamic stability, depends on the square of superficial gas velocity. Thus, as the superficial gas velocity increase rapidly, the Weber number increases exponentially. In such case, the surface tension has practically very weak effect, and the dominant term is the inertial term. Therefore, the liquid ligaments detached very fast as a results of momentum exchange and the formation of droplets increase with superficial gas velocity.

In churn turbulent flow regime, the overflow at the surface at some extent is referred by some authors as "droplet flow regime" (Colomer and Rogers, 2006), since all what could be seen are droplet detaching from the ligament due to high gas flux. This condition could be assimilated to a fluidized bed of droplet in the continuum phase (gas) (Colomer and Rogers, 2006). In terms of aerosol release from water pool, these droplets are easy to retain, as they are large enough to capture. Oppositely, droplets generated in bubbly flow regime are so tiny, which make them hard to retain(Dehbi et al., 2016).

The general trend as shown in **Figure IV-10** is that the entrainment increases as the gas velocity increases, and decrease as the distance from the water surface increases. This decrease is due to the diffusive transport. For steady state conditions, with a given superficial gas velocity, and considering the component above the pool surface, *h*, the entrainment decreases exponentially as the *h* increases.

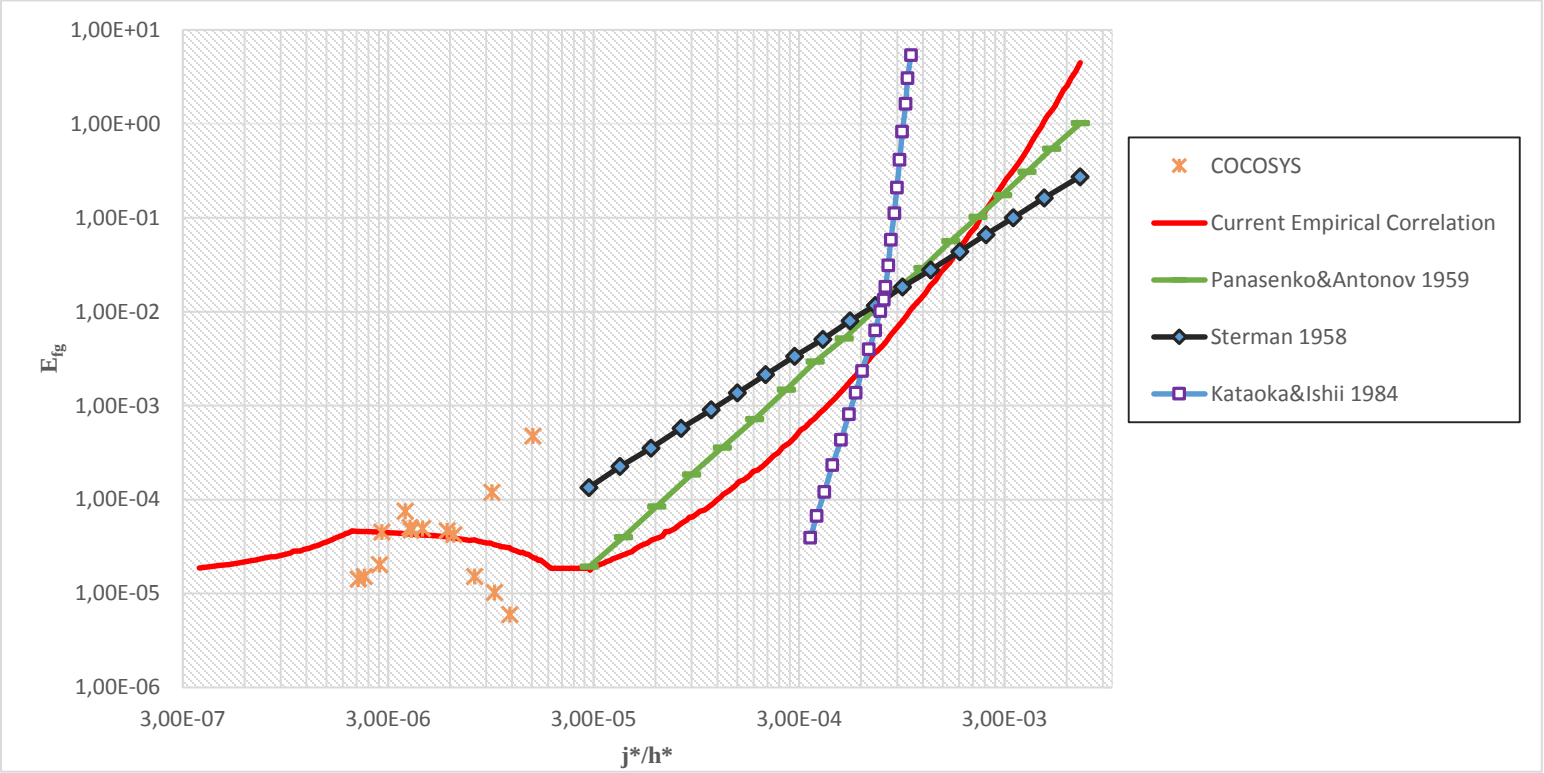

Figure IV-10 *Current Empirical correlation as a function of ratio j*/h**

Figure IV-10 represent the current correlation compared to previous semi-empirical correlation of Sterman (Sterman, 1958),Panasenko and Antonov (Panasenko and Antonov, 1959) and Kataoka and Ishii (Kataoka and Mamoru, 1983)(Chapter II of this thesis). Sterman and Panasenko and Antonov correlations underpredits the entrainment, while Kataoka and Ishii correlation over predicted the entrainment in the churn turbulent flow regime with respect to the current correlation. This might be related to the boundary condition of experimental data used by the previous authors to develop their correlations such as pressure which has showed to have a great influence on bubble dynamics and bubble geometry (Lin et al., 1998)(Wilkinson and Laurent, 1990). The over prediction in Kataoka and Ishii's correlation might also be related to the exponent in their correlation (equation II.*23*). The exponent of the ratio *j*/h** is up to 20^{th} power. In these conditions the entrainment might be affected by the Bernoulli effect when droplets pass through a break, as the experiment conducted by (Kim and No, 2003) (**Figure II-3**).

Table IV-5 below gives a comparison of the main dimensions of the facilities used by previous authors.

data	H (m)	D_H(m)	h (m)	D_p (m)	P (bar)	j_g (m/s)	E_{fg}	*Tracer*
THAI (Freitag and Schmidt, 2017)	9	3.2 or 1.9	5.9 to 8.2	1.4 or 1.6	2.5	0 to 0.1	8e-5 – 1.2e-4	CsI, NaCl
Cosandey (Cosandey, 1999)	3	1.5	2	0.6	2 to 6	0 to 0.0044	2.5e-5 – 8e-5	KI, CsI
ALPHA (Kudo et al., 1994)	5.7	3.9	1.2	0.305	1 to 15	0.04	7e-5	Na_2SO_4
REVENT (Müller and von Rohr, 1997)	3	1.5	2	0.6 to 1.5	4	0.01	6.5e-5 – 1.3e-4	KI, CsI, $BaSO_4$, SiC
REST (Bunz et al., 1992)	1.5	1.5	0.14	0.108	1	0.08	1.3e-4 – 2e-5	$BaSO_4$
Lebel et al. (Lebel et al., 2020)	1.49	0.19	0.6	0.19	1	0.37	9e-4 – 1e-3	NaCl
Zhang et al. (Zhang et al., 2016)	2.2	0.38	0.187 to 1.53	0.38	1	0.98 to 5.41	6e-3 - 10	-
Kim et al. (Kim and No, 2005)	2	0.3	1.9	0.3	1	0.35	4e-5 – 5e-2	-
Garner et al. (Garner et al., 1954)	1.37	0.3	0.61	0.61	1	1.2	2e-4 – 1.1e-3	KNO_3
Golub et al. (Golub, 1970)	0.1 to 2.2	0.2	-	0.2	1	0.5 to 2	1e-1 - 3	-

Table IV-5*Comparison of set ups of entrainment experiments*

data	H (m)	D_H(m)	h (m)	D_p (m)	P (bar)	j_g (m/s)	E_{fg}	*Tracer*
THAI (Freitag and Schmidt, 2017)	9	3.2 or 1.9	5.9 to 8.2	1.4 or 1.6	2.5	0 to 0.1	8e-5 – 1.2e-4	CsI, NaCl
Cosandey (Cosandey, 1999)	3	1.5	2	0.6	2 to 6	0 to 0.0044	2.5e-5 – 8e-5	KI, CsI
ALPHA (Kudo et al., 1994)	5.7	3.9	1.2	0.305	1 to 15	0.04	7e-5	Na_2SO_4
REVENT (Müller and von Rohr, 1997)	3	1.5	2	0.6 to 1.5	4	0.01	6.5e-5 – 1.3e-4	KI, CsI, $BaSO_4$, SiC
REST (Bunz et al., 1992)	1.5	1.5	0.14	0.108	1	0.08	1.3e-4 – 2e-5	$BaSO_4$
Lebel et al. (Lebel et al., 2020)	1.49	0.19	0.6	0.19	1	0.37	9e-4 – 1e-3	NaCl
Zhang et al. (Zhang et al., 2016)	2.2	0.38	0.187 to 1.53	0.38	1	0.98 to 5.41	6e-3 - 10	-
Kim et al. (Kim and No, 2005)	2	0.3	1.9	0.3	1	0.35	4e-5 – 5e-2	-
Garner et al. (Garner et al., 1954)	1.37	0.3	0.61	0.61	1	1.2	2e-4 – 1.1e-3	KNO_3
Golub et al. (Golub, 1970)	0.1 to 2.2	0.2	-	0.2	1	0.5 to 2	1e-1 - 3	-

In this section, it was shows how the entrainment of water droplet was affected. The effect of the bubble dynamics in the pool by analysing the flow regime and the characteristics of the bubble

size and their ability to produce droplets, either by the bubble burst in the bubble flow regime or the transition regime or by the shear of the water ligament in the churn turbulent flow regime was given. The effect of thermal-hydraulics such as the pressure has a slight effect on bubble size up to 16 bar and it was demonstrated experimentally by (Cosandey, 1999). As for the temperature, when it increases, the surface tension decrease, affecting bubble stability and their soon breakup (Poulain et al., 2018). Interestingly, the effect of temperature contribute in the aerosol agglomeration at the surface of the pool when increased. This effect of agglomeration have the ability to decrease the number of the produced droplet for bubble in the bubbly flow and transition regimes.

Droplet produced in the churn turbulent flow regime are more easily to retain than tiny droplet produced in bubbly flow regime (Dehbi et al., 2016).

V. Exploratory CFD studies

In this chapter, a summary of a CFD simulation performed, using Ansys 18.0 Fluent, is presented that was intended to simulate the entrainment of water droplets in bubbly flow regime. Several iterations were performed for verification and validation, however, this was not possible due to some challenging difficulties encountered related to computational resources.

The objective of this task is to understand the bubble behavior at the surface of the water pool concerning the stability before and after the burst. In addition, the ability of the film in producing droplet, since this latter is too small to be captured, unless the mesh is fine enough. As shown in the previous chapter, the entrainment under bubbly flow regime is of the order of 10^{-4}, and the droplets that contribute have a size of about 0.5 to 1 micron. To catch a droplet of such a size, the cell size needs to be 10 times smaller than the droplet size, which means 0.05 to 0.1 micron. First this needs exceptional computational resources to mesh the domain, and second to resolve the flow field around the droplets.

A. Geometry, Meshing and Configuration

The performed simulation consists of a bubble column rising in a stagnant water pool. It is a 2D simulation, with a computational domain of 5cm x 9cm. Water level is 5cm height, and the gas space is 4cm, which is enough to perform a statistical analysis for the entrained droplet by bubble burst. There is a column of about 50 bubbles, each bubble have a typical size of 2.5 mm diameter (typical bubble size in bubbly flow regime). This is illustrated in Figure V-1.

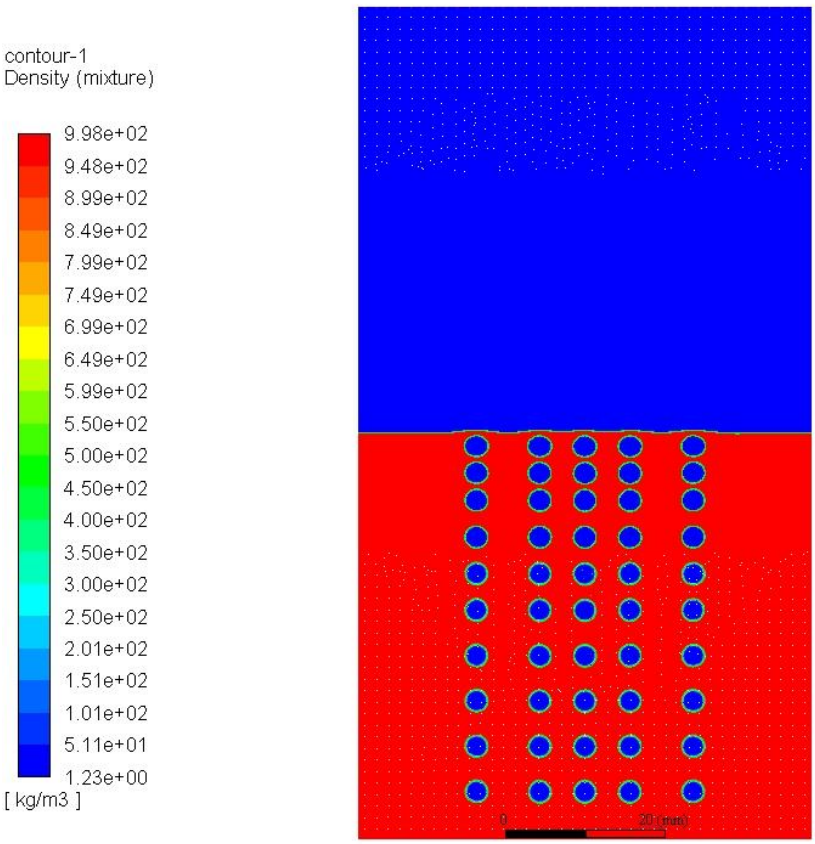

Figure V-1 Bubble column in water pool

The meshing procedure conducts to a quasi-structured mesh due to the transition from large to small elements. The domain was meshed fine enough where it should be to speed up the simulation. The refinement is done close to the surface of the water and above the surface to track the droplets (Figure V-2).

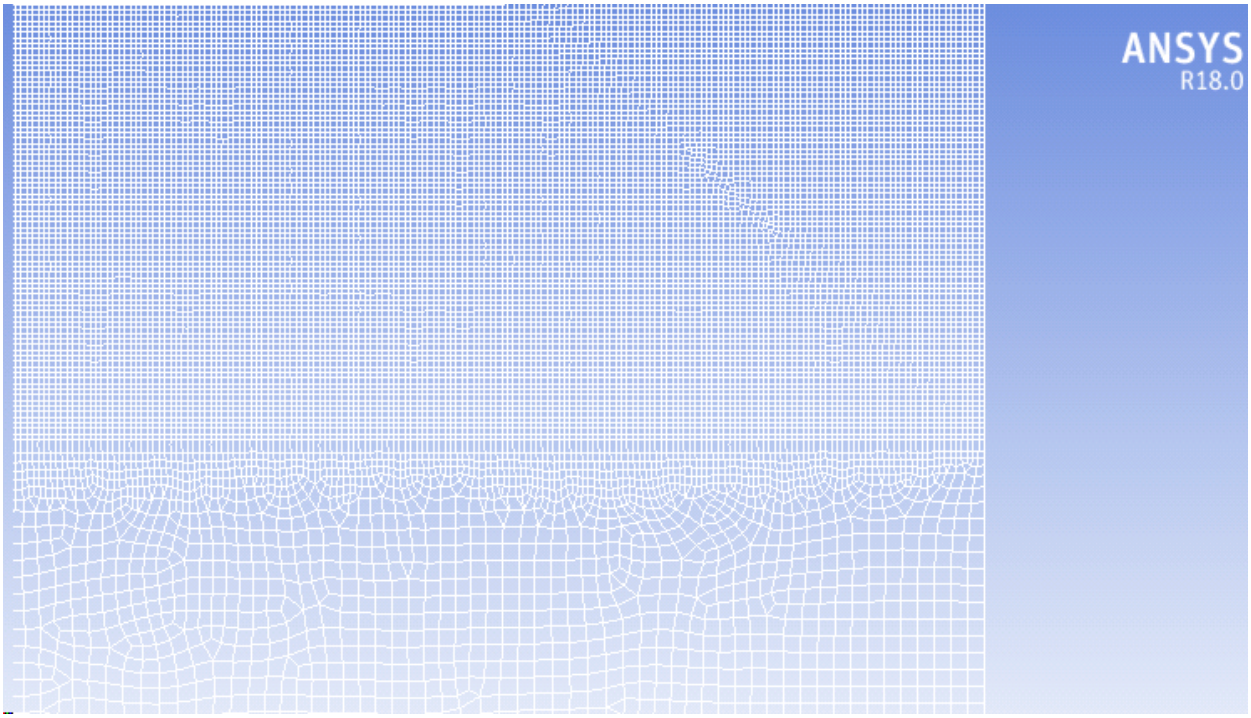

Figure V-2 Meshing of the computational domain

Three different mesh was used in the simulation for mesh independence analysis; 1) coarse mesh with a typical cell size of 45 microns, and 2) medium mesh of 30 microns and 3) fine mesh with 15 microns cell size. Table V-1 shows the details of each mesh.

Table V-1 Meshes used in the simulation

	Fine	**Medium**	**Coarse**
Smallest element size	15 μm	30 μm	45 μm
Number of elements	5 151 127	1 421 002	1 007 745

The following boundary conditions are set, which corresponds to THAI experiments WH24 a1 to a5.

- Temperature of the atmosphere = 408 K
- Water temperature = 311 K
- Pressure = 2.5 bar
- Walls = no slip,

Volume of Fluid method (Hirt and Nichols, 1981) was used for mass conservation, and Level Set method (Dervieux and Thomasset, 1979) (Sethian, 1999) (Osher and Fedkiw, 2002) for surface tracking coupled (CLSVOF).

B. Results and Challenges

This section presents some results and challenges encountered during the simulations.

After several iterations, and hundreds of bursting bubbles, only a couple of droplets was able to be captured above the water surface. As could be seen in the following figure, two droplets could be spotted at elevation 5.5 cm approximately.

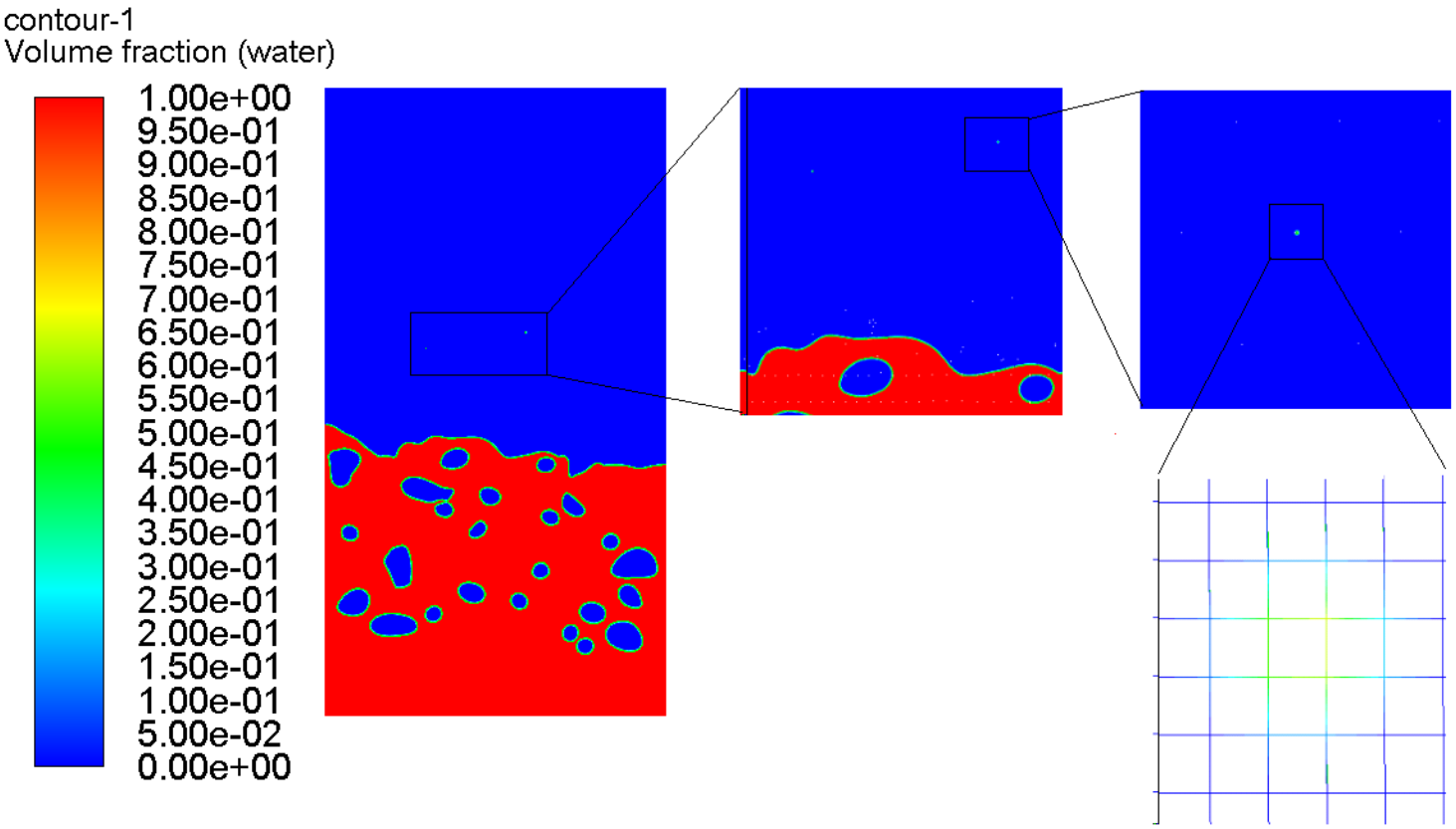

Figure V-3 Volume fraction plot for droplets analysis

Figure V-3 shows a droplet captured during the simulation. The smallest element in that simulation is 30 microns, and the droplet is barely detected by three cells. Its size could be approximated to 90 microns. Such a droplet is far from being airborne and is more likely generated by the jet after the bubble burst, since the mesh is too coarse to capture the film and its evolution. As mentioned in Chapter 1, the droplets size coming from the jet range from 100 microns to 1 mm, thus, it is trackable for the current set up. However, these droplets are not airborne.

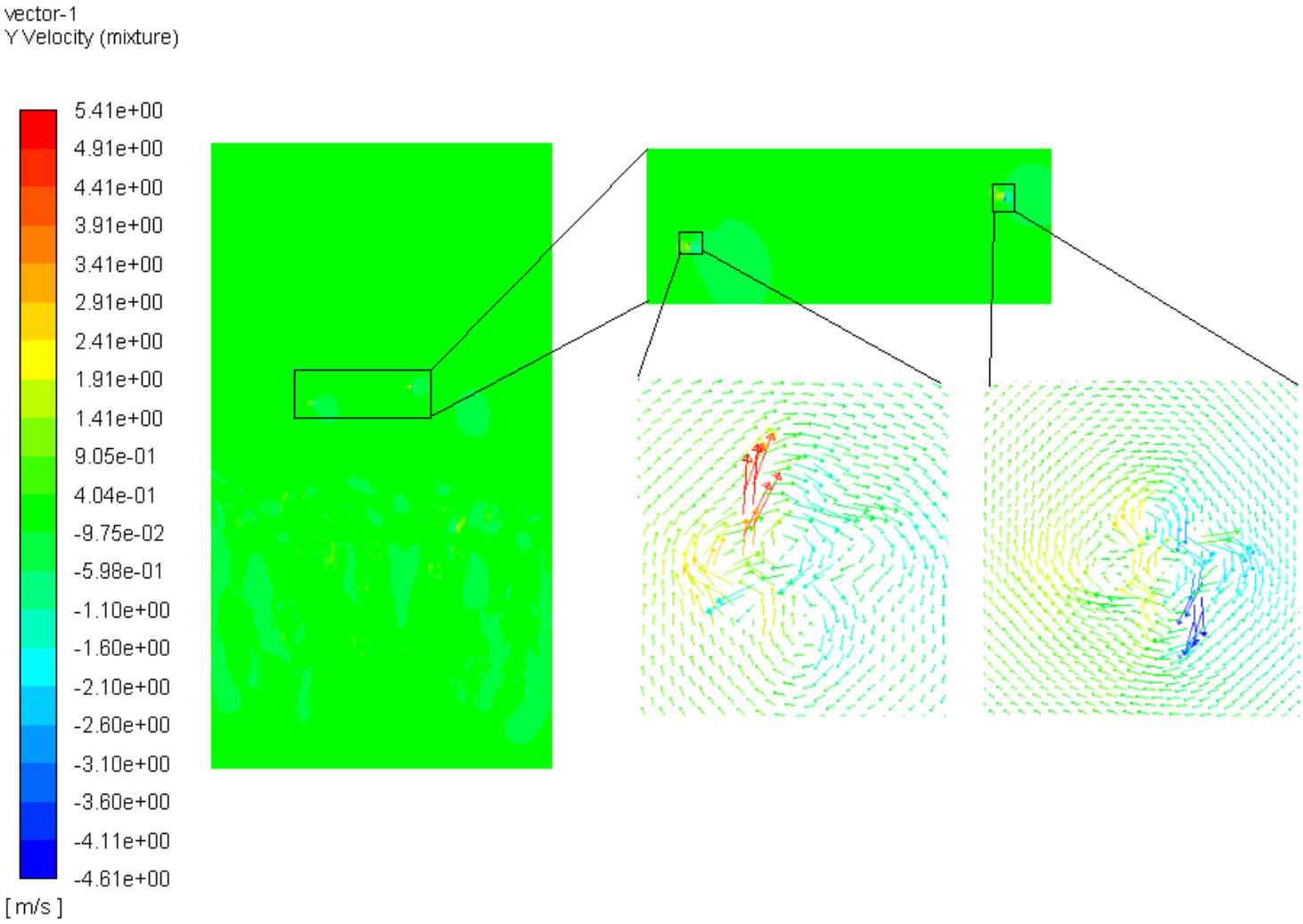

Figure V-4 Velocity plot for droplet analysis

As for the velocity, Figure V-4 Velocity plot for droplet analysis above shows, the velocity profile of the two captured droplets. The first droplet zoomed in the right hand side goes up with a velocity of 5.41 m/s and the second one have a negative velocity (downward) of 4.61 m/s. The superficial gas velocity for bubbly flow regime is up to 0.05 m/s, therefore, these droplets will definitely be de-entrained.

The simulations was performed using high performance computers HPC. Each simulation (total of three simulation for mesh independence) used a node with 28 core.

Even with such characteristics, the simulation took long time to generate few droplets which was not enough to perform a statistical analysis to quantify the entrainment in bubbly flow regime. There are several reason behind the reason not to be able to have the required results. These reasons are related to geometry of the bubble and their behavior at the water surface.

First, when the bubble is at rest at the surface of the pool, it forms a film with typical thickness of the order of 1 micron. Therefore, the smallest element size should be at least 0.1 micron in order to capture and to observe the evolution of the film as the bubble loses its integrity. Then, the droplets coming from the film have a typical size of 1 to 10 microns, thus to capture these droplets, the element size should be of the order of 0.1 to 1 micron. Once this is achieved, the complete profile of the bubble burst could be analyzed for entrainment analysis. Unfortunately, to perform such study, a substantial amount of computational resources must be accessible, since a small simulation would contained hundreds of millions of elements at least.

C. Conclusion

Despite the lack of the computational resources, one might consider some assumptions in order to have some qualitative and quantitative results.

Some recommendations could be related to the bubble study itself. The focus should be rather on the bubble than on the droplets. At such conditions, the study of one single bubble of different sizes that correspond to flow regimes, such as bubbles of a 2.5 mm diameter are found in bubbly flow regime at a pressure range of 2 to 6 bar. The computational domain should contain only one bubble and discretized accordingly to the film thickness. Same reasoning should be kept for larger bubbles found in the transition regime (between 5 and 10 mm diameter). The results of such study could give a clear insight on the trend of the entrainment in bubbly flow and transition regimes.

VI. Conclusion and Perspectives

In this thesis, empirical analysis of the entrainment of water droplets from water pool from bubbly to churn turbulent flow regime using data in the open literature and from experimental programs was carried out and the assessment was performed using numerical simulation with the lumped parameter code COCOSYS. Below, conclusion about the achievement of this work and possible future work are given.

A. Conclusion

The first part of this work provided the state of the art literature on the topic of experimental and theoretical investigation of entrainment of droplets from water pool by gas bubbles in order to define the scope. Clear deficits regarding the existing models were identified.

The next step was to analyse the entrainment phenomena through numerical simulations using THAI experimental data in order to test the effectiveness of the RUB correlation implemented in COCOSYS. As a results, the RUB correlation does not predict the entrainment beyond the transition regime, and for depressurization scenarios. Possible explanation regarding the depressurization scenarios was that the pressure effect was not taken into account in the RUB correlation.

For this purpose, an empirical correlation is proposed to predict the entrainment in bubbly flow regime, transition regime and churn turbulent flow regime, including the effect of pressure. The correlation showed good agreement with experimental data found in the open literature up to date.

The independent variable used to predict the entrainment used in the current correlation is the ratio of the dimensionless superficial gas velocity to the dimensionless height above the pool surface. This ratio has the ability to assess the entrainment prediction to cover wide range of geometries and flow regimes.

The entrainment shows an increase in bubbly flow regime, slightly decrease during the transition regime, and increase exponentially in churn turbulent flow regime. The reason behind this trend is the behaviour of the bubbles inside the pool and at the surface, since the bubbles are assumed to be uniformly sized during bubbly flow regime (production of film and jet droplets), having a size distribution in the transition regime (no jet droplets and the number of film droplet decrease with increasing bubble size), and large pockets of gas during churn turbulent flow.

This correlation could be considered as a good candidate to be implemented in computer codes since it provides wide range of applicability.

B. Perspectives

Certainly, more variable needs to be investigated theoretically and experimentally, and this fact is related to the complexity of two-phase flows in pools and at the surface. CFD simulation is efficient in simulating the pool entrainment phenomena, however such simulation require extensive computational resource especially in simulating droplets in the micron and sub-micron range, where the mesh has to be fine to capture the droplets (mesh size 10 times smaller than the captured object).

The droplets dynamics is a phenomenon that was not addressed in the analysis of the entrainment. It was assumed to be absent in the formulation of Kruzhilin, however, this phenomena affect the entrainment since the collision between droplets at and above the surface of the pool is inevitable. As a next step, the intention is to simulate the droplets dynamics by injecting them with adequate velocities that match the ejection velocity for bubbly flow, transition and churn turbulent flow regimes. The expected outcome of the droplets interaction might be coalescence or breakup. CFD simulations of such case could provide the information on droplets velocities during and after the interaction, which in turn could be used in the calculation of the frequency of the interactions. This latter also could unlock a variable or give insight to understand better the trend of the entrainment phenomena from bubbly flow to churn turbulent flow regime.

References

Akita, K., Yoshida, F., 1974. Bubble Size, Interfacial Area, and Liquid-Phase Mass Transfer Coefficient in Bubble Columns. Ind. Eng. Chem. Process Des. Dev. 13, 84–91. https://doi.org/10.1021/i260049a016

Andrews, J.M., 1960. Kinetic Study of Fluidized Solids Entrainment. Ind. Engr. Chem. 57, 85.

Arndt, S., Weber, G., Nowack, H., Spengler, C., Schwarz, S., Eschricht, D., Beck, S., 2015. COCOSYS User's Manual. Gesellschaft für Anlagen- und Reakt. mbH.

Azbel, D., 1981. Two phase flows in chemical engineering. Cambridge University Press.

Bagul, R.K., Pilkhwal, D.S., Limaye, S.P., Vijayan, P.K., Joshi, J.B., 2018a. Air Water Loop for investigation of flow dynamics in a steam drum: Steady state two-phase natural circulation experiments and validation. Nucl. Eng. Des. 328, 266–282. https://doi.org/10.1016/j.nucengdes.2017.12.024

Bagul, R.K., Pilkhwal, D.S., Vijayan, P.K., Joshi, J.B., 2019. Experimental investigations on carryover in a gravity separation-based steam drum. J. Nucl. Eng. Radiat. Sci. 5, 1–12. https://doi.org/10.1115/1.4041791

Bagul, R.K., Pilkhwal, D.S., Vijayan, P.K., Joshi, J.B., 2018b. Air Water Loop for investigation of flow dynamics in a steam drum: Carryover experiments and CFD simulation. Nucl. Eng. Des. 333, 145–160. https://doi.org/10.1016/j.nucengdes.2018.04.012

Barbosa, J.R., Hewitt, G.F., König, G., Richardson, S.M., 2002. Liquid entrainment, droplet concentration and pressure gradient at the onset of annular flow in a vertical pipe. Int. J. Multiph. Flow 28, 943–961. https://doi.org/10.1016/S0301-9322(02)00003-4

Berzal, M.E., Crespo, M.J.M., Swiderska-Kowalczyk, M., Espigares, M.M., Jimenez, J.L., 1995. State-of-the-art review on fission products aerosol pool scrubbing under severe accident conditions. Eur. Comm. Brussels, Belgium.

Blanchard, C.D., 1989. The size and height to which jet drops are ejected from bursting bubbles in seawater. J. Geophys. Res. Ocean. 94, 10999--11002.

Blanchard, D.C., Syzdek, L.D., 1988. Film Drop Production as a Function of Bubble Size. J. Geophys. Res. 93, 3649–3654.

Bunt, R., Corradini, M., Ellison, P., Farmer, M.., Francis, M., Gabor, J., Gauntt, R., Henry, C., Linthicum, R., Luangdilok, W., Lutz, R., Paik, C., Plys, M., Rabiti, C., 2015. Reactor Safety Gap Evaluation of Accident Tolerant Components and Severe Accident Analysis. NURETH-16 4661–4674.

Bunz, H., Koyro, M., Propheter, B., Schoeck, W., Wagner - Ambs, M., 1992. Resuspension of fission products from sump water. 32.05.02; LK 01; EUR-Report 3009-86-07 EL ISP D.

Clift, R., Grace, J.R., Weber, M.E., 1978. Bubbles, Drops, and Particles. Acad. Press.

Colomer, A.G., Rogers, R.L., 2006. Evaluation of alternative swell models for reactor relief. Inst.

Chem. Eng. Symp. Ser. 596–622.

Cosandey, J., 1999. Droplet production over a boiling pool during a slow depressurization. PhD thesis ETH Zürich, 179. https://doi.org/10.3929/ethz-a-010782581

Cosandey, J.O., Von Rohr, P.R., 2001. Entrainment of soluble and non soluble tracers from a boiling water surface. Nucl. Eng. Des. 208, 87–97. https://doi.org/10.1016/S0029-5493(01)00354-5

Culick, F., 1960. Comments on a ruptured soap film. J. Appl. Phys. 31, 1128–1129. https://doi.org/10.1063/1.1735765

Dapper, M., 2009. Modellierung der nassen Resuspension und Analyse des Einflusses auf den Quellterm bei Kühlmittelverluststörfällen. Selbstverlag. des Lehrstuhls für Energiesysteme und Energiewirtschaft, Ruhr-Uni. 193.

Davis, R.F., 1940. The Physical Aspect of Steam Generation at High Pressures and the Problem of Steam Contamination. Proc. Inst, lech. Eng. 144, 21.

Dehbi, A., Suckow, D., Lind, T., Guentay, S., Danner, S., Mukin, R., 2016. Key Findings from the Artist Project on Aerosol Retention in a Dry Steam Generator. Nucl. Eng. Technol. 48, 870–880. https://doi.org/10.1016/j.net.2016.06.001

Dervieux, A., Thomasset, F., 1979. A Finite Element Method For The Simulation Of Rayleigh-Taylor Instability, in: Proceedings of the Symposium Held by the International Union of Theoretical and Applied Mechanics (IUTAM). p. 597.

Freitag, M., Kühnel, A., Langer, G., 2016. Erweiterung der THAI - Anlage durch einen zweiten Druckbehälter : THAI + Extension of the THAI test facility by a second vessel : THAI +. Becker Technol. GmbH.

Freitag, M., Schmidt, E., 2017. Re-Entrainment of Fission Products from Water Pools at Elevated Temperature. Tech. Rep. No. 150 1516 – TR – WH24.

Fritz, B.G., 2006. Aerosol entrainment from a sparged non-newtonian slurry. J. Air Waste Manag. Assoc. 56, 1108–1114. https://doi.org/10.1080/10473289.2006.10464531

Garner, F.H., Ellis, S.R.M., Lacey, J.A., 1954. The size distribution and entrainment of droplets. Trans. Inst. Chem. Eng 32, 222–235.

Golub, S.I., 1970. Investigation of moisture carryover and separation in evaporation apparatus, in: Candidates Dissertation. MEI.

Golub, S.I., Weisblat, M.B., Ilyuschenko, V. V, Frolov, V.I., 1980. Estimation of transported entrainment in flash desalination plants. Proc. 7th Int. Symp. Fresh Water from Sea.

Günther, A., Wälchli, S., von Rohr, P.R., 2003. Droplet production from disintegrating bubbles at water surfaces. Single vs. multiple bubbles. Int. J. Multiph. Flow 29, 795–811. https://doi.org/10.1016/S0301-9322(03)00041-7

Gupta, S., Funke, F., Weber, G., 2015. Thai Experiments on Volatility , Distribution and Transport Behaviour of Iodine and Fission Products in Containment. Proc. Int. OECD-NEA/NUGENIA-SARNET Work. Prog. Iodine Behav. NPP Accid. Anal. Manag. March

30, April 1.

Gupta, S., Poss, G., Sonnenkalb, M., 2016. OECD / NEA THAI program for containment safety research : main insights and perspectives, in: Eurosafe Forum.

Hagendorfer, H., 2011. New Analytical Methods for Size Fractionated, Quantitative, and Element Specific Analysis of Metallic Engineered Nanoparticles in Aerosols and Dispersions. PhD thesis, École Polytech. Fédérale Lausanne.

Herranz, L.E., 2017. Pool Scrubbing in Severe Accident Sequences: Identification of Key Boundary Conditions. IPRESCA Kick off Meet.

Hirt, C.W., Nichols, B.D., 1981. Volume of Fluid (VOF) Method for the Dynamics of Free Boundaries. J. Comput. Phys. 39, 25. https://doi.org/10.1007/s40998-018-0069-1

Jamialahmadi, M., Muller-Steinhagen, H., 1990. Effect of electrolyte concentration on bubble size and gas hold-up in bubble columns. Chem. Eng. Res. Des. 68, 202–204.

Kataoka, I., Ishii, M., 1984. Mechanistic modeling of pool entrainment phenomenon. Int. J. Heat Mass Transf. 27, 1999–2014.

Kataoka, I., Mamoru, I., 1983. Mechanistic Modeling and Correlations for Pool Entrainment Phenomenon. Nureg/Cr-3304 ANL-83-37.

Kharoua, N., Khezzar, L., Saadawi, H., 2013. CFD Modelling of a Horizontal Three-Phase Separator: A Population Balance Approach. Am. J. Fluid Dyn. 3, 101–118. https://doi.org/10.5923/j.ajfd.20130304.03

Kim, Hyun, C., No, Cheon, H., 2005. Liquid entrainment and off-take through the break at the top of a vessel. Nucl. Eng. Des. 235, 1675–1685. https://doi.org/10.1016/j.nucengdes.2005.01.014

Kim, C.H., No, H.C., 2005. Liquid entrainment and off-take through the break at the top of a vessel. Nucl. Eng. Des. 235, 1675–1685. https://doi.org/10.1016/j.nucengdes.2005.01.014

Kim, C.H., No, H.C., 2003. Liquid Entrainment and Off-Take Through the Break at the Top of a Vessel. Trans. Am. Nucl. Soc. 89, 426.

Koch, M.K., Vossnacke, A., Starflinger, J., Schütz, W., Unger, H., 2000. Radionuclide re-entrainment at bubbling water pool surfaces. J. Aerosol Sci. 31, 1015–1028.

Kolokoltzev, V.A., 1952. An Investigation of the Conditions in the Steam Space of ISV Evaporators. Diss. Transl. Power Inst. 10.

Kruzhilin, G.N., 1951. The dependence of the permissible vapor load upon the pressure. Izv. Akad. Nauk. Otd. Tekh. Nauk. 7, 1106.

Kudo, T., Yamano, N., Moriyama, K., Maruyama, Y., Sugimoto, J., 1994. Experimental Study of Aerosol Reentrainment Experimental Study of Aerosol Reentrainment From Flashing Pool in ALPHA Program, in: The Third International Conference on Containment Design and Operation, Toronto, Canada. Toronto, p. 11.

Lebel, L.S., Lessard, E., Batten, K., Clouthier, T., 2020. Experimental evaluation of re-

entrainment from wet scrubber filtered containment venting systems. Nucl. Eng. Des. 369, 13. https://doi.org/10.1016/j.nucengdes.2020.110837

Lhuissier, H., Villermaux, E., 2012. Bursting bubble aerosols. J. Fluid Mech. 696, 5–44. https://doi.org/10.1017/jfm.2011.418

Lin, T.J., Tsuchiya, K., Fan, L.S., 1998. Bubble Flow Characteristics in Bubble Columns at Elevated Pressure and Temperature. AIChE J. 44, 545–560. https://doi.org/10.1002/aic.690440306

Lu, M., Xie, H., 2017a. An investigation of pool entrainment based on the method of Volume of Fluid. Nucl. Eng. Des. 318, 72–84. https://doi.org/10.1016/j.nucengdes.2017.04.006

Lu, M., Xie, H., 2017b. A Numerical Study of Liquid Carryover Based on The Volume of Fluid Model. ICONE25-66292.

Müller, M., von Rohr, P.R., 1997. Revent Program - Modelling of aerosol reentrainment from boiling pool during controlled filtered venting after a severe core melt accident. J. Aerosol Sci. 28.

NEA/CSNI, 2010. OECD/NEA THAI Project Hydrogen and Fission Product Issues Relevant for Containment Safety Assessment under Severe Accident Conditions. Final Rep. R(2010)3.

Newitt, D.M., 1954. Liquid entrainment 1. The mechanism of drop formation from gas vapour bubbles. Trans. Instn. Chem. Engrs 32, 244–261.

Osher, S., Fedkiw, R., 2002. Level set methods and dynamic implicit surfaces, Springer. https://doi.org/10.1016/s0898-1221(03)90179-9

Ouallal, M., Leyer, S., Gupta, S., 2017. Literature survey of Fission Product Aerosol Re-entrainment Modelling. NURETH-17.

Özdemir, S., 2005. Investigation of Air Bubble Motion in Water Through a Vertical Narrow Rectangular Channel by Using Image Processing Techniques. PhD thesis, METU - Middle East Tech. Univ.

Panasenko, M.D., Antonov, A.I., 1959. Correlation of mechanical carryover by steam. Teploenergetika 6.

Paradissiadis, I., Widmer, F., 1984. Prediction of Liquid Entrainment in Evaporators. Chem. Eng. Process. Process Intensif. 18, 249–253.

Poulain, S., Villermaux, E., Bourouiba, L., 2018. Ageing and burst of surface bubbles. J. Fluid Mech. 851, 636–671. https://doi.org/10.1017/jfm.2018.471

Qiu, S.Z., Sun, D.C., Tian, W.X., Xiang, Y., Su, G.H., 2015. Experimental and Theoretical Research on Liquid Entrainment in AP1000 ADS Blow - down Phase of SBLOCA. NURETH-16.

Resch, F., Afeti, G., 1992. Submicron Film Drop Production by Bubbles in Seawater. J. Geophys. Res. 97, 3679–3683.

Rozen, A.M., Golub, S.I., Davydov, I.F., Gostinin, G.I., 1970. Some Laws Governing Drop

Carry Over, in: Soviet Physics Doklady. p. 648.

Rozen, A.M., Golub, S.I., Votintseva, T.I., 1976a. Calculating droplet carryover with bubbling. Teploenergetika 23, 59.

Rozen, A.M., Golub, S.I., Votintseva, T.I., 1976b. On the nature of degree of dependence of transported carryover on vapor velocity with bubbling. Teploenergetika 23, 55.

Ruzicka, M.C., Zahradník, J., Drahoš, J., Thomas, N.H., 2001. Homogeneous-heterogeneous regime transition in bubble columns. Chem. Eng. Sci. 56, 4609–4626. https://doi.org/10.1016/S0009-2509(01)00116-6

Santiago, M.R. de, 1991. Etude de l'entrainement de gouttelettes a la surface libre du liquide dans une colonne a bulles. PhD thesis, Univ. Joseph FOURIER.

Santiago, M.R. de, Marvillet, C., 1991. Pool entrainment phenomenon: Measurement of size and velocity distributions of droplets at several distances above the bubbling surface. Int. Commun. Heat Mass Transf. 3, 499–511.

Schmidt-Naujok, E.W., Balewski, B., Freitag, M., Gupta, S., 2013. Wet resuspension of insoluble material from a boiling sump. Tech. Rep. No 1501361–TR–TH25.

Schmidt, E.W., Gupta, S., Freitag, M., Poss, G., Von Laufenberg, B., 2015. Wet resuspension of insoluble material from a boiling sump. Tech. Rep. No.1501361–TR–TH25.

Sethian, J.A., 1999. Level set methods and fast marching methods.

Shah, Y.T., Kelkar, B.G., Godbole, S.P., Deckwer, W. -D, 1982. Design parameters estimations for bubble column reactors. AIChE J. 28, 353–379. https://doi.org/10.1002/aic.690280302

Spiel, Donald E, 1998. On the births of film drops from bubbles bursting on seawater surfaces smaller than their parents and which have upward velocity oscillation. J. Geophys. Res. 103, 907–918.

Spiel, Donald E., 1998. On the births of film drops from bubbles bursting on seawater surfaces. J. Geophys. Res. Ocean. 103, 24907–24918. https://doi.org/10.1029/98JC02233

Spiel, D.E., 1992. Acoustical measurements of air bubbles bursting at a water surface: Bursting bubbles as Helmholtz resonators. J. Geophys. Res. 97.

Sterman, L.S., 1958. On the theory of steam separation. Sov. Physics-Technical Phys. 3, 1440–1451.

Sterman, L.S., 1957. The correlation of experimental data for vapour bubbling through a liquid. Zh. Tekh. Fiz. 26, 1519.

Sterman, L.S., 1952. Kotloturbostroenie. no. 5.

Sterman, L.S., Antonov, A.I., Surnov, A. V., 1957. An investigation of steam quatility at 185 atm. Teploenergetika 3, 17.

Sterman, L.S., Antonov, A.I., Surnov, A. V, 1958. An Investigation of the Steam Quality at 185 atm Using Radioactive Isotopes. Teploteh. i Gidrodynamika.

Styrikovich, M.A., Petukhov, V.I., Kolokoltsev, V, A., 1964. The effect of gas phases density on the extent of droplet entrainment. Teploenergetika 11.

Styrikovich, M.A., Sterman, L.S., Surnov, A. V, 1955. An Investigation of the Carry Over of Salt by Steam Using Radioactive Isotopes. Teploenergetika 2.

Sun, D.C., Tian, W.X., Qiu, S.Z., Su, G.H., Zhang, P., Liu, J.C., Ma, Y.Y., 2014. Scaling analysis of AP1000 ADS-4 entrainment and depressurization. Prog. Nucl. Energy 74, 71–78. https://doi.org/10.1016/j.pnucene.2014.01.019

Sun, D.C., Xiang, Y., Tian, W.X., Liu, J.C., Zhang, P., Qiu, S.Z., Su, G.H., 2015. Experimental investigation of upper plenum entrainment in AP1000. Prog. Nucl. Energy 80, 80–85. https://doi.org/10.1016/j.pnucene.2014.12.003

Taylor, G., 1959. The dynamics of thin sheets of fluid. III. Disintegration of fluid sheets. Proc. R. Soc. London. Ser. A. Math. Phys. Sci. 253, 313–321. https://doi.org/10.1098/rspa.1959.0196

Toba, Y., 1959. Drop Production by Bursting of Air Bubbles on the Sea Surface (II) Theoretical Study on the Shape of Floating Bubbles. J. Oceanogr. Soc. Japan 15, 121–130. https://doi.org/10.5928/kaiyou1942.15.121

Viles, J.C., 1993. Predicting liquid re-entrainment in horizontal separators. JPT, J. Pet. Technol. 45, 405–409. https://doi.org/10.2118/25474-PA

Wallis, G.B., 1970. Annular two-phase flow, Part 1: A simple theory. J. Fluids Eng. Trans. ASME. https://doi.org/10.1115/1.3424950

Wallis, G.B., 1962. The Onset of Droplet Entrainment in Annular Gas-Liquid Flow. Schenectady, NY.

Wei, Y., Chen, H., Gu, H., Chen, L., Yu, X., 2020. Experimental investigation of the puncture position and film rolling speed of bubbles bursting under different liquid pool conditions. Prog. Nucl. Energy 129, 13. https://doi.org/10.1016/j.pnucene.2020.103510

Westgarth, R., 1964. Chamber geometry in multi-stage flash evaporators. U.S. Dep. Commer. Off. Tech. Serv.

Wilkinson, P.M., Laurent, L.L., 1990. Pressure and gas density effects on bubble break-up and gas hold-up in bubble columns. Chem. Eng. Sci. 45, 2309–2315. https://doi.org/10.1016/0009-2509(90)80110-Z

Wilson, T.W., Ladino, L.A., Alpert, P.A., Breckels, M.N., Brooks, I.M., Browse, J., Burrows, S.M., Carslaw, K.S., Huffman, J.A., Judd, C., Kilthau, W.P., Mason, R.H., McFiggans, G., Miller, L.A., Najera, J.J., Polishchuk, E., Rae, S., Schiller, C.L., Si, M., Temprado, J.V., Whale, T.F., Wong, J.P.S., Wurl, O., Yakobi-Hancock, J.D., Abbatt, J.P.D., Aller, J.Y., Bertram, A.K., Knopf, D.A., Murray, B.J., 2015. A marine biogenic source of atmospheric ice-nucleating particles. Nature 525, 234–238. https://doi.org/10.1038/nature14986

Wurster, S., Meyer, J., Kolb, H.E., Kasper, G., 2015. Bubbling vs. blow-off - On the relevant mechanism(s) of drop entrainment from oil mist filter media. Sep. Purif. Technol. 152, 70–79. https://doi.org/10.1016/j.seppur.2015.08.012

Xiang, Y., Wu, Y.W., Sun, D.C., Tian, W.X., Zhang, P., Qiu, S.Z., Su, G.H., 2016. Experimental simulation of liquid entrainment in ADS-4 depressurization line in AP1000. Prog. Nucl. Energy 91, 295–301. https://doi.org/10.1016/j.pnucene.2016.05.006

Yan, P., Jin, H., He, G., Guo, X., Ma, L., Yang, S., Zhang, R., 2019. CFD simulation of hydrodynamics in a high-pressure bubble column using three optimized drag models of bubble swarm. Chem. Eng. Sci. 199, 137–155. https://doi.org/10.1016/j.ces.2019.01.019

Yeh, G., Zuber, N., 1960. On The Proplem of Liquid Entrainment. Report.

Zenz, F.A., Weil, N.A., 1958. A theoretical-empirical approach to the mechanism of particle entrainment from fluidized beds. AIChE J. 4, 472–479. https://doi.org/10.1002/aic.690040417

Zhang, J., Chen, J.J.J., Zhou, N., 2012. Characteristics of jet droplet produced by bubble bursting on the free liquid surface. Chem. Eng. Sci. 68, 151–156. https://doi.org/10.1016/j.ces.2011.09.019

Zhang, P., Chen, P., Li, W., Di, Z., Zhang, L., Hu, X., Zou, Y., 2016. An experimental study of pool entrainment in high gas flux region. Prog. Nucl. Energy 89, 191–196. https://doi.org/10.1016/j.pnucene.2016.02.017